

EFFECTS OF ASYMMETRIC LEADING EDGE

FLAP DEFLECTION ON DELTA WINGS

By

CARLOS IZE

Bachelor of Physics
São Paulo University
São Carlos, Brazil
1988

Master in Mechanical Engineering
São Paulo University
São Carlos, Brazil
1991

Submitted to the Faculty of the
Graduate College of the
Oklahoma State University
in partial fulfillment of
the requirements for
the Degree of
DOCTOR OF PHILOSOPHY
July, 1998

COPYRIGHT

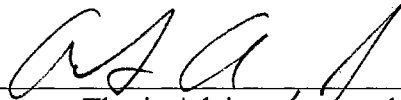
By

Carlos Izé

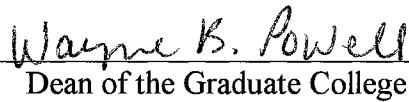
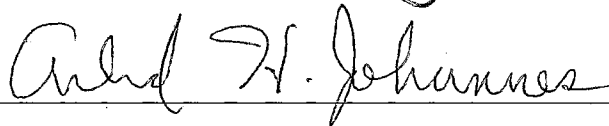
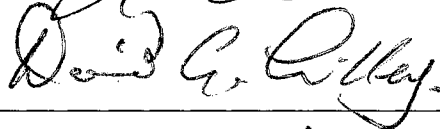
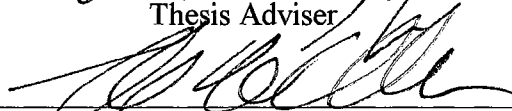
Graduation Date
July, 1998

EFFECTS OF ASYMMETRIC LEADING EDGE
FLAP DEFLECTION ON DELTA WINGS

Thesis Approved:



Thesis Adviser



Wayne B. Powell
Dean of the Graduate College

PREFACE

The effect that leading edge vortex flaps have on delta wings with 65° and 80° leading edge swept angle has been studied. The study combines both experimental and computational methodologies. The experimental investigation focuses on static measurements, while the computational focuses on the quasi-steady and dynamic characteristics of leading edge vortex flaps. A torque sensor was constructed to measure the roll moment of the delta wing. A simple free to roll system was also developed to qualify the effect of the leading edge vortex flaps on the delta wings. Flow visualization was performed to determine the path and the separation points of the vortices over the wing. Preliminary results indicate that the leading edge vortex flaps have an interesting phenomenon on the wings. When the flaps are deflected anti-symmetrically, and as the angle of attack of the wing increases, the wing rolls toward the downward flap: does not roll or roll towards the upward flap. The cause for this is that for low angles of attack, as the leading edge flap is deflected upwards, the local angle of attack is increased, and vice versa on the opposite flap. This creates a roll moment towards the downward deflected flap. At large angles of attack, the crossflow becomes dominant due to the leading edge vortex formation. A downward flap deflection results in stronger vortex over the wing, resulting in a roll moment in the direction of the upward flap.

ACKNOWLEDGMENTS

I wish to express my sincere appreciation to my major advisor, Dr. Andrew S. Arena, Jr., for his intelligent supervision, constructive guidance, inspiration and friendship. My sincere appreciation extends to my other committee members Dr. David G. Lilley, Dr. Frank W. Chambers and Dr. Arland H. Johannes, whose guidance, assistance, encouragement, and friendship are also invaluable. I would like to thank Dr. Ronald L. Dougherty for giving me the opportunity to become a Teaching Assistant. I also would like to thank James Davis for helping me in the use of the mechanical shop facilities.

More over I would like to express my sincere gratitude to my friends that provided suggestions and assistance during this study: Mr. Joseph Conner and Mr. Reed Jackson.

Thanks also go to my parents for their support and encouragement. I would like to give my special appreciation to my wife Claudia, for her patience, strong encouragement at times of difficulty which were not few, love and understanding throughout this whole process. Finally, I would like to thank all the Professors that I worked with as a Teaching Assistant for all the opportunities they gave to me.

“There are more things in heaven and earth, Than are dreamt of in your philosophy.”

William Shakespeare

“Earth is the cradle of Humanity, but one can't live in the cradle forever.”

Konstantin A. Tsiolkovsky

“Imagination is more important than knowledge.” **Albert Einstein**

“Resistance is futile.” **The Borg**

“Live Long and Prosper.” **Vulcan Salute**

TABLE OF CONTENTS

I.	INTRODUCTION.....	1
	1.1 Problem Statement.....	1
	1.1.1 Vortex Flaps Effects.....	4
	1.1.2 Trip Wires Effect.....	6
	1.2 Literature Review.....	8
	1.3 Summary.....	19
	1.4 Objectives of the Investigation.....	20
II.	EXPERIMENTAL APPARATUS.....	21
	2.1 Wind Tunnel Facility.....	21
	2.2 Delta Wings.....	21
	2.3 Surface Pressure Distribution.....	27
	2.4 Torque Sensor.....	28
	2.4.1 Mechanical Component.....	28
	2.4.2 Electronic Component.....	31
	2.5 Surface Oil Apparatus.....	33
	2.6 Free to Roll Apparatus.....	34
III.	COMPUTATIONAL MODEL.....	37
	3.1 Flow Model.....	37
	3.2 Energy Exchange Concept.....	40
IV.	COMPUTATIONAL RESULTS AND DISCUSSION.....	43
	4.1 Model Validation.....	43
	4.2 Quasi-Steady Effects.....	46
	4.3 Spanwise Camber Effects.....	50
V.	EXPERIMENTAL PROCEDURE.....	54
	5.1 Rational for Experimental Approach.....	54
	5.2 List of Experiments Conducted.....	55
	5.3 Roll Moment Measurement.....	57
	5.4 Surface Pressure Measurement.....	62

5.5	Trip Wires Effect.....	63
5.6	Surface Flow Visualization.....	64
5.7	Free to Roll Flow Visualization.....	64
VI.	EXPERIMENTAL RESULTS AND DISCUSSIONS.....	65
6.1	Roll Moment Characterization.....	65
6.1.1	Validation.....	65
6.1.2	Roll Moment Coefficient with Asymmetric Flap Deflection.....	67
6.2	Trip Wires Effect on Roll Moment.....	72
6.2.1	80° Wing Without Flap Deflection.....	73
6.2.2	80° Wing With Asymmetric Flap Deflection.....	74
6.3	Surface Pressure Measurement.....	76
6.3.1	Pressure Distribution Over the 80° Wing Without Flap Deflection.....	76
6.3.2	Pressure Distribution Over the 80° Wing With Asymmetric Flap Deflection.....	79
6.4	Flow Visualization.....	84
6.4.1	Static Surface Flow Visualization for the 80° Delta Wing.....	84
6.4.2	Static Surface Flow Visualization for the 65° Delta Wing.....	97
6.5	Free to Roll System.....	106
6.6	Roll Reversal Phenomenon.....	108
VII.	CONCLUSIONS AND RECOMMENDATIONS.....	112
7.1	Conclusions.....	112
7.2	Recommendations.....	116
	REFERENCES.....	117
	APPENDIXES.....	121
	APPENDIX A - Torque Sensor Construction.....	122
	A.1.1 Mechanical Part.....	121
	A.1.2 Electronic Part.....	127
	APPENDIX B - Computer Code Used for Data Acquisition.....	129

LIST OF TABLES

Table	Page
1. Roll moment measurements.....	56
2. Surface pressure measurements.....	56
3. Roll moment coefficient over the 80° delta wing obtained from the pressure coefficient.....	79

LIST OF FIGURES

Figure	Page
1.1 Leading-edge vortex on a delta wing (Marchman 1981).....	2
1.2 Vortex formation over a slender delta wing.....	3
1.3 Concept of vortex flap: a) flat delta wing and b) delta wing with LEVF deflected downward (Rinoie and Stollery 1994).....	5
1.4 Pressure distribution over a delta wing for laminar (a) and turbulent (b) flow (Hummel 1978).....	7
1.5 Upper vortex flap (UVP) concept (Rao 1982).....	9
1.6 Delta wing with vortex flap and vortex plate (Rinoie and Stollery 1994)....	11
1.7 Tabbed vortex flap (Hoffler and Rao 1985).....	12
1.8 Cavity flap with independent extension and rotation (Rao 1985).....	13
1.9 Apex fence flap concept (Hoffler et. al 1985).....	13
1.10 Combination of apex flap and vortex flap on a 74° sweep wing.....	14
1.11 Double delta wing used by Walton and Katz (1992).....	15
1.12 Roll angle history of the damped oscillations from Walton and Katz (1992).....	16
1.13 Roll angle history of the damped oscillations from Roberts and Arena (1994).....	16
1.14 Model and flaps used by Levin and Seginer (1994).....	17
2.1 80° sweep angle delta wing.....	22
2.2 65° sweep angle delta wing.....	23

2.3	80° sweep angle delta wing with 20% leading edge vortex flap.....	24
2.4	65° sweep angle delta wing with 20% leading edge vortex flap.....	25
2.5	80° sweep angle delta wing with trip wires.....	26
2.6	Sketch of plain delta wing surface pressure model	28
2.7	Round piece and stripe used to build the torque sensor.....	29
2.8	Torque sensor with the strain gages.....	29
2.9	Vertical support of the sting	30
2.10	Setup for the static experiments.....	31
2.11	Electronic circuit of the strain gages and amplifier.....	32
2.12	Setup of the moment acquisition system.....	33
2.13	Primary parts of the free to roll system.....	34
2.14	System connected to the wind tunnel floor.....	35
2.15	Control of the pitch position of the delta wing.....	35
2.16	Control of the yaw position of the delta wing.....	36
3.1	Crossflow delta wing model.....	38
3.2	The roll rate boundary condition.....	39
3.3	Geometry of the leading edge vortex flap.....	40
3.4	Conceptual stable and unstable roll moment trajectories.....	41
3.5	Conceptual sketch of limit cycle roll moment diagram.....	41
4.1	Experimental wing rock time history (Arena 1992).....	44
4.2	Computational wing rock time history.....	44
4.3	Wing rock envelope.....	45
4.4	Calculated roll moment vs. roll angle.....	46

4.5	Roll moment vs. roll angle from experiment (Arena 1992).....	46
4.6	Unsteady and quasi-steady roll moment coefficient vs. roll angle.....	47
4.7	Spanwise vortex position for the unsteady and quasi-steady runs.....	48
4.8	Normal vortex position for the unsteady and quasi-steady runs.....	48
4.9	Vortex strength for unsteady and quasi-steady runs.....	49
4.10	Roll moment time history, when flaps are activated.....	50
4.11	Flap deflection time history.....	51
4.12	Damping effect of roll moment of wing rock control.....	51
4.13	Normal vortex position during control of wing rock.....	52
5.1	Calibration curve for the torque sensor.....	58
5.2	Displacement curve for the torque sensor.....	58
5.3	(a) Normal coupling curve. (b) Lateral coupling curve.....	59
6.1	Roll moment vs. roll angle for different angles of attack for the 80° wing.....	66
6.2	Roll moment vs. roll angle for different angles of attack for the 65° wing.....	67
6.3	Effect of flap deflection on C_l for different angles of attack for the 80° wing.....	68
6.4	Effect of asymmetric flap deflection for opposite flap angles.....	69
6.5	Effect of flap deflection on C_l for different angles of attack for the 65° wing.....	70
6.6	Comparison between experiment and model 25° flap deflection, for the 80° wing.....	71
6.7	Roll moment for different trip wire position over the wing.....	73
6.8	Effect of trip wire on the 80° wing with asymmetric flap deflection.....	75

6.9	Pressure coefficient for the 80° wing with and without trip wires.....	77
6.10	Pressure coefficient for the 80° wing with asymmetric flap deflection.....	80
6.11	Pressure coefficient for the 80° wing with asymmetric flap deflection.....	82
6.12	Pressure distribution of the 80° wing with asymmetric flap deflection at several roll angles.....	83
6.13	Surface flow field for a 80° wing at $\alpha=30^\circ$ and $\phi=0^\circ$	86
6.14	Vortex breakdown effect on a 80° wing at $\alpha=40^\circ$ and $\phi=0^\circ$	87
6.15	80° wing at $\alpha=30^\circ$ and $\phi=0^\circ$ (a), (b) and (c).....	89
6.16	80° wing at $\alpha=30^\circ$ and $\phi=10^\circ$ (d), (e), (f).....	90
6.17	80° wing at $\alpha=30^\circ$ and $\phi=20^\circ$ (g), (h), (i).....	91
6.18	80° wing at $\alpha=30^\circ$ and $\phi=30^\circ$ (j), (k), (l).....	92
6.19	80° wing at $\alpha=15^\circ$ and $\phi=0^\circ$ (a), (b), (c).....	94
6.20	80° wing at $\alpha=30^\circ$ and $\phi=0^\circ$ (d), (e), (f).....	95
6.21	Secondary separation line for the 80° wing at $\alpha=15^\circ$ and 30°	96
6.22	65° wing at $\alpha=15^\circ$ and $\phi=0^\circ$ (a) and (b).....	98
6.23	65° wing at $\alpha=15^\circ$ and $\phi=10^\circ$ (c) and (d).....	99
6.24	65° wing at $\alpha=15^\circ$ and $\phi=20^\circ$ (e) and (f).....	100
6.25	65° wing at $\alpha=15^\circ$ and $\phi=30^\circ$ (g) and (h).....	101
6.26	65° wing at $\alpha=10^\circ$ and $\phi=0^\circ$ (a) and (b).....	102
6.27	65° wing at $\alpha=15^\circ$ and $\phi=0^\circ$ (c) and (d).....	103
6.28	65° wing at $\alpha=20^\circ$ and $\phi=0^\circ$ (e) and (f).....	104
6.29	65° wing at $\alpha=30^\circ$ and $\phi=0^\circ$ (g) and (h).....	105
6.30	Behavior of the delta wings for different angles of attack.....	107

6.31	Flap effect at low angles of attack.....	109
6.32	Change in vortex position, for asymmetric flap deflection on the 80° wing.....	110
6.33	Vortex breakdown position for delta wings (Wentz and Kohlman 1971).....	111
A1	Main parts of the torque sensor.....	122
A2	Final assemble of the strips and the supports.....	123
A3	Support for the torque sensor and for the wing.....	124
A4	Final assemble of the torque sensor with wing support and sensor support.....	125
A5	Placement of the strain gages on the torque sensor.....	126
A6	Schematic of the electronic circuit for the strain gages and amplifier.....	128

NOMENCLATURE

English Symbols

b	Wing Trailing Edge Span
c	Chord of the Wing
C_l	Roll Moment Coefficient
C_p	Pressure Coefficient
d	Distance
D	Diameter of the Trip Wire
E	Energy
F	Force
L	Moment
n	Unit Normal Vector
p	Total Pressure
p_∞	Freestream Static Pressure
q_∞	Dynamic Pressure
s	Wing Half Span = $b/2$
S	Wing Area
t	Time
t^*	Non-Dimensional Time
TiO_2	Titanium Dioxide
u_L	Uncertainty in Moment
U_{cl}	Uncertainty in Roll Moment Coefficient
V	Volts
V_{out}	Output Voltage
x	Axial Body-Fixed Coordinate
y	Spanwise Body-Fixed Coordinate
z	Normal Body-Fixed Coordinate

Greek Symbols

α	Angle of Attack
δ	Flap Deflection Angle
ΔE	Change in Energy
ϕ	Roll Angle
$\dot{\phi}$	Roll Rate
Φ	Total Velocity Potential
∇	Gradient Operator
Λ	Delta Wing Sweep Angle

Γ_l Left Vortex Circulation
 Γ_r Right Vortex Circulation
 Ω Ohm

Abbreviations

AC..... Alternate Current
HP..... Hewlett Packard
LEVF..... Leading Edge Vortex Flaps
L/D..... Lift to Drag Ratio
M..... Mach Number
Pa..... Pascal
PC..... Personal Computer
TW..... Trip Wire
UVF..... Upper Vortex Flap

CHAPTER I

INTRODUCTION

1.1 Problem Statement

It is known that the aerodynamics of highly swept delta wings is considerably different from conventional wings. Delta wings and other highly swept wings are designed primarily for transonic and supersonic flight. Therefore, their performance at subsonic speeds is not optimal. Subsonic regimes are usually at landing, takeoff, initial climb and many maneuvers, making the wing to have a poor performance. At these speeds it is often necessary to operate at high angles of attack to generate the needed lift. Due to their shape, delta wings can generate large lift at low speeds due to the action of their leading edge vortices; however, the effect of these vortices is not always beneficial.

As stated by Marchman(1981), on most highly swept and delta wings the leading edge radius is not sufficiently large to prevent flow separation along the leading edge. It is this separation that forms the vortex on the upper surface of the wing as shown in figure 1.1.

The strength of the leading edge vortex is normally sufficient to result in flow reattachment over the wing's upper surface and, consequently, in the production of lift up to large angles of attack. The low pressure in the vortex itself adds to the lifting force on the wing. The vortices also tend to be unstable in yaw due to vortex bursting over the wing.

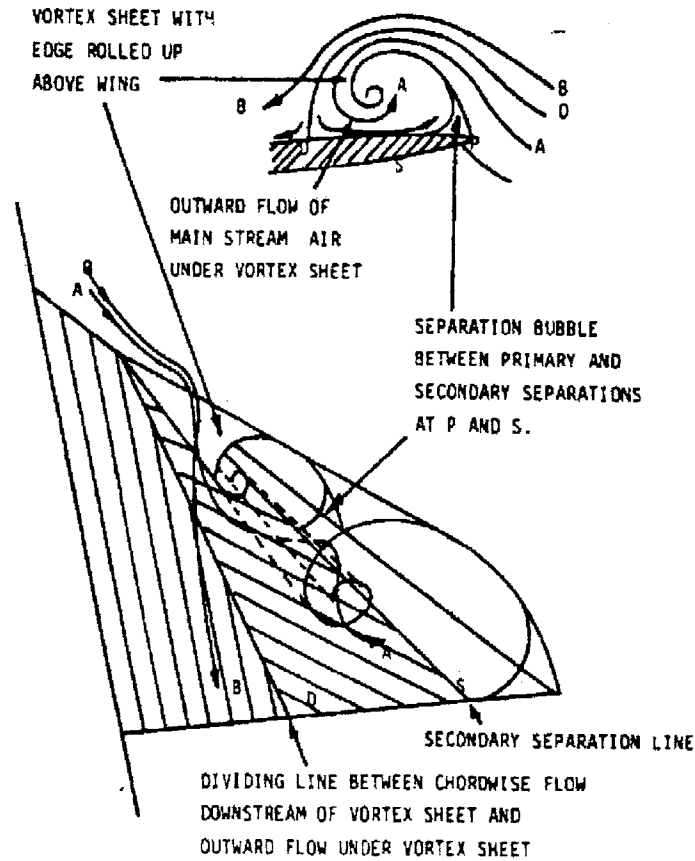


Figure 1.1. Leading -edge vortex on a delta wing. (Marchman 1981)

The vortices over the wing induce additional velocities at the upper surface of the wing. Therefore an additional lift occurs which depends non-linearly on the angle of incidence of the wing. The steep pressure gradient between the minimum of pressure and the leading edge of the wing causes flow separation which takes the form of a small secondary vortex as shown in figure 1.2. At the upper surface of the wing this secondary vortex induces additional velocities.

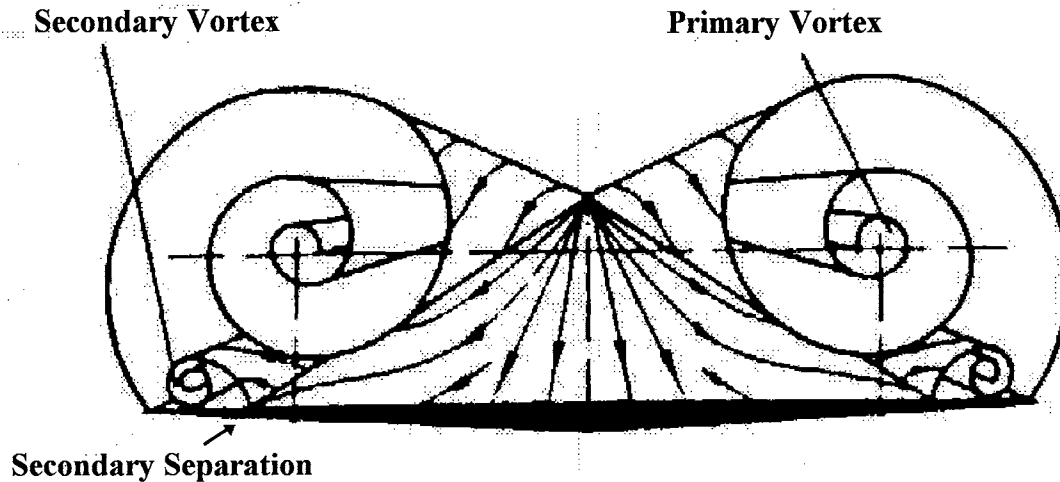


Figure 1.2. Vortex formation over a slender delta wing.

For delta wings with sweep angles greater than 75° , an interesting phenomenon occurs, as the angle of attack increases. A self-induced oscillatory dynamic roll motion starts to build on the wing as shown by Nguyen, Yip and Chambers (1981), Levin and Katz (1984). This oscillation, called “wing rock”, is initiated by some external perturbation and grows in amplitude and frequency until converging on a steady state limit cycle.

The wing rock has been found to be independent of initial conditions and results in a time averaged loss in lift. This phenomenon can occur at any airspeed, and has been known to occur in a variety of aircraft with highly swept wings as shown by Arena (1992).

Susceptibility to wing rock may result in a limiting of the flight envelope, particularly in the landing and other high angle of attack phases of flight. One of the main characteristics of wing rock is the vortices. After wing rock is initiated the amplitude of the motion grows in time due to the instability created by a time lag in the position of the leading edge vortices.

A relatively recent focus of wing rock research is how can wing rock be avoided or suppressed after it starts. Several ways to suppress wing rock have been proposed. A variety of primarily passive methods have been presented in the literature including leading edge fins (Synolakis et. al 1993), flow dividers on the top of the wing surface (Ng, Skaff and Kountz 1994), leading edge tangential blowing (Wong 1992). The feasibility of active wing rock control has also been presented (Walton and Katz 1992), and (Roberts and Arena 1994).

1.1.1 Vortex Flap Effects

A delta wing is often used as a main wing for aircraft such as the next generation, high speed civil transport, and most modern military aircraft. It is known that the L/D ratio of the delta wing at low speeds is relatively poor. To improve the L/D ratio, and therefore, improve the takeoff and climb performance of delta wing aircraft, it was proposed the use of leading edge vortex flap by Rao (1979).

The leading edge vortex flap (LEVF) is a full span deflectable surface at the leading edge of a delta wing. With the flaps deflected downward, a leading edge separation vortex may be formed over the forward facing flap surface as shown in figure 1.3 by Rinoie and Stollery (1994).

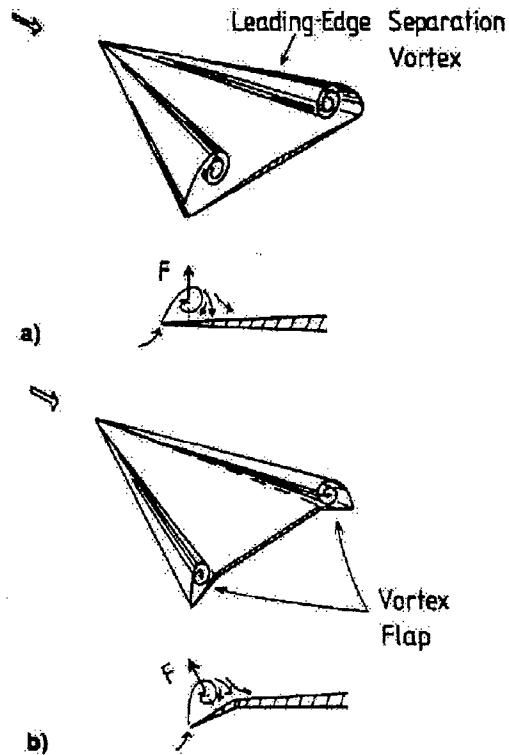


Figure 1.3. Concept of vortex flap: a) flat delta wing and b) delta wing with LEVF deflected downward (Rinoie and Stollery 1994).

The suction force generated by the vortex acts on the flap surface and generates a thrust component. Hence, the drag is reduced and the L/D ration improved.

It has been shown that leading edge vortex flaps have a significant effect on the vortex flow over delta wings. Many investigators have addressed the effects of vortex flaps on delta wing flowfield, primarily through symmetrical deflections. It has been shown, experimentally and computationally, that when the flaps are deflected symmetrically there is an improve in lift and drag over the wing.

There have also been computational and experimental investigations showing that anti-symmetric flap deflection has the capability to damp wing rock. These investigations address only the control of wing rock, not showing the flow aerodynamics for different conditions, like different angles of attack, different roll angles, etc.

The main objective of this investigation is the study of the effect of the vortex flaps on the roll moment, pressure distribution and behavior of the wing at different angles of attack. This will allow a better understanding of the physics of the effect of asymmetric leading edge flap deflection and will show when and how the flaps are effective.

1.1.2 Trip Wires Effect

Due to the limitations on most wind tunnels, it is difficult to achieve a Reynolds number higher than 2,000,000. For this reason there have been few studies considering high Reynolds numbers over delta wings and almost none the considered the Reynolds number over a wing with the use of leading edge vortex flaps deflected symmetrically or asymmetrically. As shown by Hummel (1978), there is a difference when the flow over a plain delta wing is laminar and when is turbulent. The main result is the difference in the pressure distribution over the wing for laminar flow and for turbulent flow, as shown in figure 1.4.

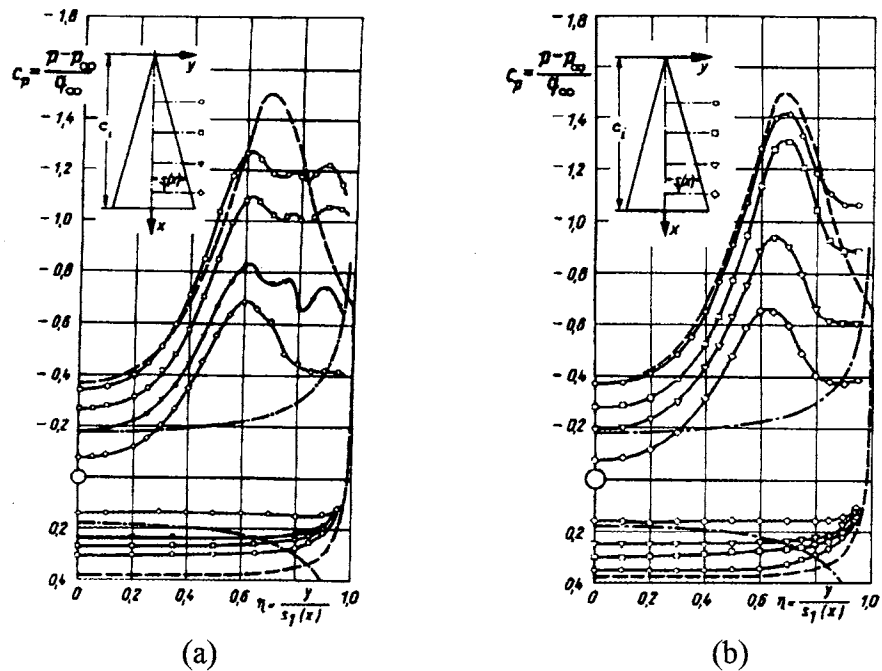


Figure 1.4. Pressure distribution over a delta wing for laminar (a) and turbulent (b) flow (Hummel 1978).

It can be seen that the pressure distribution for the laminar flow is different than that for the turbulent flow. The reason for this is that there is a vorticity effect that increases the suction in the region of the secondary vortex. The laminar boundary layer separates earlier than the turbulent boundary layer, leading to a large secondary vortex, while the turbulent boundary layer remains attached longer, forming a small secondary vortex.

Most of the research done with leading edge vortex flaps over delta wings in wind tunnels have a Reynolds number between 400,000 and 900,000 which is in the range of laminar flow. Therefore there is no data showing the difference of the flow behavior, for low and high Reynolds numbers. The difference of pressure distribution between laminar and turbulent flow, will probably make the roll moment different for these two conditions.

In another study performed by Carcaillet, et al. (1986) the Reynolds number was increased by increasing the velocity of the wind tunnel. Their results are similar to those obtained by Hummel. For this reason, the flow over delta wings with flap deflection (symmetric and asymmetric) will probably show some difference for different Reynolds number.

Due to this difference in pressure over the wing, for laminar and turbulent flow, it is important to determine how the vortex flaps and these two flow conditions interact with each other over the wings.

The effect that the turbulent flow have over the wings, by tripping the boundary layer, will be investigated in parallel with the asymmetric flap deflection studies.

1.2 Literature Review

On most highly swept and delta wings the leading- edge radius is not sufficiently large to prevent flow separation along the leading edge. This separation results in a vortex on the upper surface of the wing. The strength of the leading vortex may be sufficient to reattach the flow and to produce lift at large angles of attack. The low pressure in the vortex adds to the lift force on the wing, but it also adds drag force due to the rearward inclination of the resulting force vectors.

Subsonic wind tunnel tests were performed by Marchman, et al.(1980), to determine the improvement on the performance of the use of leading edge vortex flaps on delta wings. Various flap sizes and deflection angles were examined and lift-to-drag ratio improvement of up to 40% were found at moderate angles of attack on 60° and 75° swept wings. It was concluded that symmetric, downward LEVF's are effective in moving the

wing's leading edge vortex onto the flaps, tilting the vortex-induced force vector forward to produce thrust or reduce the wing's drag while maintaining attached flow and lift on the wing's upper surface.

In another study, Marchman (1981) showed that inverted flaps on the 60° delta wing gives a substantial increase in lift to drag ratio. The data from the 60° delta wing was compared with that from the 75° delta wing, showing that the LEVF effectiveness is stronger as sweep angle is increased.

The effect that LEVF has on 60° sweep delta wings at yaw angles up to 20° was studied by Marchman and Thomas (1981). It was found that the same improvement that the LEVF had, remained at yaw angles up to 20°, showing that the use of LEVF in yaw is not detrimental and may improve some aspects of yawed flight for delta wings.

A different kind of vortex flap, called Upper Vortex Flap (UVF), was studied by Rao (1982) in a 74° delta wing. The idea was to have the flaps hinged along the leading edges and deployed from the wing upper surface, as shown in figure 1.5.

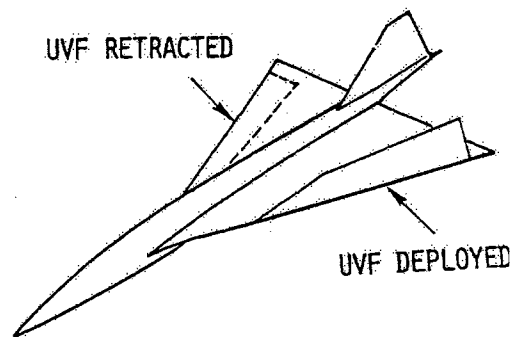


Figure 1.5. Upper Vortex Flap (UVF) concept (Rao 1982)

Results indicated that there is an increase in lift at zero and low angles of attack, and improvement in the longitudinal stability, and an augmented roll control at high angles of attack when the flaps are deflected asymmetrically in combination with elevons.

The influence of the fuselage on the aerodynamic behavior of a 60° delta wing with leading edge vortex flaps was studied by Marchman and Hollins (1982). Results showed that $C_{l_{max}}$ is increased due to fuselage lift, and the fuselage did not affect the ability of vortex flaps to significantly increase L/D of the wings.

The effects trailing edge flaps have on LEVF, were studied by Schoonover and Ohlson (1982), in a supersonic interceptor model designed for efficient cruise at $M=3.0$. Their tests were conducted at $M_\infty=0.3$ and were performed to study pitch moment. The results show that a combination of vortex flaps and trailing edge flaps can improve the model performance. At lift levels typical of maneuvering flight, the addition of a vortex flap provides a significant improvement in the leading-edge suction by shifting the vortex outboard onto a forward facing surface. The combined vortex flap deflection and trailing edge flap deflection provides better performance than deflection of either surface alone.

The influence that a trailing edge vortex has on the leading edge vortex flap was studied by Grantz and Marchman (1983) on 60° and 75° delta wings. Results indicated that the vortex flowfield of the 75° was not substantially improved with the deflection of trailing edge flaps. Changes occurred on the marginal vortices of the 60° wing. The deflection of trailing edge flaps resulted in substantial increase in lift coefficient at low angles of attack without sacrificing performance.

A study of the effects of the combination of vortex flap with vortex plates, shown in figure 1.6, was performed by Rinoie and Stollery (1994) in a 60° delta wing.

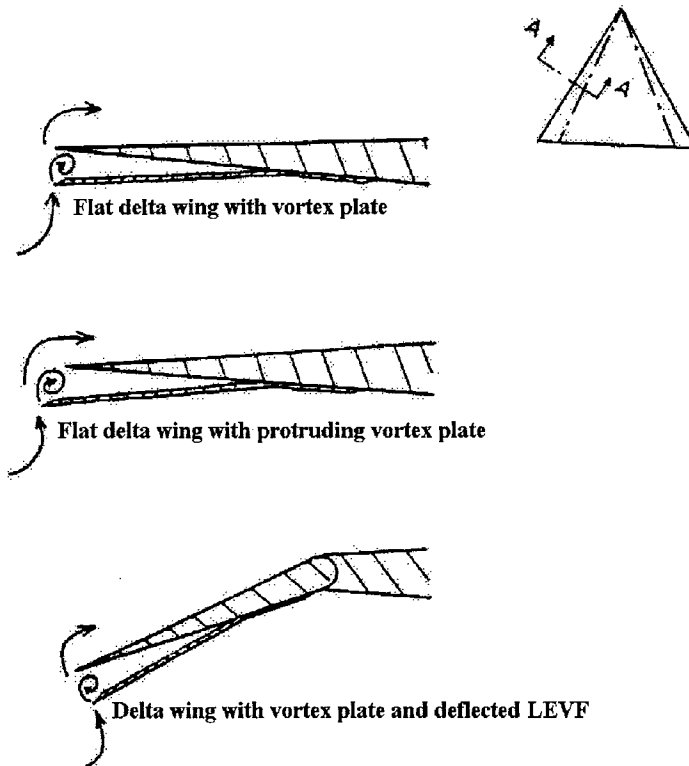


Figure 1.6. Delta wing with vortex flap and vortex plate (Rinoie and Stollery 1994).

The performance of the vortex flap protruding from the leading edge of the datum delta wing is comparable to that of the vortex plate. However, when the vortex plate is used with the vortex flap deflected, it showed no benefit.

A different vortex flap were investigated by Hoffler and Rao (1985). They studied a tabbed vortex flap, as shown in figure 1.7.

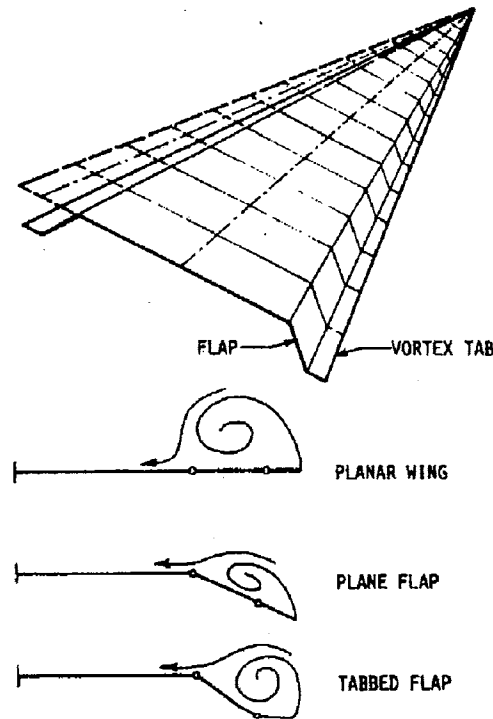


Figure 1.7. Tabbed vortex flap (Hoffler and Rao 1985).

The results show that for a 74° delta wing at $M=0.3$, the tab can augment the flap vortex thrust considerably; however, an excessive tab drag component may cancel this benefit. They concluded that on the basis of lift-to-drag ratio improvements achieved, it cannot be asserted that the potential benefits over properly designed plane vortex flaps of equal area will be such as to justify the added mechanical complexity of the tabbed flap.

An extension of the vortex flap concept was explored by Rao (1985). A retractable lower surface flap mounted on a translating hinge was studied, on a 60° delta wing, allowing chordwise extension as well as deflection, the two movements being independently controlled, as shown in figure 1.8.

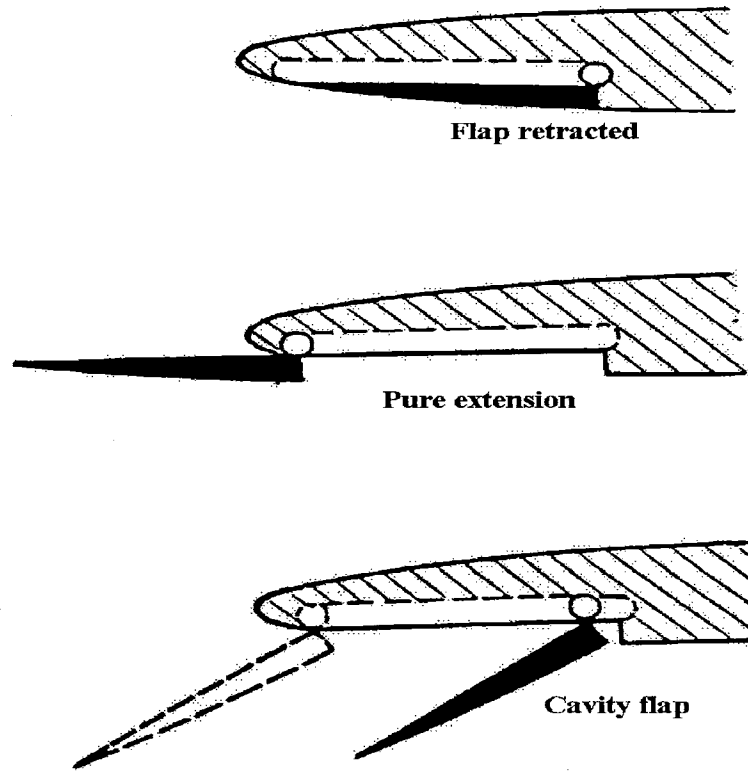


Figure 1.8. Cavity flap with independent extension and rotation (Rao 1985).

Results indicate that the cavity flap was at least equal to the conventional leading-edge flap in L/D improvement.

An investigation of the effects produced by “apex fences” flaps on a 60° delta wing, shown in figure 1.9, was studied by Hoffler, et al. (1985).

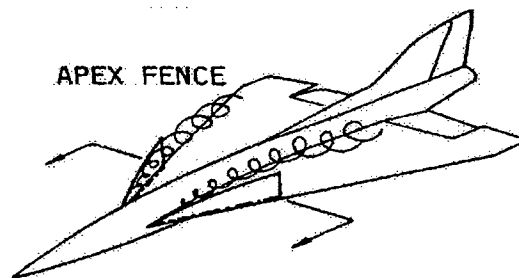


Figure 1.9. Apex fence flap concept (Hoffler et. al 1985).

It was found that the apex fence produced opposite effects over the wing apex region in the low alpha and high alpha regimes. At low angles of attack fence vortices augmented the suction level over the apex, whereas at high angles of attack the apex suction was reduced from the basic wing case.

An analytical study of the aerodynamics of a delta wing with LEVF's was made by Oh and Tavella (1986). They used a vortex sheet model and particular attention was given to the influence of angle of attack and flap deflection on lift and drag forces. Their results show that the drag is reduced as the LEVF's are deflected symmetrically, and downward, but it shows a reduction in lift which does not agree with any of the previous experimental results.

An experimental study of apex flap in combination with vortex flap on a 74° delta wing, shown in figure 1.10, were made by Hsing et al.(1991).

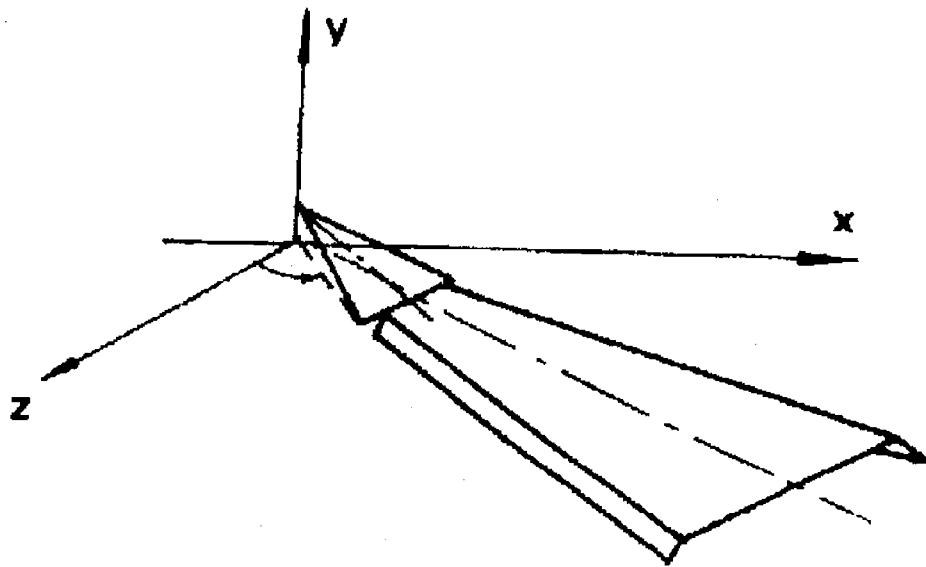


Figure 1.10. Combination of apex flap and vortex flap on a 74° sweep wing.

Their results show that deflecting the apex flap downward will further reduce the drag and hence increase the ratio lift/drag. It was found that wings with vortex flaps properly sized with apex flaps can produce higher lift than without it.

A experimental study of leading edge vortex flaps applied to control of wing rock was made by Walton and Katz (1992). They used vortex flaps in a free to roll double delta wing, shown in figure 1.11, and the motion of the flaps was synchronized with the wing rolling oscillations in such a way that when the wing rolled right the left flap was deflected upward and the right flap downward, and vice-versa when the wing rolled left.

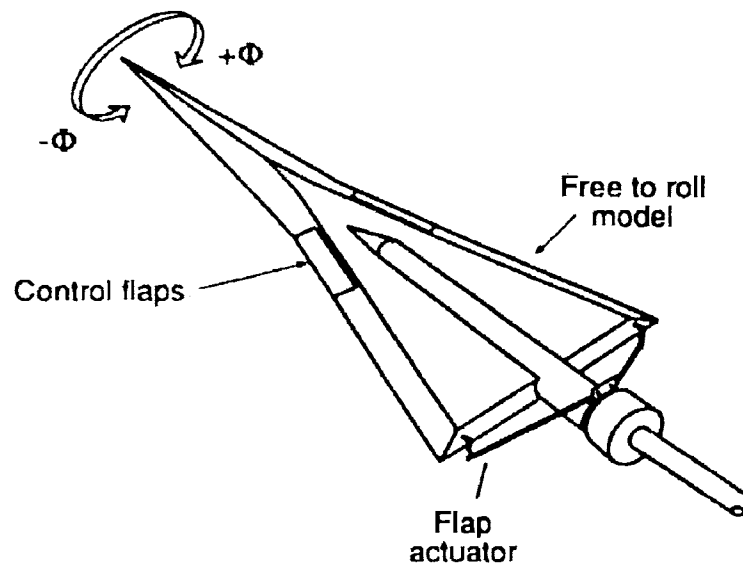


Figure 1.11. Double delta wing used by Walton and Katz (1992)

Their results demonstrated that the amplitude of the self induced roll oscillations can be reduced by the use of leading edge vortex flaps, as shown in figure 1.12.

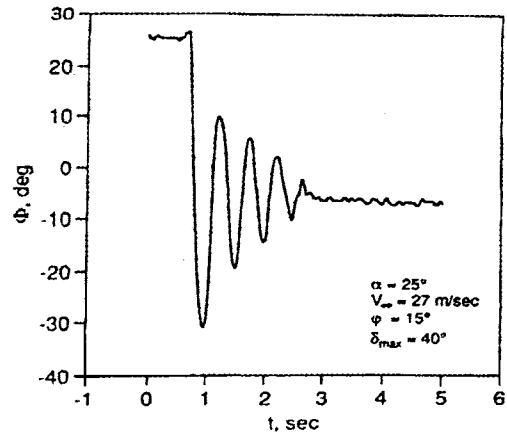


Figure 1.12. Roll angle history of the damped oscillations from Walton and Katz(1992).

A method that uses vortex flap on the leading edge of an 80° delta wing to aid in understanding and evaluating wing rock suppression methodologies was studied by Roberts and Arena (1994). A method that uses a vortex flap on each leading edge has been implemented in this study to suppress the wing rock motion. By controlling the characteristics of separation, through derivative feedback control, the vortex flaps have suppressed the wing rock motion completely. Their results, shown in figure 1.13, are comparable with those from Walton and Katz, shown in figure 1.12.

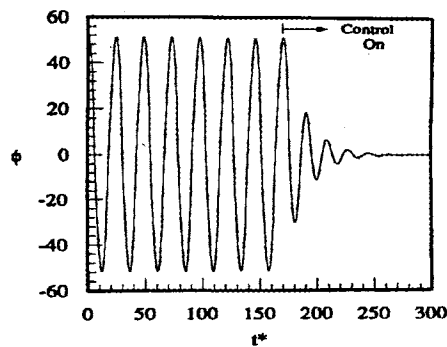


Figure 1.13. Roll angle history of the damped oscillations from Roberts and Arena (1994).

Different sizes and different geometry's of the leading edge vortex flaps, as shown in figure 1.14, were studied by Levin and Seginer (1994).

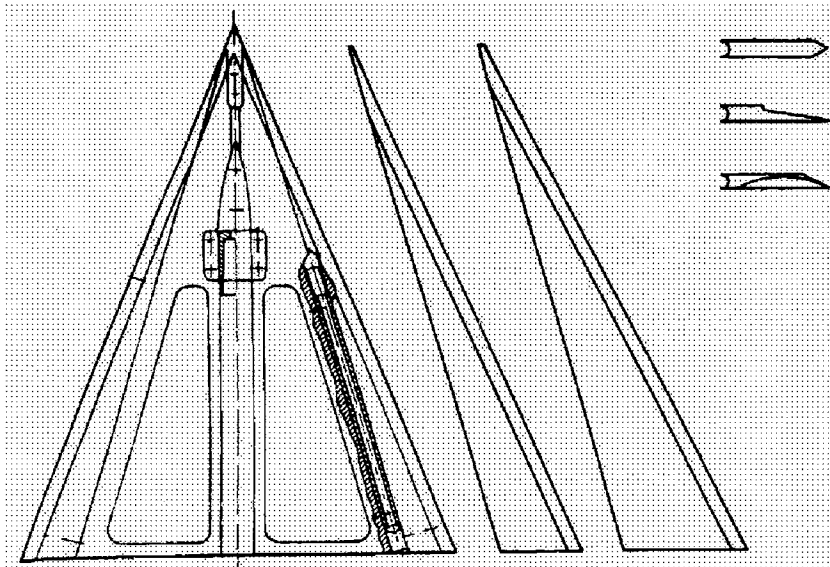


Figure 1.14. Model and flaps used by Levin and Seginer (1994).

Their results show that the physical size of the vortex flap does not affect the characteristics of the flap effect. The same basic phenomena is repeated with all the symmetrical flaps of different aspects ratios. However, it increasingly affects the magnitude of the flap influence on the lift curve slope, the drag coefficient, and the aerodynamic efficiency, as the flaps grow larger.

The effect of spanwise blowing on a delta wing with vortex flaps was studied by Traub (1996). The study showed that spanwise blowing can improve the performance of the leading edge vortex flaps. Results showed that blowing generates substantial increase in lift beyond $\alpha = 13^\circ$.

The use of apex flap on a 75° delta wing to control a pitch-up motion from $\alpha = 28^\circ$ to $\alpha = 50^\circ$ was investigated by Schaeffler and Telionis (1996). During the pitch-up motion an apex flap was deployed and time history of the pressure distribution was obtained. Results indicate that the flaps were effective in delaying stall only if deployed before vortex breakdown had moved over the wing.

Measurements of the three component velocities, the total pressure, the dynamic pressure and the static pressure distributions over the vortex flap and the wing surface on a 70° delta wing were made by Rinoie et al. (1996). The measurements confirmed that the maximum lift/drag ratio is attained when a separated vortex is formed on the vortex flap and when its spanwise length coincides with the vortex spanwise length. It was also determined that the leading edge separation vortex formed on a vortex flap shows similar characteristics to the one formed on a plain delta wing.

The effects of leading edge flaps on leading edge vortices and vortex breakdown were investigated by Deng and Gursul (1996). It was found that the effect of flaps and sensitivity of breakdown location strongly depend on angle of attack and flap angle. Velocity measurements showed that, with the varying flap angle, large changes take place in the size and location of vortex core, in axial and swirl velocity profiles, and in the structure of the secondary vortex.

The study performed by Rinoie et. al (1996), in a 70° delta wing, showed that the maximum L/D ration over the wing is obtained when a separated vortex is formed on the vortex flap and its spanwise length coincides with the vortex flap spanwise length.

The computer model used by Roberts and Arena (1994), was modified by Ize and Arena (1997a) to investigate the use of leading edge vortex flaps as a method to change

the spanwise camber of a 80° delta wing. Their investigation focused on the effects that spanwise camber has on delta wings in roll. Their results indicate that the effects of both the quasi-steady boundary condition as well as spanwise camber proportional to roll rate are similar in that both contribute to roll damping.

In another study conducted by Ize and Arena (1997b), the effect of leading-edge vortex flaps on roll moment of delta wings over a wide range of angle of attacks was explored. Leading edge flaps with conical planforms were mounted on flat plate delta wings of 65° and 80° sweep angles and deflected anti-symmetrically. Results indicate that for the 80° wing, asymmetric flap deflection increases the roll control effectiveness as angle of attack increases. For the 65° wing, the effectiveness is also a function of angle of attack, with significant decrease beyond a certain point.

1.3 Summary

As it can be seen, vortex flaps can be used in controlling a delta wing in roll, and can increase the lift/drag ratio, when used properly. However, there are some aspects of the vortex flaps that were not studied entirely. Some of these aspects are: **i)** Will the flaps be efficient when vortex breakdown is present? **ii)** How does Reynolds number affect the vortices over the wing with and without flaps? **iii)** How do the vortices change with the vortex flaps?

These are some of the questions that this work will try to answer.

1.4 Objectives of the Investigation

The motivation for the present work is to further investigate the effect that anti-symmetric leading edge flap deflection has on delta wings, and identify the physical phenomena associated with the roll control provided by LEVF's. Also determine how does Reynolds number affect flow separation and reattachment over the wings with and without flaps.

The investigation has been performed in a 80° and a 65° sweep angle delta wings, with LEVF's and conventional flaps at trailing edge (elevons). The wings have been subjected to an experimental study which includes:

- i) Measurement of the roll moments. (80° and 65° wings)
- ii) Static surface flow visualization of the delta wings (80° and 65° wings)
- iii) Measurement of the pressure distribution at one chord station on the top surface of the 80° wing with and without flap deflection.
- iv) Reynolds number effect in the roll moments and in the pressure distribution on the 80° wing with and without flap deflection.

The different types of measurements are correlated with each other to obtain a better understanding of the effects of LEVF's over the delta wings.

The effects of the LEVF's over the delta wings has also been investigated with a computational model. The model represents the separated flowfield above the wing as discrete system of two vortices in an inviscid flow. The position and strength of each vortex is captured by the formulation of specific boundary conditions. The model was also used to study the quasi-steady effects over the 80° wing.

CHAPTER II

EXPERIMENTAL APPARATUS

2.1 Wind Tunnel Facility

The experiments were conducted in the open circuit wind tunnel at the Oklahoma State University. The tunnel is powered by a 125 hp AC motor, which drives the flow through anti-turbulence screens, the contraction section, the interchangeable test section, and diffuser. The contraction cone at the inlet has a 15 to 1 contraction ratio. The diffuser section attaches to a 0.93 x 0.93 m cross section and is 2.81 m of long interchangeable test section. The test section diverges through an angle of 5.6° to a circular radius where the fan is located. A circular straw box consisting of drinking straws aligned with the flow was mounted between the diffuser and the fan to reduce atmospheric disturbance from outside. A pitot-static tube and an inclined manometer were used to measure the pressure inside the wind tunnel.

2.2 Delta Wings

Four delta wings were used for the investigation. Two with a 65° sweep angle and two with a 80° sweep angle. All were made out of 0.3175 cm thick aluminum, and the planform area were equal to 428 cm^2 for all wings. The wings had a 45° bevel at the bottom of the leading edge. Two of the wings had flaps on them. One 65° and one 80° wing had vortex flaps.

A sketch of the wings without flap deflection is shown in figure 2.1 and 2.2.

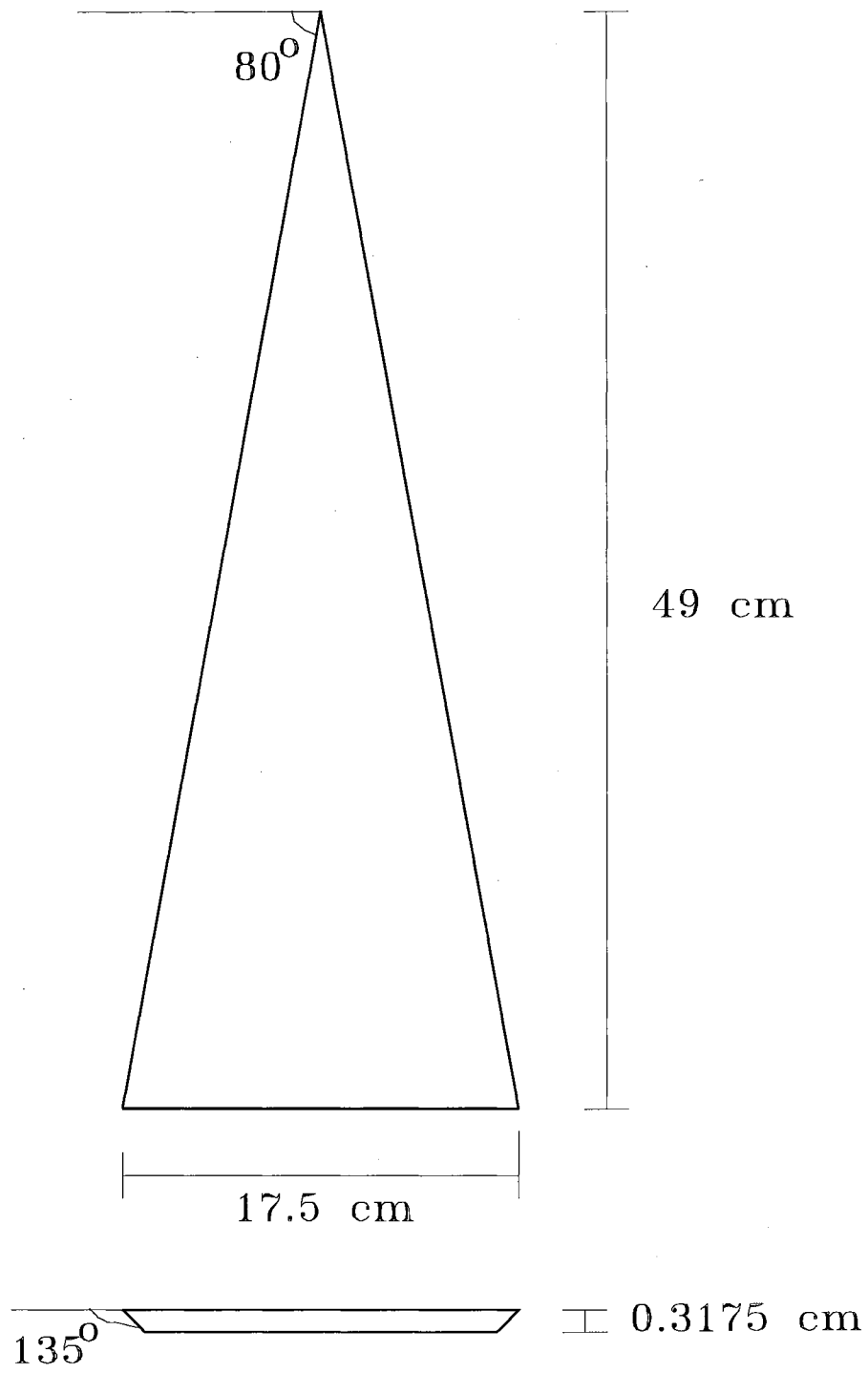


Figure 2.1. 80° sweep angle delta wing.

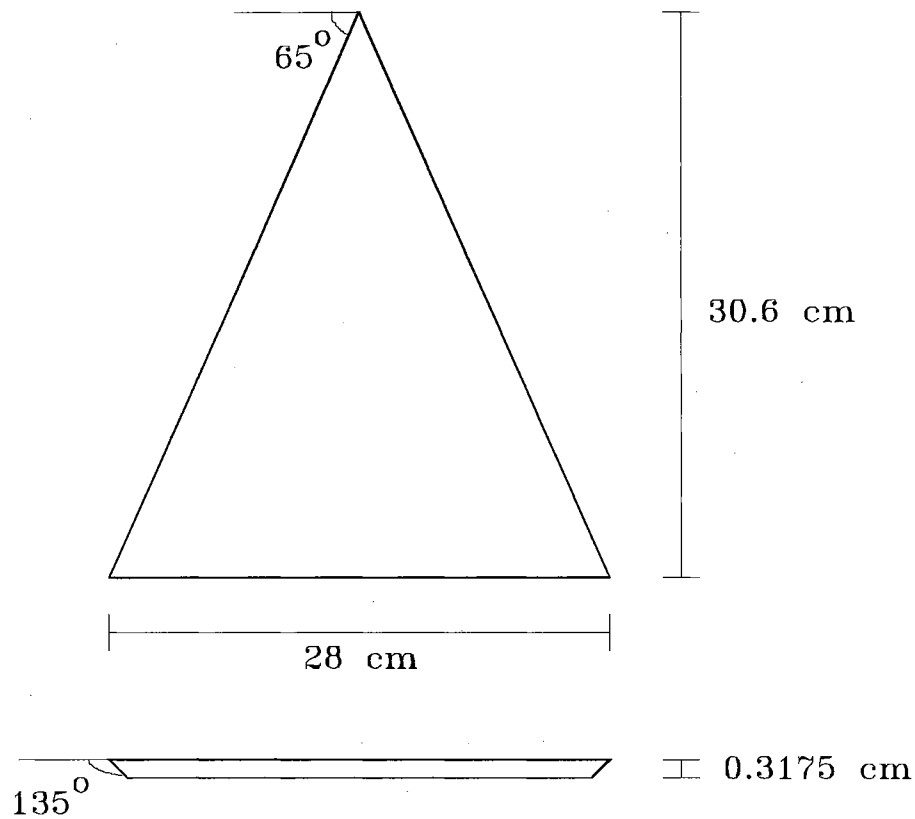


Figure 2.2. 65° sweep angle delta wing (not in scale).

The vortex flaps were cut at each chord station such that the flap span was 20% of the local span, yielding a conical planform. The flaps were set at $\delta=25^\circ$ anti-symmetrically with the left flap being downward and the right flap upward. A small groove was milled on each side of the wing so that the flaps could be deflected to the desired angle. A silicon sealant was used to close the gaps between the flaps and the wing. A sketch of the models with vortex flaps is shown in figures 2.3 and 2.4.

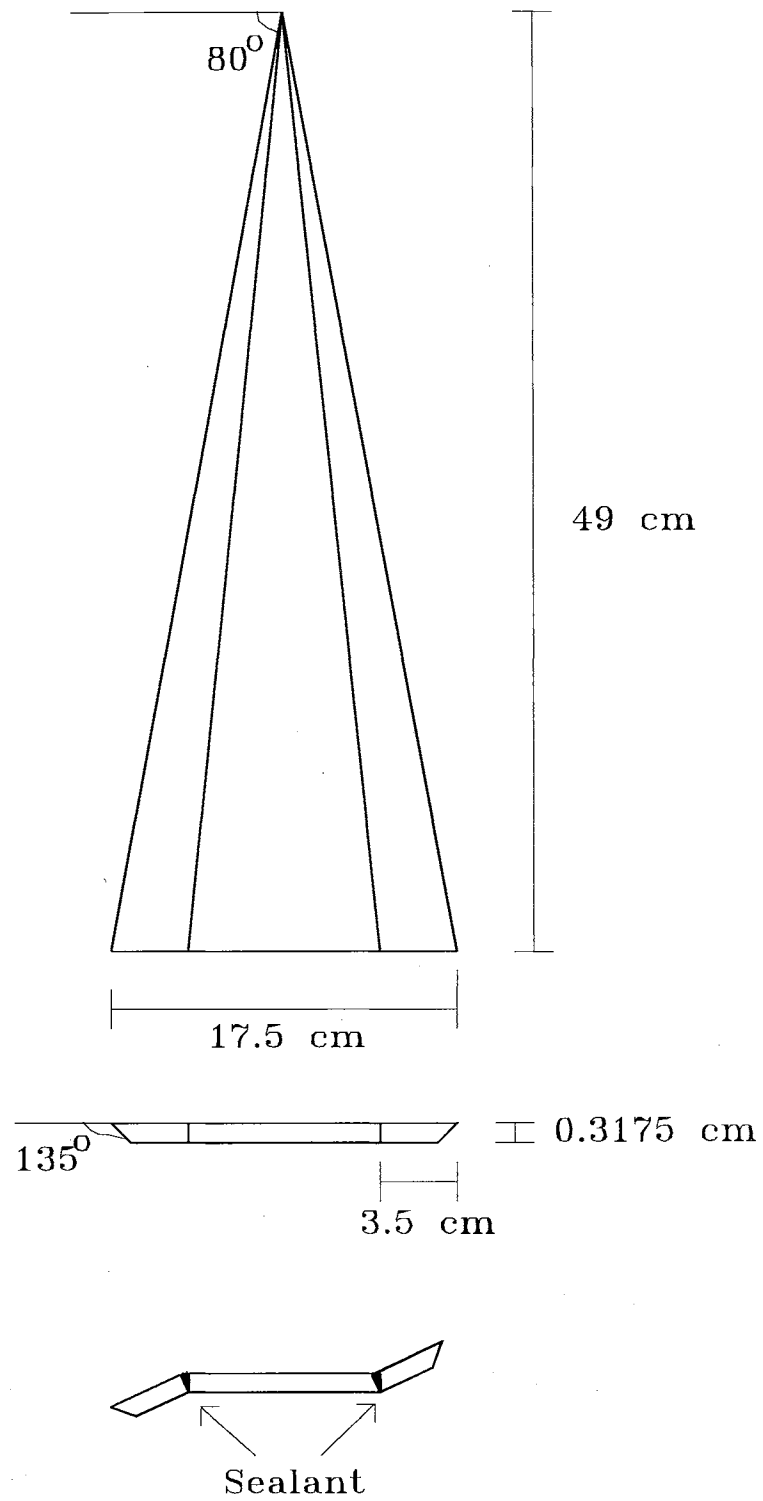


Figure 2.3. 80° sweep angle delta wing with 20% leading edge vortex flap.

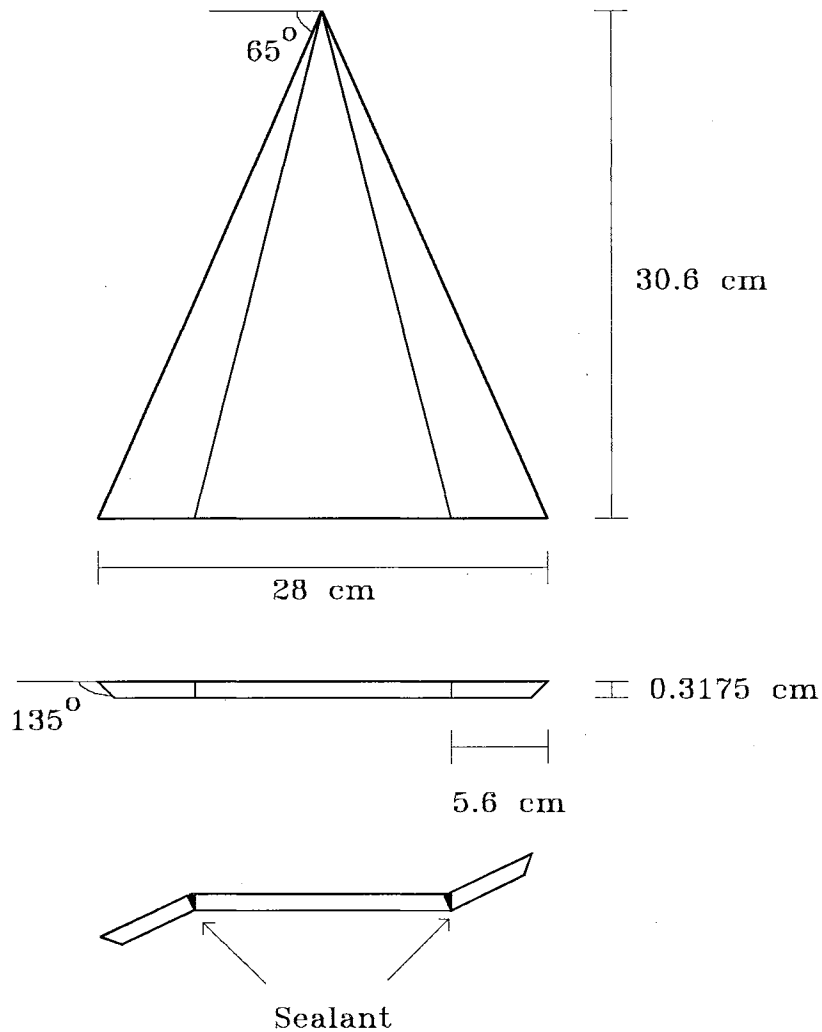


Figure 2.4. 65° sweep angle delta wing with 20% leading edge vortex flap.

In two different experiments, trip wires were placed on the top of the plain wings. The trip wires had a relative diameter of $D/s = 0.0053$, which is the same relative diameter used by Hummel (1978). For the 80° wing the trip wires were placed in two different locations. In one of the experiment, they were placed at half of the semi-span of the wing and at the chord of the wing, and on another experiment at 1/3 of the semi-span of the wing measured from the center of the wing and at the chord of the wing. The wing in figure 2.5, shows the trip wires at 1/3 of the semi-span from the center line of the wing.

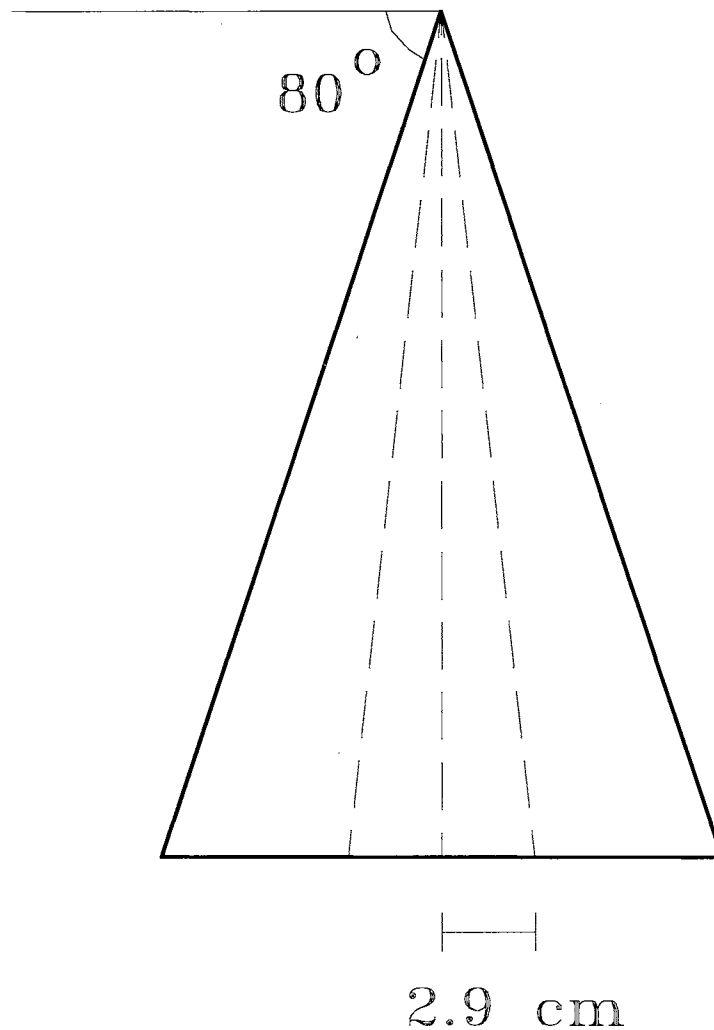


Figure 2.5. 80° sweep angle delta wing with trip wires.

On the 65° plain wing, the trip wires were placed on 1/2 of the semi-span and at the chord of the wing.

For the 80° wing with flaps, experiments were performed with the trip wires placed at 1/3 of the semi-span measured from the center of the wing and one at the center of the wing. There was no experiments performed with the 65° wing having asymmetric flap deflection and the trip wires.

2.3 Surface Pressure Distribution

To measure the pressure over the wings 4 rectangular grooves were machined into the top of the models to accommodate 0.238 cm square cross-section brass tubing. The tubes which lay in the spanwise grooves were cut in four parts. The spanwise tubes were placed at 75% chord station. This station was chosen because it allows a good spatial resolution in the pressure taps. The total number of taps on the plain 80° wing was 60, but only 32 were used. The pressure of the taps were taken in a cosine distribution, that means, a cosine distribution was performed on the 60 holes, and only the pressure on 32 of the total of holes was measured. The cosine distribution was used to reduce the number of data necessary to take, with sufficient resolution distribution over the wing. The method of cosine spacing distribution is frequently used to divide the chord of an airfoil into panels with larger density near the edges of the airfoil, where it is necessary to have a better resolution of the flow. Using this method to make the distribution of the pressure taps, gave a better resolution near the leading edge of the wing. There were 14 taps on each of the outer tubes and 16 on the inner tubes. On the 80° delta wing with flaps, there were 58 pressure taps, but again only 32 were used, using also cosine distribution. There were 11 on the flaps and 17 on the inner tubes. The tubes going to the trailing edge of the wing were round brass tubes of 1.5 mm internal diameter. The round tubes were glued on the square tubes with epoxy. The surface pressure model can be seen in figure 2.6.

The holes were drilled 2 mm apart, the closest holes to the leading edge of the wing was at 3 mm from it. The 4 chambers were independent of each other allowing the use of a scanning valve to measure the pressure on each array independently from each

other. The scanning valve was then connected to a Validyne D15 pressure transducer for data acquisition. Rubber tubes connected to the round brass tubes on the trailing edge of the wing were taped on the sting in order to reduce interference on the flow of the trailing edge of the wing.

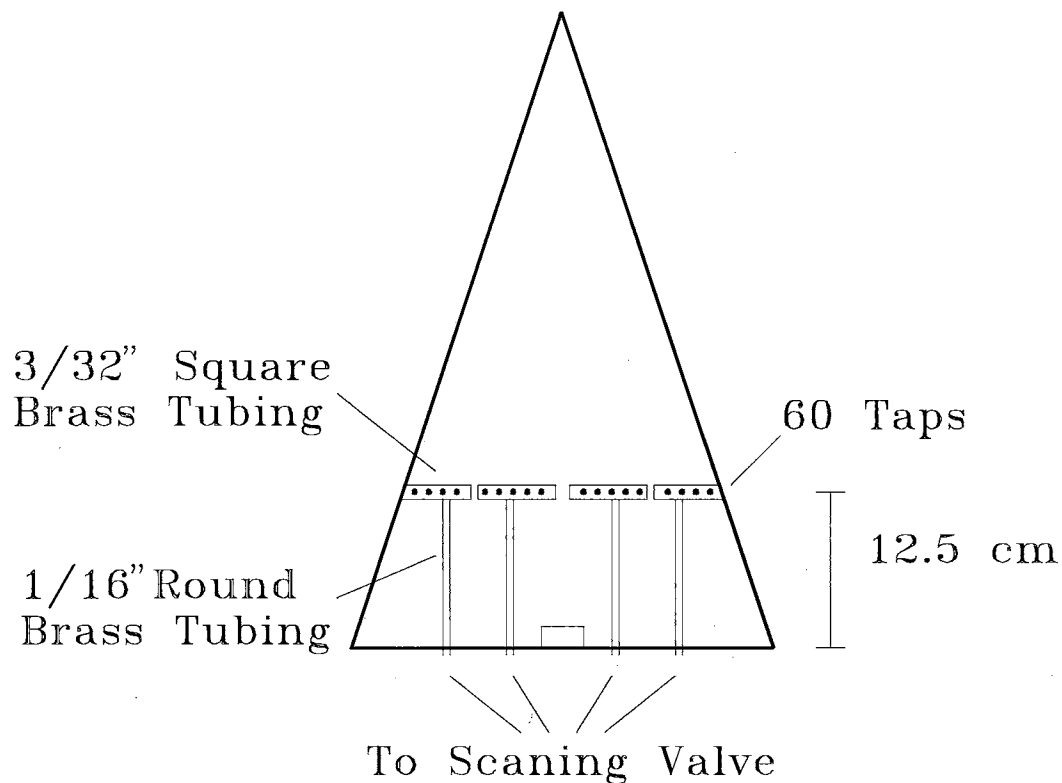


Figure 2.6 .Sketch of plain delta wing surface pressure model.

2.4 Torque Sensor

2.4.1 Mechanical Component

The torque sensor was a cruciform type, and was used to measure the roll moment of the wings. It was made out of 2 round pieces of aluminum with 4 strips of aluminum connecting the round pieces in a cruciform shape. The pieces are shown in figure 2.7.

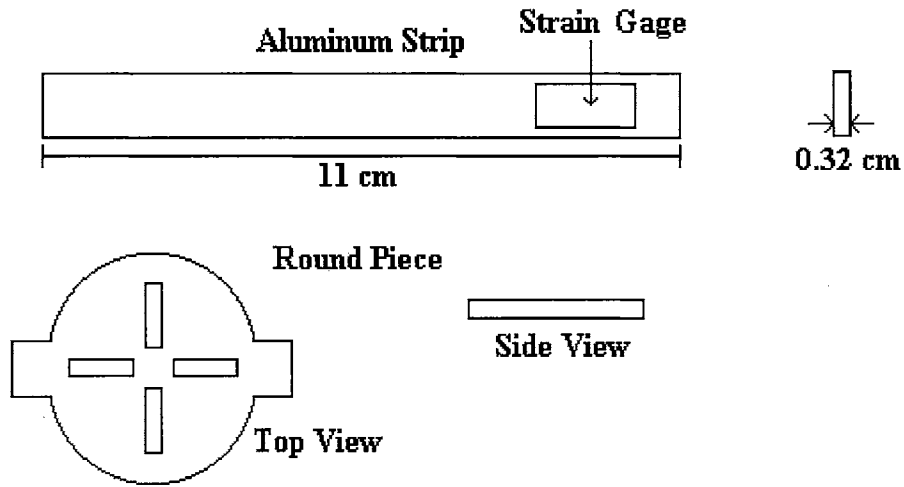


Figure 2.7. Round piece and stripe used to build the torque sensor.

To measure the torque, 4 strain gages were placed in 2 of the stripes, opposite to each other, creating a temperature compensated Wheatstone bridge. A complete step by step on how to built the torque sensor is shown in Appendix A. A sketch of the torque sensor is shown in figure 2.8.

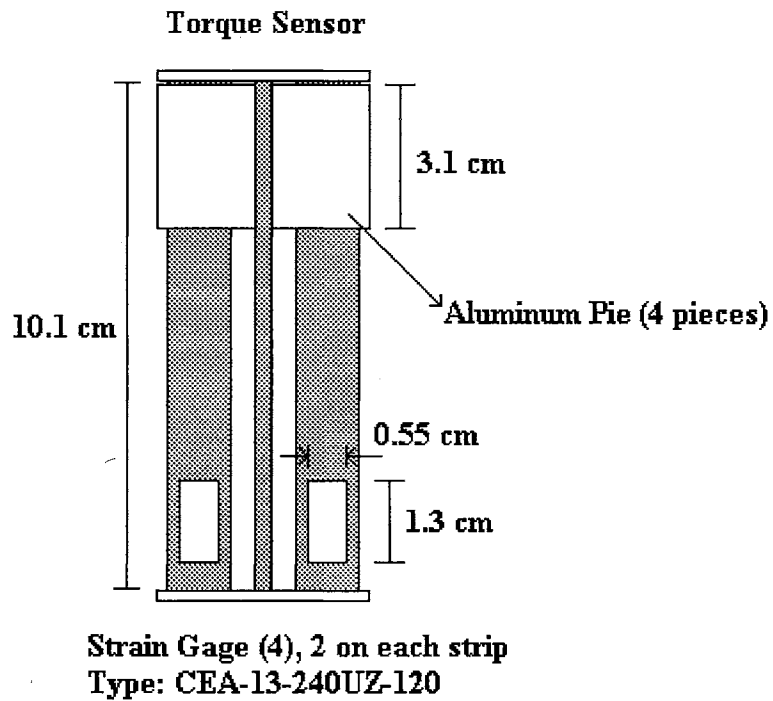


Figure 2.8. Torque sensor with the strain gages.

Due to high vibration of the torque sensor and fluttering at high angles of attack, a 2.5 cm diameter piece of solid cylinder, made of aluminum was cut in 4, and was placed at the upper part of the stripes.

Calibration was accomplished by placing the delta wing without flap deflection on the torque sensor, and than using known weights at a given moment arm. Checks were done periodically, to verify that the sensor was working properly. The wing and the sensor were sting mounted in a vertical support. The sting was long enough, so it would not interfere with the flow coming from the trailing edge of the delta wing. The diameter of the sting was smaller than the diameter of the toque sensor support, to avoid interference on the flow. The vertical support had a round slot, making it possible to change the angle of attack of the system easily, as shown in figure 2.9. The vertical support was then connect to the wind tunnel floor, parallel to the incoming flow.

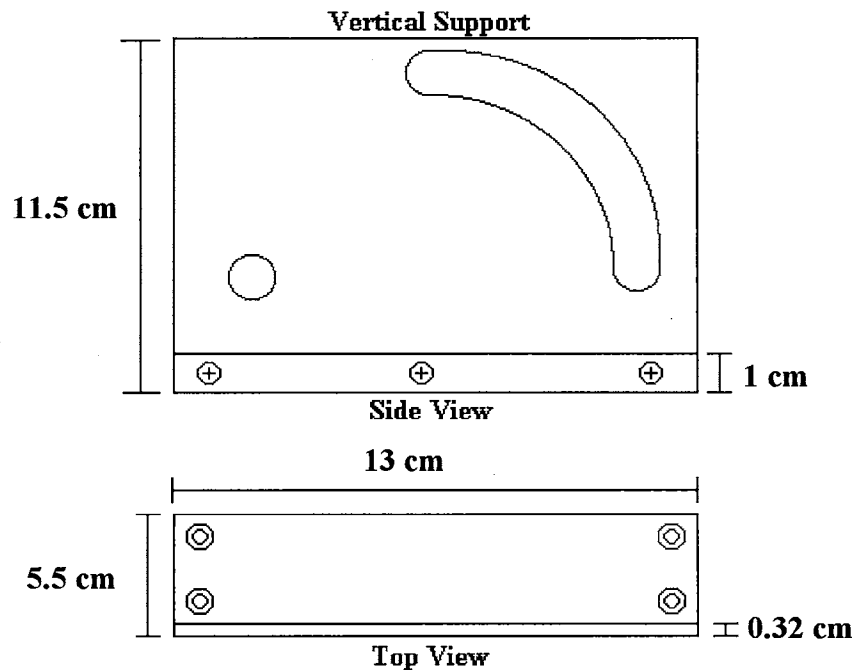


Figure 2.9. Vertical support of the sting.

The complete setup of the wing connected to the torque sensor is shown in figure 2.10.

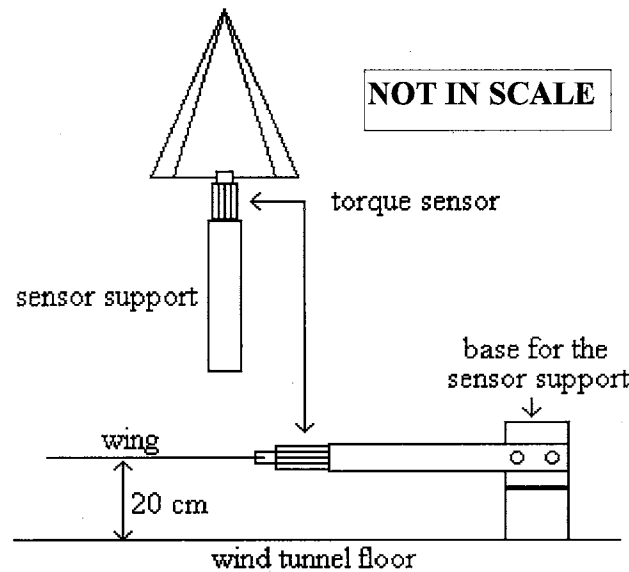


Figure 2.10. Setup for the static experiments.

2.4.2 Electronic Component

To determine the moment exerted on the gages, it was necessary to measure the output voltage from the Wheatstone bridge. The output voltage was too small to be measured directly. In order to be measurable, the voltage was amplified 680 times, using a simple amplifier circuit. Two 10 ohm, 20 turn potentiometers were placed in the system in order to be able to zero the voltage of the system. The electronic circuit of the system is shown in figure 2.11.

A variable power supply was used to supply the input voltage for the strain gages and the power for the amplifier. The input power for the amplifier was set at ± 11 Volts.

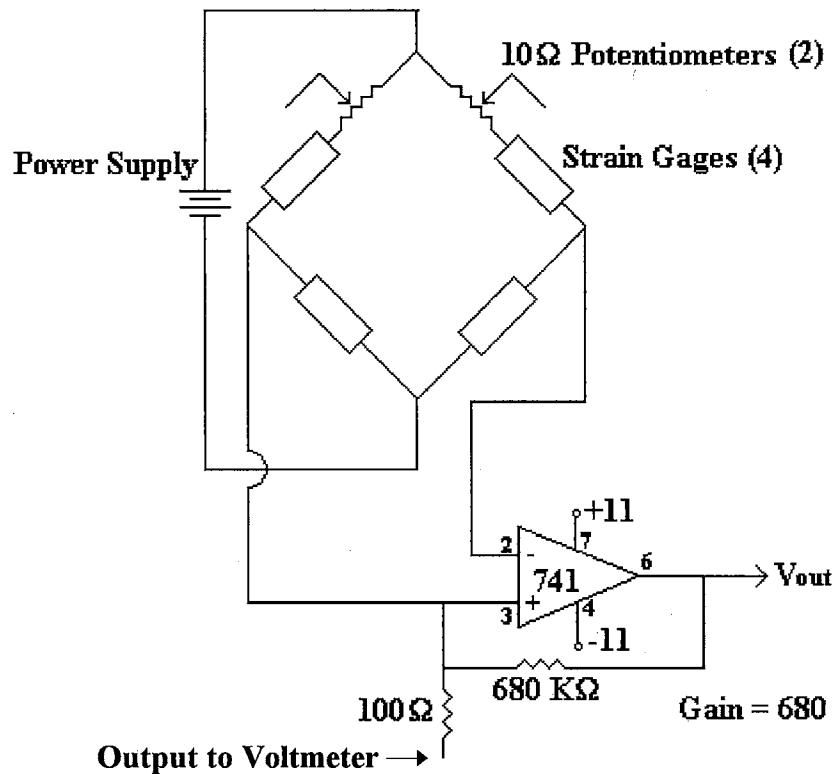


Figure 2.11. Electronic circuit of the strain gages and amplifier.

The input power to the gages from the power supply was set at +2.11 Volts and -1.76 Volts.

The amplified output voltage from the strain gages was read in 3 different places: i) directly from a voltmeter, ii) in an HP digital oscilloscope, and iii) using a data acquisition board, connect to a 386 PC based computer. The voltage used to plot all the graphics came from the data acquisition board. The board was set to take 1000 samples and average it, and keep taking the 1000 samples until the system was turned off. The oscilloscope was used to verify if there was any oscillation on the wing during the data acquisition phase that could start a fluttering on the torque sensor and the wing and

damage the system. The voltmeter was used just to compare the voltage with the one given by the data acquisition board. The setup of the moment acquisition system is shown in figure 2.12.

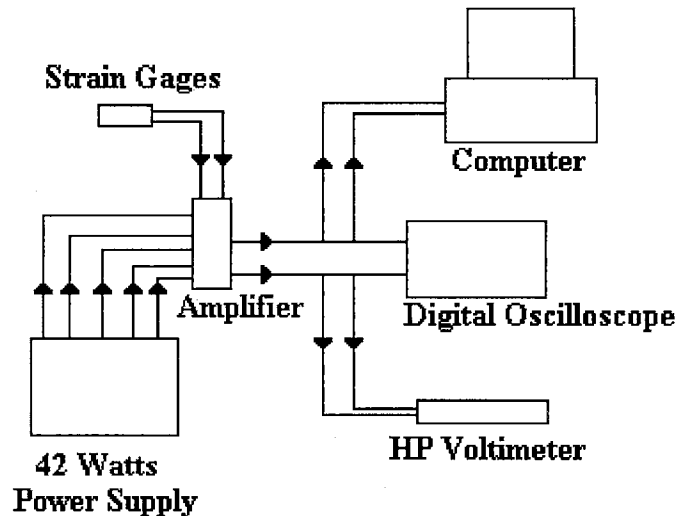


Figure 2.12. Setup of the moment acquisition system.

A program in C, shown in the Appendix B, was written to acquire the output voltage from the torque sensor. This voltage was shown on the screen during the entire experiment, making it possible to see any unusual changes on the system.

2.5 Surface Oil Apparatus

The apparatus used for surface oil visualization consisted simply of the surface oil, a foam brush, and a 35 mm camera. The surface oil was a mixture of fifteen parts of kerosene, five parts of TiO_2 powder (Titanium Dioxide), and one part of Oleic Acid. Flood lamps were used to illuminate the model to obtain good lighting for the camera.

2.6 Free to Roll Apparatus

The free to roll system consisted of two small bearings placed at each end of a plastic tube, that worked as a sleeve, with a steel shaft going through it, as shown in figure 2.13.

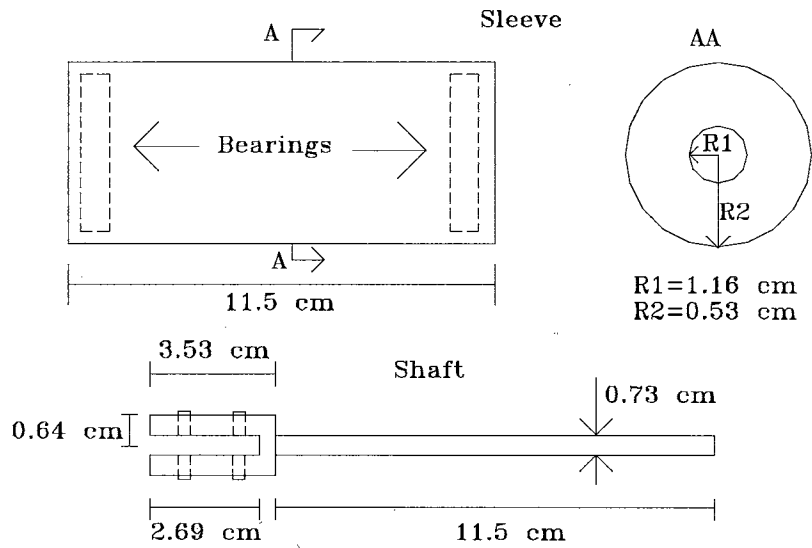


Figure 2.13. Primary parts of the free to roll system.

The system was press fit inside a steel tube, and the tube was then attached to the same vertical support shown in figure 2.9. The vertical support was attached to a horizontal plate that was then attached to the floor of the wind tunnel. The complete setup of the system is shown in figure 2.14.

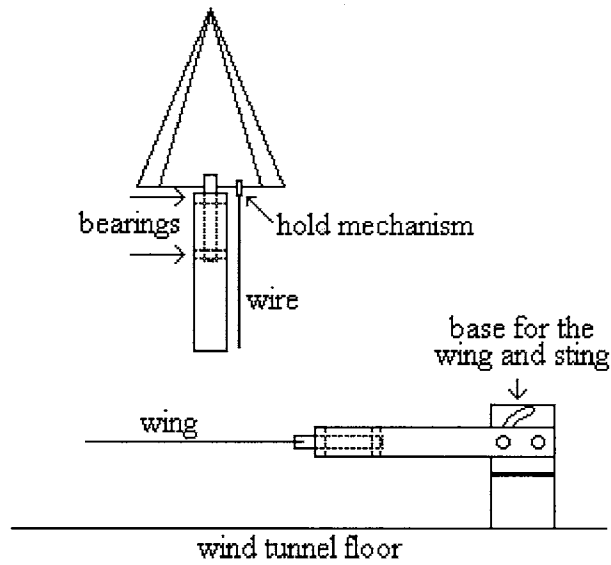


Figure 2.14. System connected to the wind tunnel floor.

The wings were held at the shaft by 4 set screws, in order to adjust the wing in pitch and yaw directions, and align it with relation to the shaft and the flow of the air, as shown in figures 2.15 and 2.16.

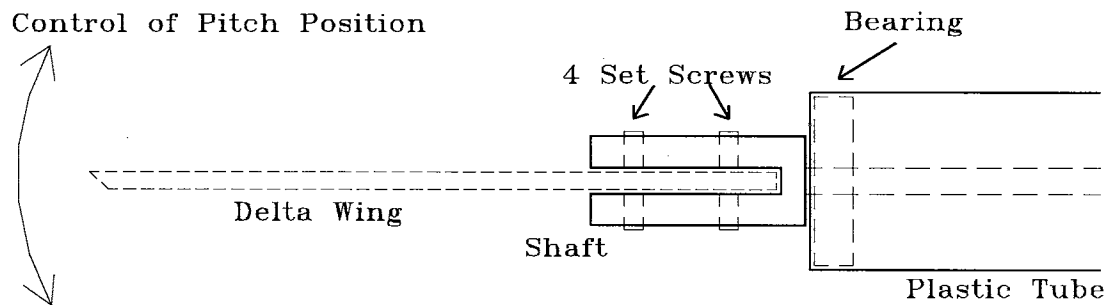


Figure 2.15. Control of the pitch position of the delta wings.

Control of Yaw Position

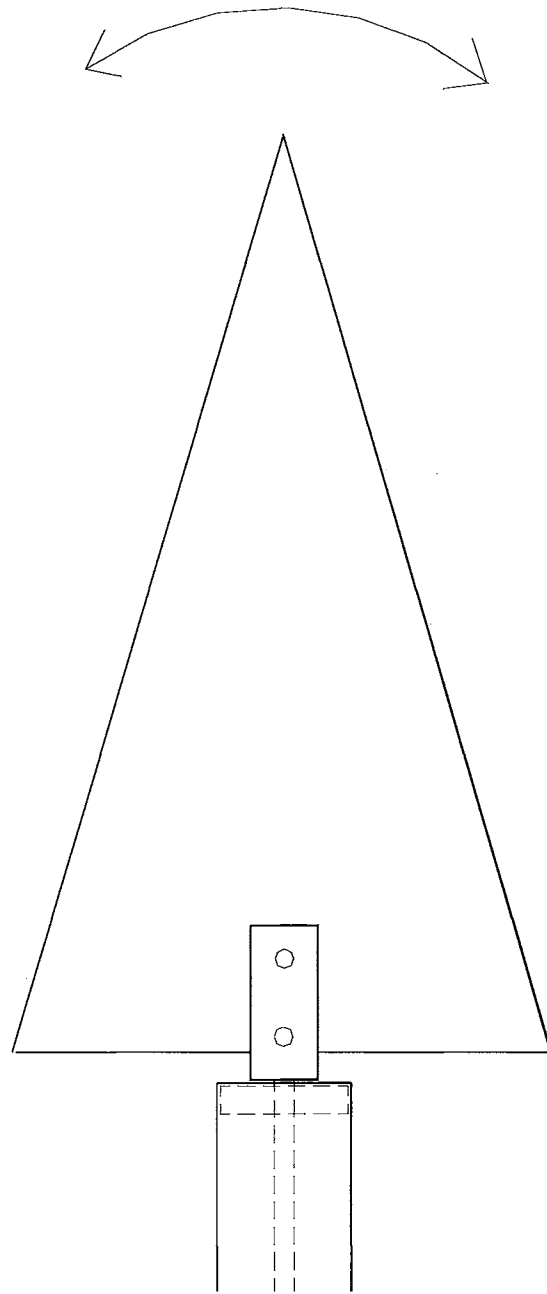


Figure 2.16. Control of the yaw position of the delta wings.

CHAPTER III

COMPUTATIONAL MODEL

3.1 Flow Model

The computational analysis for this study was performed using a modified inviscid model developed by Arena and Nelson. It was shown that the essential characteristics of the unsteady delta wing can be captured by modeling only the primary flow characteristics. The solution to the present model is obtained by using a panel technique where the body geometry is represented by a distribution of constant strength sources and vortices. The model assumes that the flowfield is incompressible, inviscid and unsteady. The governing equation of the flowfield is then

$$\nabla^2 \Phi = 0 \quad (3.1)$$

The model also assumes that the wing is a slender body. The slender wing assumption states that gradients with respect to the x direction are negligible compared to y and z directions in the crossflow plane.

To obtain the solution to the 2D Laplace's equation for flow on a body, boundary conditions must be stipulated on the boundary itself and in the far field at infinity. The boundary condition on the boundary is such that the flow must be tangent to the surface of the body. The far field boundary condition states that the perturbation velocity in the flow field must be zero at infinity. Stated another way, the total potential of the flowfield at infinity must be equal to the potential of the freestream itself.

On the surface of the body

$$\nabla\Phi \cdot n = V_n \quad (3.2)$$

In the far field at infinity,

$$\nabla\Phi = q_\infty \sin\alpha \quad (3.3)$$

The original model assumes conical flow over a slender wing which implies that all cross sections of the flow over the wing are the same, varying only by a linear scaling factor. Allowing the wing to undergo unsteady rolling motions requires the solution of unsteady boundary and zero-force conditions, and the transfer of inertial coordinates into a body fixed frame. As for the boundary conditions, the far field boundary condition will be automatically satisfied by using singularity solutions that satisfy the boundary condition. The tangential flow boundary condition is imposed by developing a set of linear equations which specify the normal flow on the body to be zero. A diagram of the model is shown in figure 3.1.

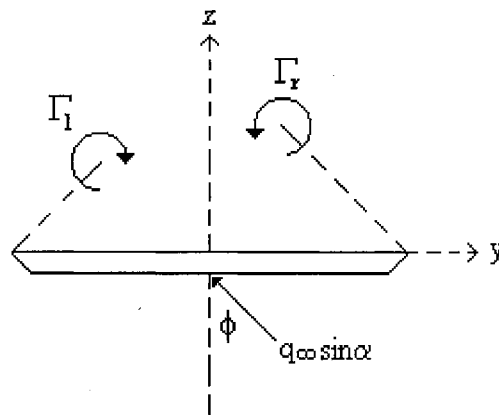


Figure 3.1. Crossflow delta wing model.

The code also assumes an inviscid, incompressible, unsteady model by using potential vortices to model the leading edge vortices. The time dependent aerodynamics

solution is coupled to a single-degree-of-freedom dynamics solver such that the solution is marched in time.

The quasi-steady aerodynamic calculations are accomplished by fixing the wing at a given roll angle, and applying the roll rate boundary condition. This is accomplished over a range of roll angles and roll rates consistent with the time history obtained during wing rock simulation. The effect of the roll rate applied to the static delta wing as a boundary condition is shown in figure 3.2.

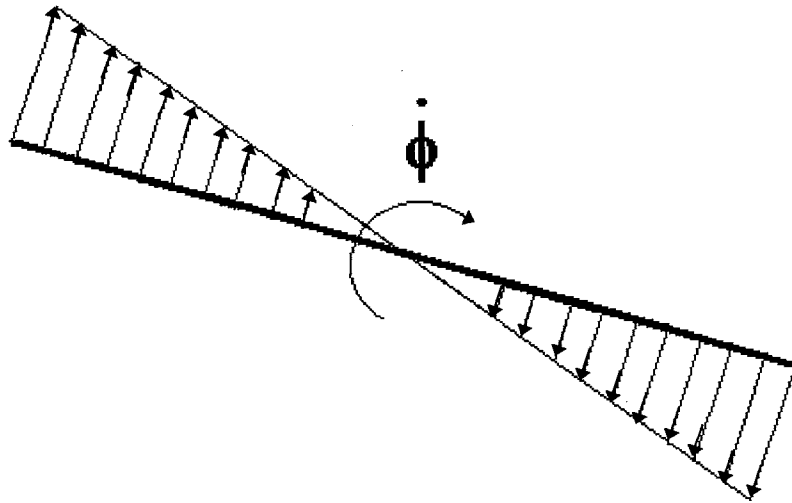


Figure 3.2. The roll rate boundary condition.

The program was then modified, allowing the use of the leading edges of the wing to model vortex flaps. The vortex flaps modify the characteristics of the separation and therefore the primary vortex position and strength. Since the model was developed using a conical assumption, the flaps must also be conical along the entire leading edge, to comply with the primary model assumption.

The implementation of the flaps using panel methods is shown in figure 3.3.

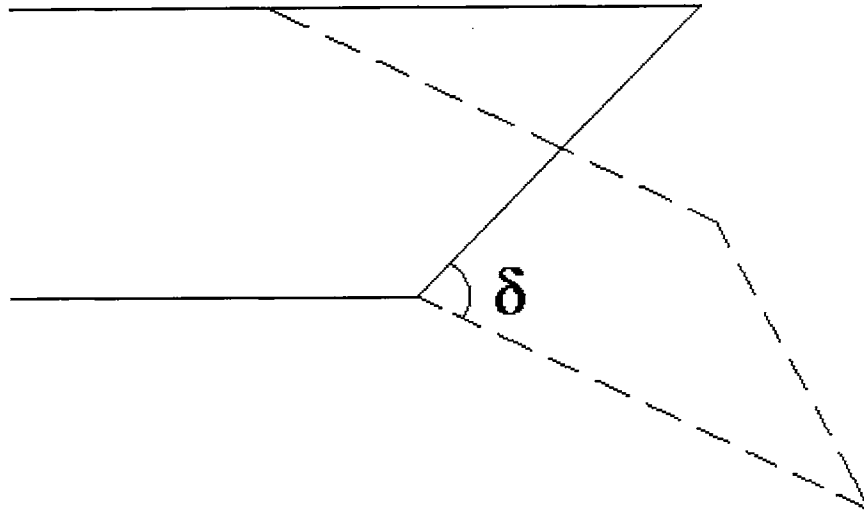


Figure 3.3. Geometry of the leading edge vortex flap.

The bevel of the delta wing is rotated about its lower corner, while the connecting panel stretches to close the shape of the delta wing body. This implementation represents the leading edge flap deflection. Flap deflection angles are calculated during the coupled solution, such that any practical deflection strategy may be assessed.

3.2 Energy Exchange Concept

A useful tool which has been used in analyzing wing rock is the concept of energy exchange, presented by Nguyen, Yip and Chambers (1981). It can be shown that the total energy exchanged between the wing and the fluid, during one free-to-roll cycle is given by

$$\Delta E = qSb \int_{t_1}^{t_2} C_l \dot{\phi}(t) dt \quad (3.4)$$

It can be shown that the net energy exchanged in a cycle is directly proportional to the areas of the loops of the graph of C_1 vs. ϕ , shown in figure 3.4.

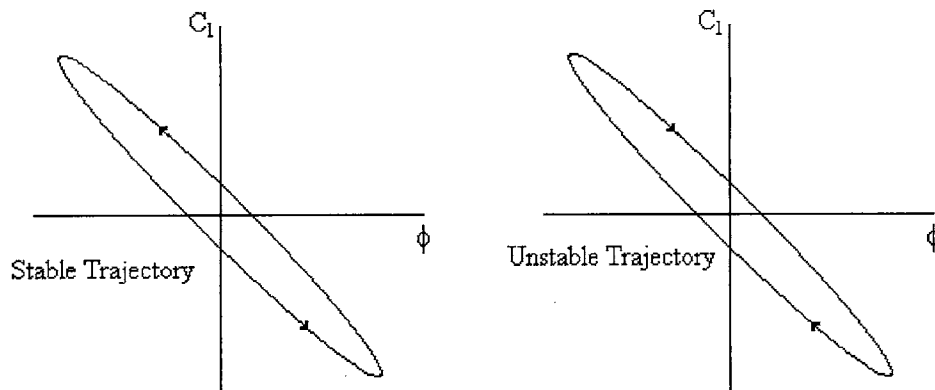


Figure 3.4 Conceptual stable and unstable roll moment trajectories.

The direction of the loop determines whether the system is gaining or losing energy. If $\Delta E < 0$, the system is losing energy to the fluid, (damping), and if $\Delta E > 0$, the system is gaining energy from the fluid, (negative damping). $\Delta E = 0$ means that there is no net energy exchange and the system is in equilibrium. A theoretical depiction of a limit cycle moment diagram can be seen in figure 3.5.

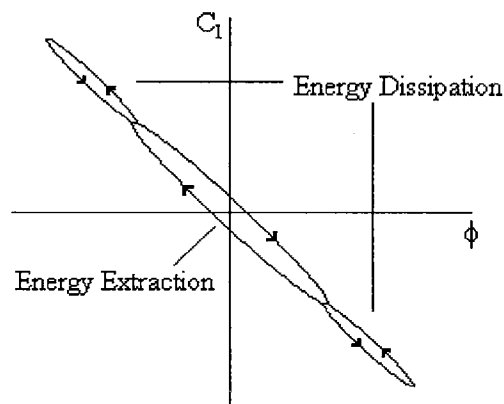


Figure 3.5. Conceptual sketch of limit cycle roll moment diagram.

For a limit cycle to exist, the area inside the clockwise loop must equal the sum to the areas inside the counterclockwise loops.

Experimental and computational studies made by Arena and Nelson (1990, 1991, 1994) indicate that after wing rock is initiated by some initial perturbation, the amplitude of the motion grows in time due to the instability created by a lag in the position of the leading edge vortices, until the damping contributions balance the instability and result in an equilibrium oscillation. The greater the damping contribution to roll moment, the lower the oscillation amplitude and vice versa. The nonlinear damping contribution from the top surface of the wing creates the damping lobes necessary to keep the motion from diverging and appears to be due to the unsteady behavior of leading edge vortex strength.

CHAPTER IV

COMPUTATIONAL RESULTS AND DISCUSSION

4.1 Model Validation

Before being used in the present investigation, the computational model was validated extensively. Static and dynamic tests were conducted and compared with experimental data obtained by Arena (1992). The model predicted the limit cycle oscillation qualitatively and quantitatively, as well as captured the dominant flowfield mechanisms observed in experiment. Representative validation results are presented here. Further discussion of validation runs may be obtained in Arena and Roberts (1994).

It is important to note that vortex breakdown on the wing is not necessary for wing rock limit cycle oscillation to occur. Since the model does not account for vortex breakdown, the dynamic model cannot accurately predict wing rock amplitudes when breakdown is affecting the flowfield. This limits the model to angles of attack less than approximately 33° for an 80° delta wing.

All of the data in the present investigation is presented for the 80° delta wing for which a significant experimental test base is available. An example of a wing rock time history obtained experimentally for an 80° swept delta wing at 30° angle of attack may be seen in figure 4.1.

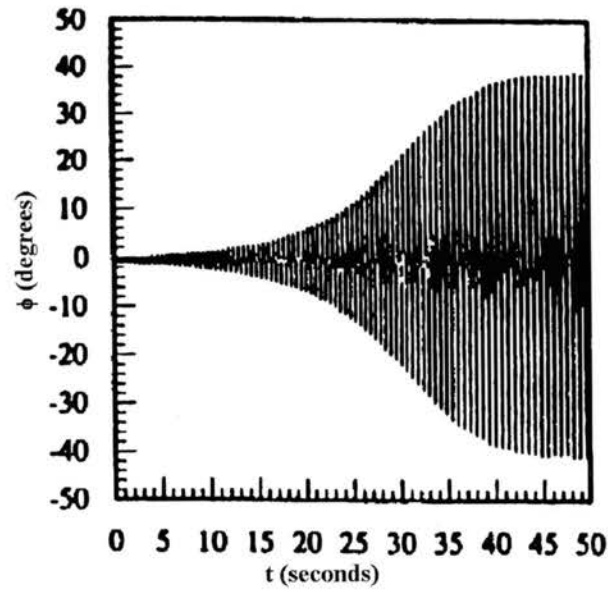


Figure 4.1. Experimental wing rock time history (Arena 1992).

The predicted time history using the computational model can be seen in figure

4.2.

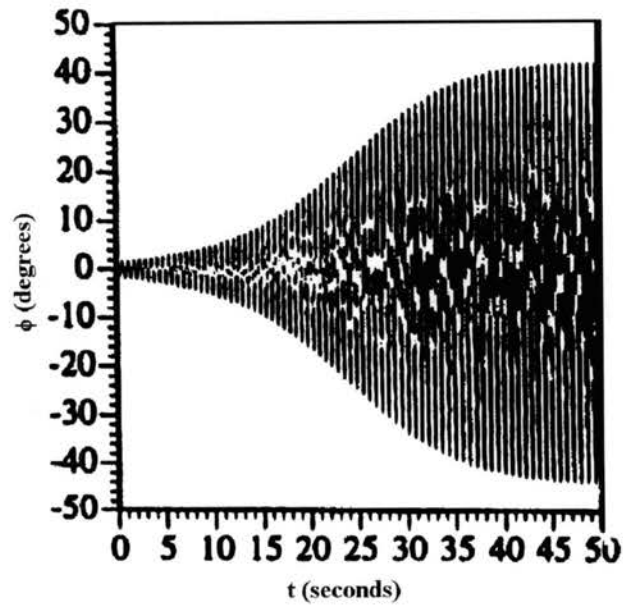


Figure 4.2. Computational wing rock time history (Roberts and Arena 1994).

The envelope of angle of attack showing the amplitude wing rock oscillations is shown in figure 4.3.

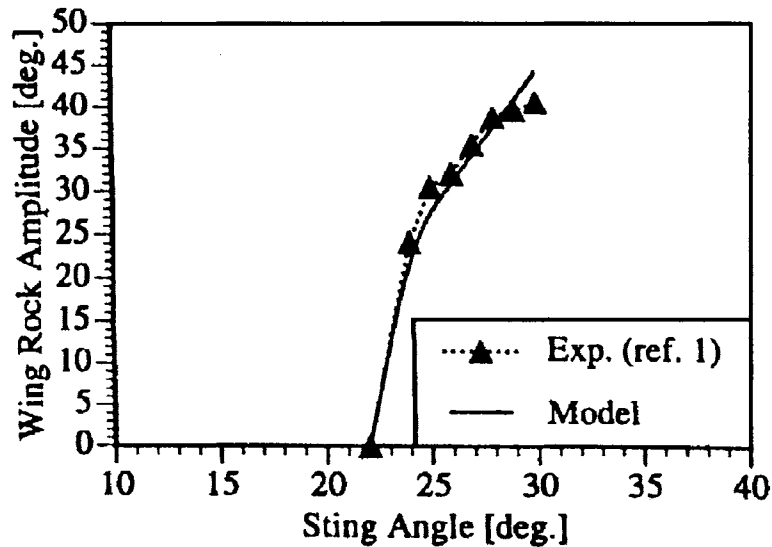


Figure 4.3. Wing rock envelope (Arena 1992).

Experiment and the computational model are in good agreement with both predicting wing rock beginning at approximately 22° for the 80° wing.

Values of time, roll angle, roll rate and roll moment coefficient and flowfield characteristics were obtained, and stored during the simulation of the model. A complete cycle at the steady state amplitude was then selected and the roll moment diagram was plotted, as shown in figure 4.4.

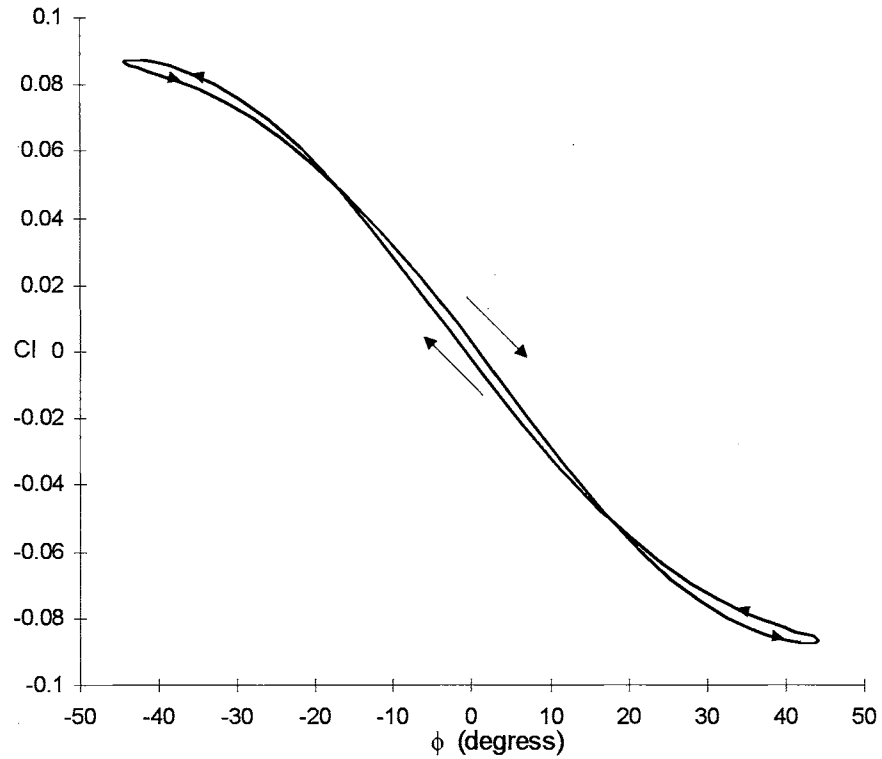


Figure 4.4. Calculated roll moment vs. roll angle.

The plot shows the characteristic loops correspondent to the limit cycle of wing rock. The two counterclockwise damping loops and the inner clockwise loop. Good agreement is observed between the model and experiment, shown in figure 4.5.

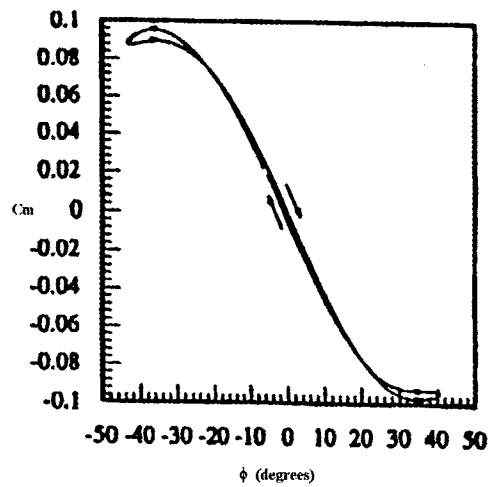


Figure 4.5. Roll moment vs. roll angle from experiment (Arena 1992).

By comparing the results from the model and experiment, it can be determined that the model is able to capture the major aspects of wing rock which lends confidence in further use of the model as a tool for investigating other aspects of the wing rock motion including quasi-steady effects, and spanwise camber changes.

4.2 Quasi-Steady Effect

Utilizing the roll angle and roll rate information during wing rock, quasi-steady runs were accomplished as discussed in the methodology. Figure 4.6 is a plot of the unsteady, and the quasi-steady roll moment vs. roll angle.

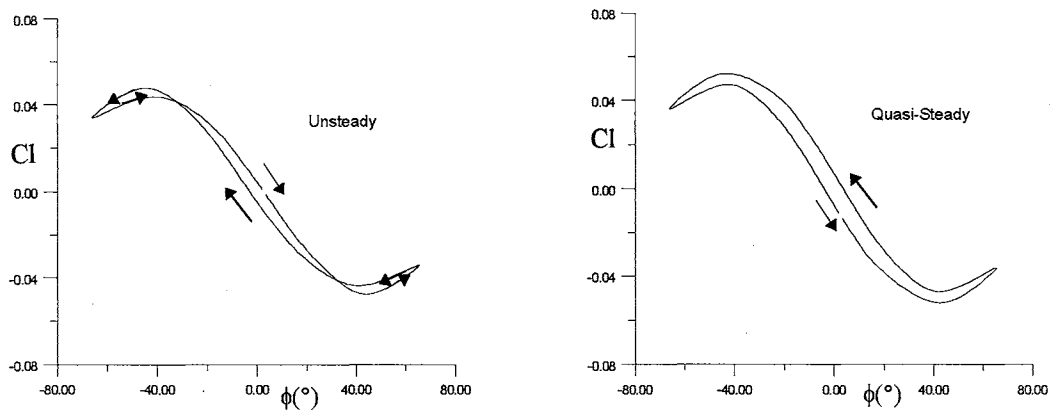


Figure 4.6. Unsteady and quasi-steady roll moment coefficient vs. roll angle.

Unlike the unsteady equivalent, there is only one direction with regard to the hysteresis for the quasi-steady plot. The entire plot is in the counterclockwise direction. This is significant in that it is clear from the sense of the loop that quasi-steady effects alone cannot sustain wing rock. Since it is the clockwise loop that is indicative of a destabilizing or unstable system, this system clearly cannot undergo wing rock, and has damping only.

A plot for the variation of the spanwise position of the vortices, for the unsteady and quasi-steady effects is shown in figure 4.7.

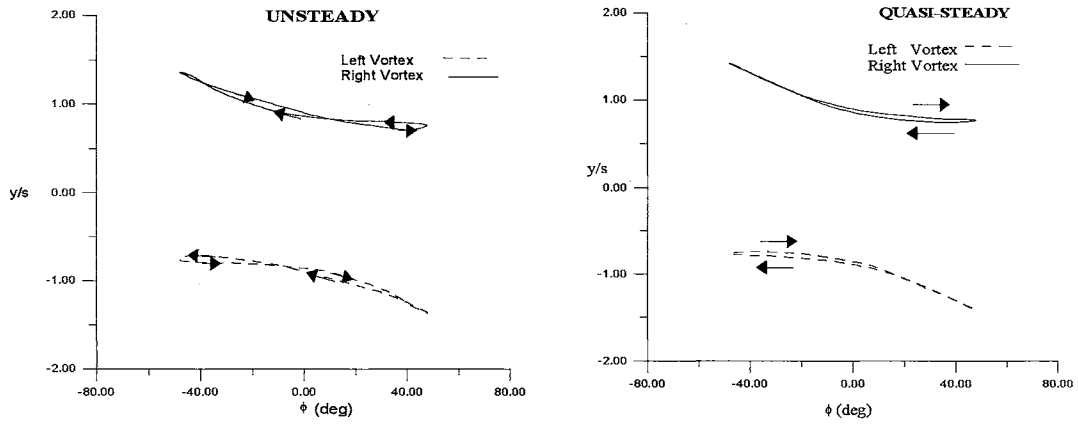


Figure 4.7. Spanwise vortex position for the unsteady and quasi-steady runs.

For the spanwise vortex position there is very little variation between the unsteady and quasi-steady runs. Quasi-steady effects do not significantly effect change spanwise vortex position. This was expected, since there is little hysteresis in spanwise vortex position during wing rock.

The variation of the normal position of the vortices, for the unsteady and quasi-steady effects is shown in figure 4.8.

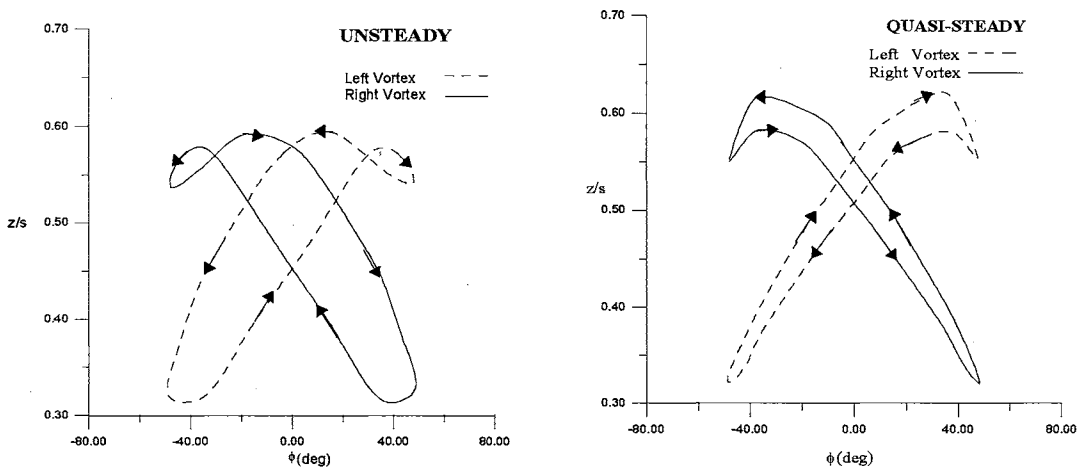


Figure 4.8. Normal vortex position for the unsteady and quasi-steady runs.

The normal vortex position data show that there is a significant difference between the unsteady and quasi-steady hysteresis behavior. It can be seen that the direction of the hysteresis for the quasi-steady runs is opposite to that observed during wing rock.

The behavior of vortex strength for the quasi-steady and unsteady runs is shown in figure 4.9.

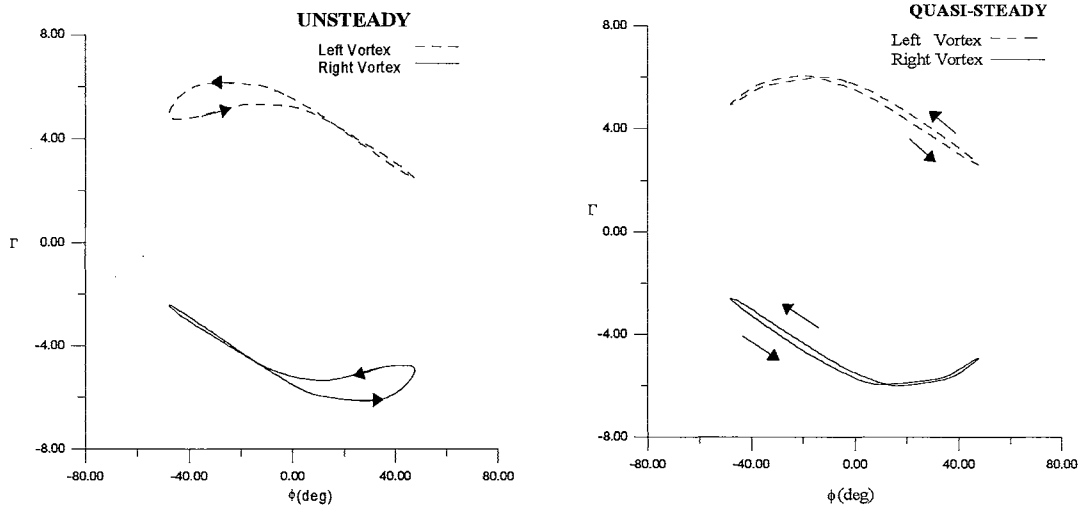


Figure 4.9. Vortex strength for the unsteady and quasi-steady runs.

As discussed previously, the apparent effect of the vortex strength hysteresis during wing rock is to generate the damping lobes necessary to limit the oscillation and produce a limit cycle. As can be seen in the figure, the direction of the hysteresis is the same, however, the magnitude of the hysteresis is reduced.

The results observed in the vortex position data are significant in that they suggest a rationale for the hysteresis behavior observed in the quasi-steady simulations. In the quasi-steady case, the hysteresis in vortex position normal to the wing is opposite to that observed in the unsteady case, which suggests that the hysteresis in the normal vortex position is due to a convective time lag. This is important because it indicates that the

instability causing wing rock is caused primarily by unsteady effects. The quasi-steady boundary condition can only generate a damping contribution to the motion.

4.3 Spanwise Camber Effects

In a previous study by Roberts and Arena (1994) steady and unsteady effects of asymmetric leading edge flap deflections on the 80° wing were discussed. In the present effort, flaps are activated in an anti-symmetric sense, proportional to roll rate.

The effect of the flap deflections on the wing rock oscillation, can be seen in figure 4.10.

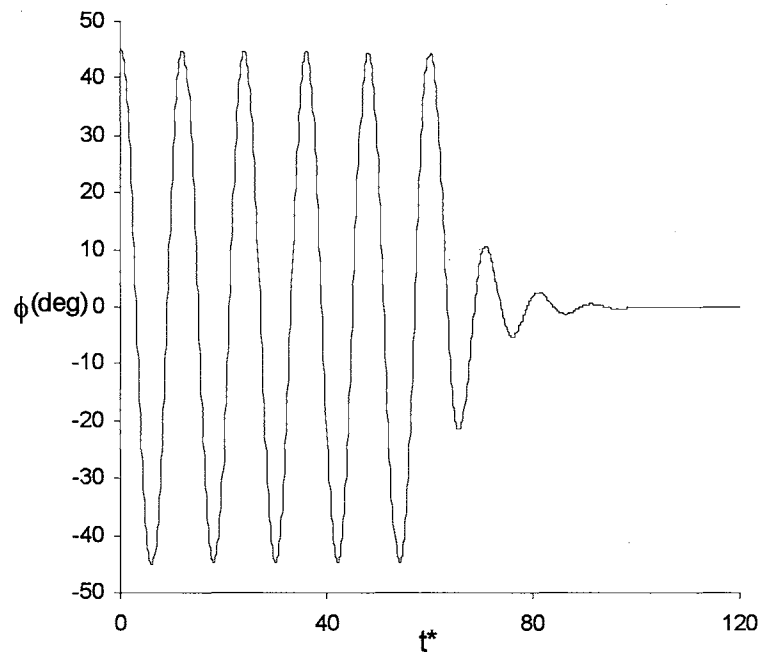


Figure 4.10. Roll moment time history, when flaps are activated.

Several cycles of steady state wing rock are shown prior to flap activation. Anti-

symmetric flap activation proportional to roll rate occurs at a nondimensional time of approximately 50, as shown in figure 4.11, after which the motion rapidly decays.

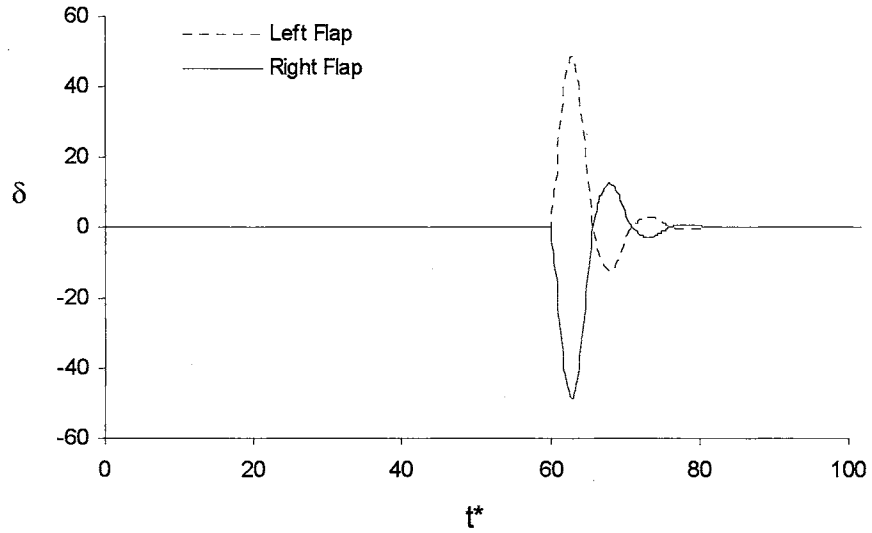


Figure 4.11. Flap deflection time history.

The behavior of the moment hysteresis for this time history may be seen in figure 4.12.

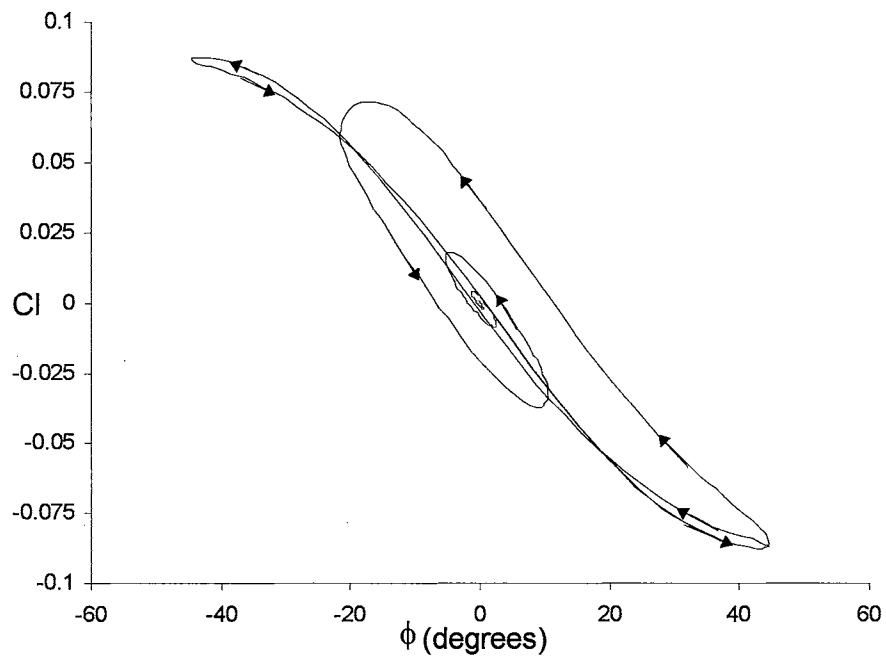


Figure 4.12. Damping effect of roll moment of wing rock control.

During the cycle of the wing rock oscillation before control is turned on, the cycle still exhibits the three major hysteresis loops as seen in figure 3.5, indicating that the limit cycle motion has reached steady state. When control is turned on, the roll moment rapidly decreases in a counter clockwise spiral toward zero moment indicating the significant damping contribution added by the flap activation.

An explanation for the resulting damping after flap activation may be seen in figure 4.13 which is a plot of the position of a vortex for the time history.

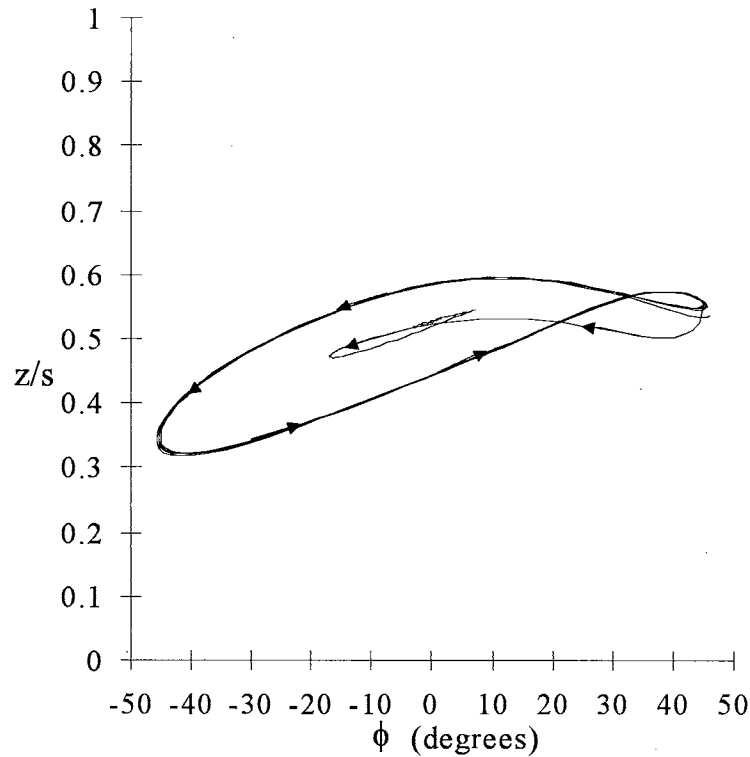


Figure 4.13. Normal vortex position during control of wing rock.

The left vortex only is shown for clarity. During wing rock, the large time lag which was discussed previously is observed. After the flaps are activated, the lag is quickly eliminated. The ability to mitigate the lag in vortex position, may also be observed through a forced oscillation in roll while flaps are activated proportional to roll rate.

The variation of spanwise camber due to the flaps which results in a damping of the wing rock motion should be noted. As seen in figure 4.11, the flap on the downward going wing is deflected downward, and vice-versa on the upward going wing.

CHAPTER V

EXPERIMENTAL PROCEDURE

5.1 Rational for Experimental Approach

The primary goal of the experimental investigation was to determine the effects that asymmetric deflection of the vortex flaps have on the flow over slender delta wings. This has been accomplished by studying the flow over a 80° and a 65° leading edge sweep delta wing. The 80° wing was chosen because it undergoes wing rock at high angles of attack, and the 65° was chosen because it does not undergo wing rock at any angle of attack. There is also a large amount of data related to the 65° sweep wing, that can be used to compare with the results obtained in this investigation. It was possible to compare the difference in behavior between the two wings. The 65° wing also has a characteristic that vortex breakdown starts at the trailing edge of the wing at approximately 20° angle of attack, while for the 80° wing it starts at angles of attack higher than 35° (Wentz and Kohlman 1971).

Ideally the Reynolds number for all the experiments should be the same and be on the order of 10^6 to assure a real simulation. Unfortunately the torque sensor had some limitations which made it difficult to maintain the same Reynolds numbers for both wings. Due to the way the torque sensor was constructed, the maximum dynamic pressure that could be applied to it, with the 80° wing was 249 Pa. A higher pressure would make the 80° wing to start to flutter when placed at 30° angle of attack. The stress would be so high that the sensor would have broken. Therefore different Reynolds number were used for the wings.

In order to determine the roll moment of the wings, a torque sensor in a cruciform format was built. The torque sensor was built to measure the torque generated by the wings when placed at different positions. The sensor was built in such a way to minimize the pitch moment and the yaw moment generated by the wings when they were being tested.

Surface pressure distribution is the means by which the flowfield generates roll moments, for this reason measurements of the surface pressure were performed for the 80° delta wing. The measurements were performed for different angles of attack and different roll angles, to complement the information given by roll moment data.

Since the characteristics of the flow over the wings change when the flaps are deflected, a simple free to roll apparatus was built to qualitatively investigate the motion of the wings when the flaps were deflected.

Surface flow visualization was also performed to investigate the effects that the trip wires have on the boundary layer and the flow over the wings.

5.2 List of Experiments Conducted

The experiments in the investigation were conducted using the 80° and the 65° wings with no flaps, and the wings with asymmetric leading edge flap deflection. Reynolds number was 700,000 for the 80° wing and 403,000 for the 65° wings. The experiments conducted until now are shown in tables 1 and 2:

1) Measurement of the roll moment:

		Plain Wing		Flapped Wing		Flapped Wing
		With and Without TW		Without TW		With TW
		$\Lambda=65^\circ$	$\Lambda=80^\circ$	$\Lambda=65^\circ$	$\Lambda=80^\circ$	$\Lambda=80^\circ$
$\alpha \backslash \phi$		-40° to 40° with 10° increment		0°		0°
10°		YES	YES	NO	NO	NO
15°		YES	NO	NO	NO	NO
30°		NO	YES	NO	NO	NO
-2° to 30° with 2° increment		NO	NO	YES	YES	YES

Table 1. Roll moment measurements.

2) Static flow visualization for the flat wings ($\alpha=7^\circ, 15^\circ, 30^\circ, 40^\circ$, for the $\Lambda=80^\circ$ wing and $\alpha=10^\circ, 15^\circ, 20^\circ, 30^\circ$, for the $\Lambda=65^\circ$ wing, for $\phi=0^\circ, 10^\circ, 20^\circ, 30^\circ$, for both wings). The experiments were performed with and without trip wires.

3) Surface pressure measurement:

		$\Lambda=80^\circ$		
		Plane Wing		Flapped Wing
		With and Without TW		With and Without TW
$\alpha \backslash \phi$		15°, 30°, 40°	0°, 2°, 5° 15°, 20°, 25°	30°
0°		YES	YES	YES
10°		YES	NO	YES
20°		YES	NO	YES
30°		YES	NO	YES

Table 2. Surface pressure measurements.

4) Qualitative flow visualization of the wings, in the free to roll apparatus. Several angles of attack.

5.3 Roll Moment Measurement

The torque sensor and the data acquisition system were used to obtain the roll moment coefficient for all the wings used in the investigation. This data was used in other aspects of the experimental investigation, including correlation with flow visualization, surface pressure distribution, and the model motion on the free to roll apparatus. The sensor was found to be suited for the measurements, since it was able to measure less than 0.0042 N.m of torque, which corresponds to a weight of 5g placed at the tip of the 80° wing.

The first step for using the sensor, was to perform a calibration. The 80° delta wing was connected to the torque sensor, and the system was then connected in a table. Small holes were made on the tip of the trailing edge of the wings, so weights could be hung there. The wing was placed at $\alpha=0^\circ$ and $\phi=0^\circ$, and a series of weights were hung on the wing one at a time and the respective voltage recorded.

By measuring the difference in voltage with and without the weight on the wing, it was possible to determine a calibration curve for the torque sensor. The calibration curve is shown in figure 5.1.

The data follows a linear curve, which was expected since the torque sensor is symmetric and the wing is also symmetric.

The torque sensor was made out of aluminum strips, which are malleable. When the wing was placed on the torque, and experiments conducted, the torque sensor would try to rotate, but since the strips are malleable they would twist.

To ensure that only the torque of the wing would be used, the twist or physical displacement of the torque sensor was also measured. The procedure to measure the

displacement was the same as the one used to measure the moment. Weights were hung on the sides of the wing, and the displacement of the wing in roll was measured.

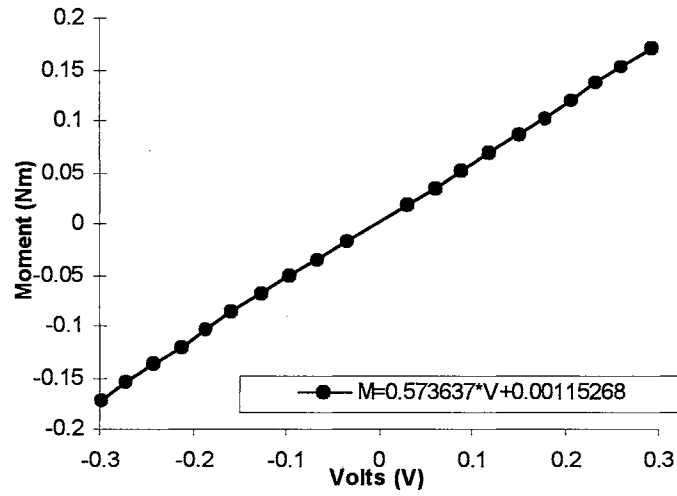


Figure 5.1. Calibration curve for the torque sensor.

The measurement was done on both sides of the wing to ensure that the system was symmetrical. The displacement calibration curve is shown in figure 5.2.

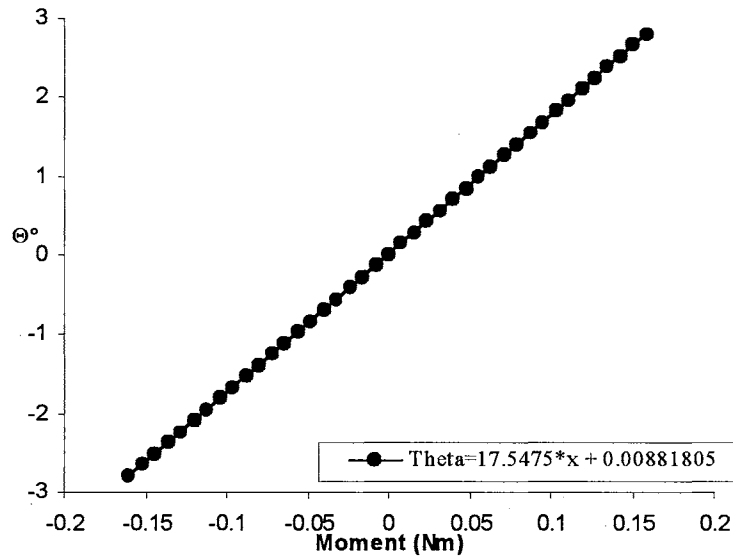


Figure 5.2. Displacement calibration curve for the torque sensor.

Again the curve is linear, showing that the system is symmetric with relation to displacement.

By knowing the moment generated by the wing it is possible to determine the angle displacement of the wing. For the experiments with the flat wings and the vortex flap wings, the maximum displacement angle was less than 2.5° .

When the wing was placed at high angles of attack, there was a force on the normal direction, that would pitch the wing up. At roll angles different than zero, there was also a lateral force on the yaw direction. These forces are also referred as normal and lateral forces.

To ensure that there would be no normal or lateral force generated by the torque sensor, the coupling on these two directions was measured. The graphs in figures 5.3(a) and 5.3(b), shows the measurement of normal and lateral coupling.

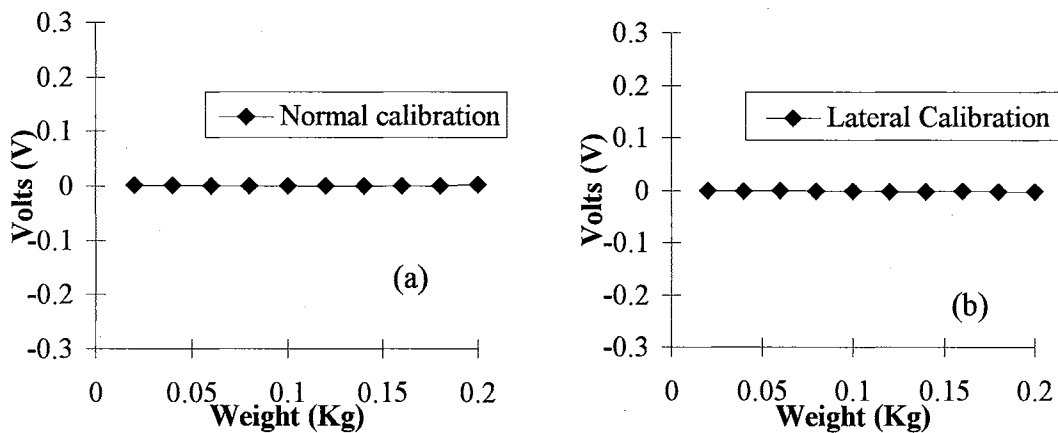


Figure 5.3. (a) Normal coupling curve. (b) Lateral coupling curve.

It can be seen that even when a weight of 0.2Kg is applied to the torque sensor, there is no measurable voltage difference. This indicates that normal and lateral forces are not coupled with roll moment.

The uncertainty on the calibration of the torque sensor arose mainly from the measurement of the distance from the center of the wing and the weights used for the calibration. Using the equation of moment, given by

$$L = F \cdot d \quad (5.1)$$

and using Kline's equation for uncertainty, given by

$$u_L = \sqrt{\frac{\partial L}{\partial m} \Delta m + \frac{\partial L}{\partial d} \Delta d} \quad (5.2)$$

it was possible to determine that the maximum uncertainty of the calibration of the torque sensor is 4%.

The uncertainty on the measurement of the voltage necessary to find the moment, was mainly from the sensitivity of the strain gage bridge and resolution of the A-D board used. These uncertainties are small compared to the uncertainty in the calibration and are often ignored.

Due to the high sensitivity of the torque sensor, the voltage difference after each run would not go back to zero. It was necessary to take 3 to 4 measurements to observe the voltage to come back to zero or close to zero voltage difference after each run. The probable cause for this was a combination of stiffness and inertia of the aluminum strips used. It was observed that after 3 or 4 runs the voltage would come back to zero or at least 4 mV from zero. Since it was impossible to get a zero voltage difference, most of the time, a maximum of 4mV was set as a limit from which the voltage difference could come back to its original value after each run. This difference corresponds to a roll moment of approximately of 0.0018. This value corresponds to 2% of the maximum value measured, which occurred at a roll angle of 30° and to 6% of the minimum value measured., which

occurred at a roll angle of 10°. At a roll angle of 0°, there was no roll moment or it was very small, in the order of 0.0018.

The roll moment coefficient was found using

$$C_l = \frac{2L}{V^2 b S} \quad (5.3)$$

where the velocity is given by

$$V = \sqrt{\frac{2q}{\rho}} \quad (5.4)$$

therefore

$$C_l = \frac{L\rho}{q.b.S} \quad (5.5)$$

Using Kline's method in the roll moment equation yields

$$U_{C_l} = \sqrt{\frac{\partial C_l}{\partial L} \Delta L + \frac{\partial C_l}{\partial q} \Delta q + \frac{\partial C_l}{\partial b} \Delta b + \frac{\partial C_l}{\partial S} \Delta S} \quad (5.6)$$

Using the uncertainty of calibration found in equation 5.2, and using the uncertainty of the manometer to be 0.05 in H₂O = 12.45 Pa, and taking the maximum value of the moment obtain during calibration which as 0.1707 N.m for 0.2 Kg of weight placed at 0.085 m from the center of the wing, and knowing the area of the wing to be 0.0431 m², the maximum uncertainty obtain is 5%. This value of uncertainty is within the maximum value of uncertainty acceptable for experimental results, which is around 5%.

5.4 Surface Pressure Measurement

The surface pressure acquisition system described in section 2.4 was used to obtain the surface pressure distribution on the wing at 75% chord station. This chord station was chosen because it was far enough from the trailing edge of the wing, to avoid the end effect of the vortices on the trailing edge. It was also a chord station where a good resolution of the pressure distribution could be obtained. Pressure measurement was taken at several angles of attack and roll angles, as shown in section 2.4.

Before beginning any pressure acquisition, the pressure transducer was calibrated. After that all of the taps on the surface of the model were then covered with thin transparent tape. Before acquiring any data, the chambers in the wing were checked for leaks. This was possible since the application of the tape would create a residual pressure in the chambers which could be measured by the transducer. The voltage referent to the pressure would show in the voltmeter and if it was non-zero and stable, there were no leaks in the system. 1 tap was selected in each slot of the wing and a pin was used to puncture the tape. The chamber pressure would immediately fall to zero. The scanning valve was then rotated to the next slot and the process repeated for each of the slots. The tunnel was then turned on and the data acquisition program began. 2000 data points were taken at each tap over a period of 10 seconds and then averaged. Then a new tap was selected by using the scanning valve, and the process repeated. The transducer was calibrated each day it was used.

The pressure coefficient is calculated using the standard expression for C_p

$$C_P = \frac{p - p_\infty}{q} = \frac{\Delta p}{q} \quad (5.5)$$

The pressure transducer reference used was the static free stream pressure from the pitot-static tube. This allowed a direct calculation of the pressure coefficient using equation 5.5.

The uncertainty on the pressure coefficient is mainly due to the calibration of the pressure transducer which was found to be a maximum of 5%.

The pressure coefficient for the 80° wing with and without trip wires can be numerically integrated to find the lift generated over the wing. One of the simplest numerical method that can be used is the Trapezoid Rule, which fills the space between two data points with a rectangle whose height is equal to the value of the function at one of the data points, and whose width is equal to the width of the interval, and puts a line between the two data points. This rule is stated as:

$$I = \sum_{i=1}^{n-1} \frac{(y_i + y_{i+1})}{2} (x_{i+1} - x_i) \quad (5.6)$$

Even though this is a simple numerical integration, its approximation is good enough for the purpose of this study.

5.5 Trip Wires Effect

To determine the effect that the change in flow condition has on the flow over the 65° and 80° delta wing, trip wires were placed on the top of the wing, as mentioned in Section II. Experiments were performed with the trip wires at two different location. Initially the trip wires were placed at ½ of the semi-span and on the center of the wing. Then the trip wires were placed at 1/3 of the semi-span, measured from the center of the wing, and one in the center. The reason to have two locations for the trip wires was

because some of the results showed that for the 1/2 semi-span location, the boundary layer could have been already separated, before getting to the wires.

On the 65° delta wing, the trip wires were placed only at half of the semi-span. The experiments conducted with the 65° wing were limited to roll moment measurements and flow visualization.

5.6 Surface Flow Visualization

The surface flow visualization substance mixture used for the study was presented in section 2.3. The procedure for conducting the surface flow visualization was to apply a layer of the mixture to the wings surface with a foam brush. The layer of mixture was made as thin as possible so that gravity would not cause the mixture to run as the model was rotated at different roll angles. The wings were then placed at a static angle of attack and roll angle and the tunnel was turned on. After the mixture had dried sufficiently, the wings were removed from the tunnel and placed on a black piece of cloth and illuminated with flood lights to obtain the photographs.

5.7 Free to Roll Flow Visualization

The flow visualization was done by placing the wing into the free to roll system at the desired angle of attack. The wing was then hooked to a release mechanism connected to the outside of the wind tunnel. The wings were hooked at $\phi=0$. After that the wind tunnel was turned on, and when the desired flow velocity was achieved the wing was released and its behavior observed.

CHAPTER VI

EXPERIMENTAL RESULTS AND DISCUSSIONS

6.1 Roll Moment Characterization

The Reynolds number used for the 80° wing was 700,000, and for the 65° was 403,000. This Reynolds number was chosen in order to obtain the maximum signal from the torque sensor while not exceeding the maximum stress that the torque sensor could withstand. To raise the Reynolds number to 700,000 on the 65° sweep wing the pressure would have to be raised to 747 Pa. That would bring the wing tunnel velocity close to the maximum velocity set, and would break the sensor. To decrease the Reynolds number to 403,000 on the 80° sweep wing the pressure would have to be decreased to 100 Pa, which would be too small for the investigation. For this reason what was kept constant was the dynamic pressure of the air flow, which was 249 Pa. The dynamic pressure used proved to be enough to show several different phenomenon over both wings.

6.1.1 Computational Validation

From the calibrations curves it was determined that the torque sensor was working properly and could be used to measure the moment of the wings. A series of experiments were conducted to compare the experimental results with the computer model. Since the model has a limitation on the angle of attack that it can be used, the experiments were limited at 15° and 30° angles of attack for the 80° wing, and at 10° and 15° angles of attack for the 65°

The experiments were made for several roll angles and the two angles of attack mentioned above, using the plane wings. The experimental results were compared with the computer model which was extensively used and showed to be valid, presented in section III, for $\alpha=10^\circ$ to 30° . For the 80° wing the moment coefficient is shown in figure 6.1.

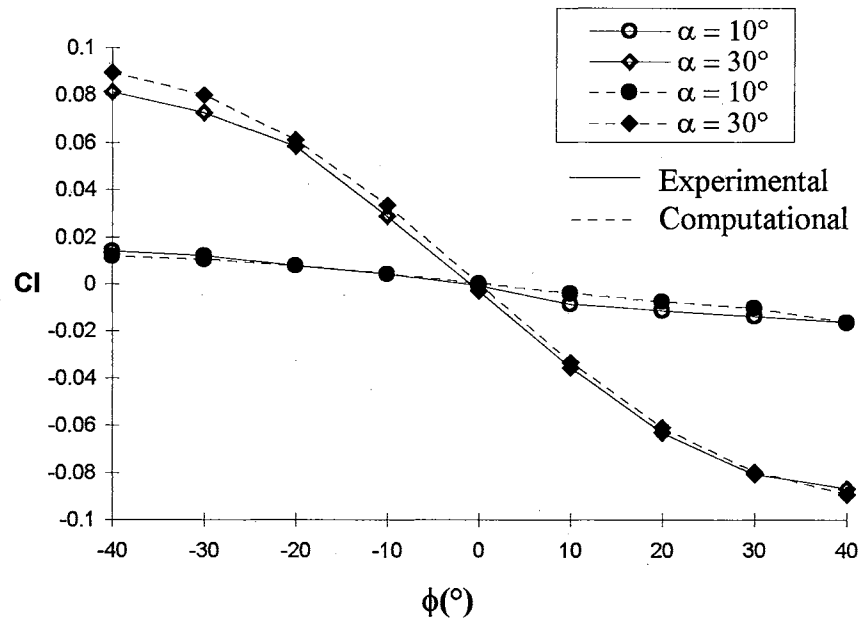


Figure 6.1. Roll moment vs. roll angle for different angles of attack for the 80° wing.

Good agreement is observed between the experimental data and the computer model. As mentioned before, the model uses potential vortices to model the leading edge vortices, over the wing. Therefore for the 80° sweep wing at small angles of attack the vortices are not formed, and the assumption in the code is not valid. For angles of attack higher than 32° , vortex breakdown starts to appear on the wing, which is not modeled in the code. Therefore the use of the code was limited to 10° and 30° angle of attack for the 80° wing.

For the 65° wing, the moment is shown in figure 6.2.

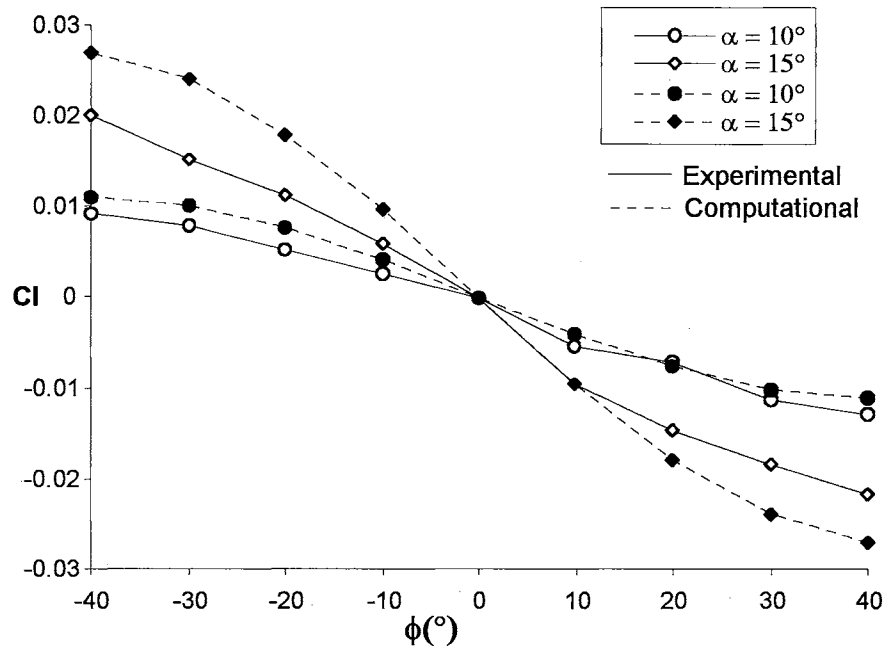


Figure 6.2. Roll moment vs. roll angle for different angles of attack for the 65° wing.

Prediction is reasonable with increasing error at larger angles of attack. This behavior would be expected due to the assumptions in the model which improve with increased sweep angle.

From these results it was concluded once again that the computer model is able to capture the flow physics over the wings, and is only limited by the angles of attack where the vortices are not presented or where there is vortex breakdown.

6.1.2 Roll Moment Coefficient With Asymmetric Flap Deflection

The effect of a 25° anti-symmetric flap deflection on the 80° wing is shown in figure 6.3.

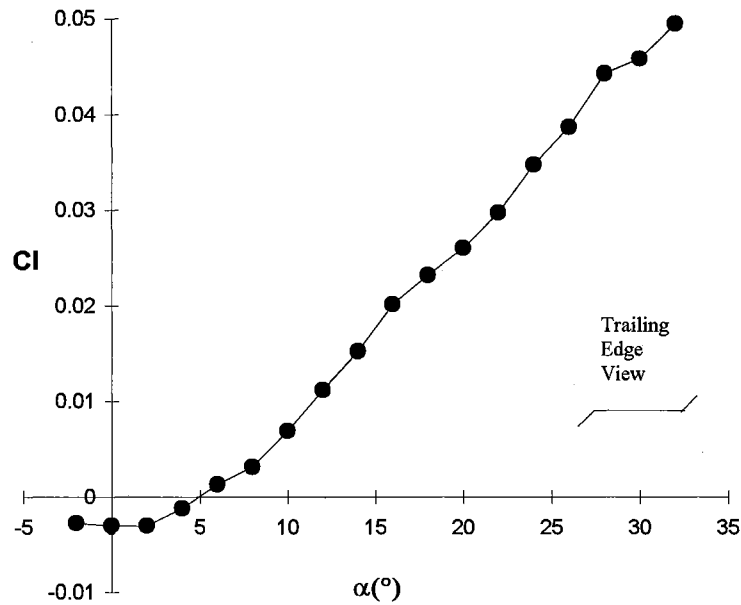


Figure 6.3. Effect of flap deflection on C_l for different angles of attack for the 80° wing.

The plot shows that the moment coefficient increases for angles of attack higher than 7° indicating an improvement in control effectiveness. If the angle of attack is around 7° , all control effectiveness is lost, and for angles of attack smaller than 5° an interesting phenomenon may be seen in which, anti-symmetric flap deflection produces moment in the opposite direction.

To determine if the wing would have the same behavior with the flaps deflected in the opposite direction, a wing was built with the left flap deflected upward and the right flap deflected downward. This should cause the wing to roll right at low angles of attack and roll left at high angles of attack. The graph in figure 6.4 shows the graph for both wings,

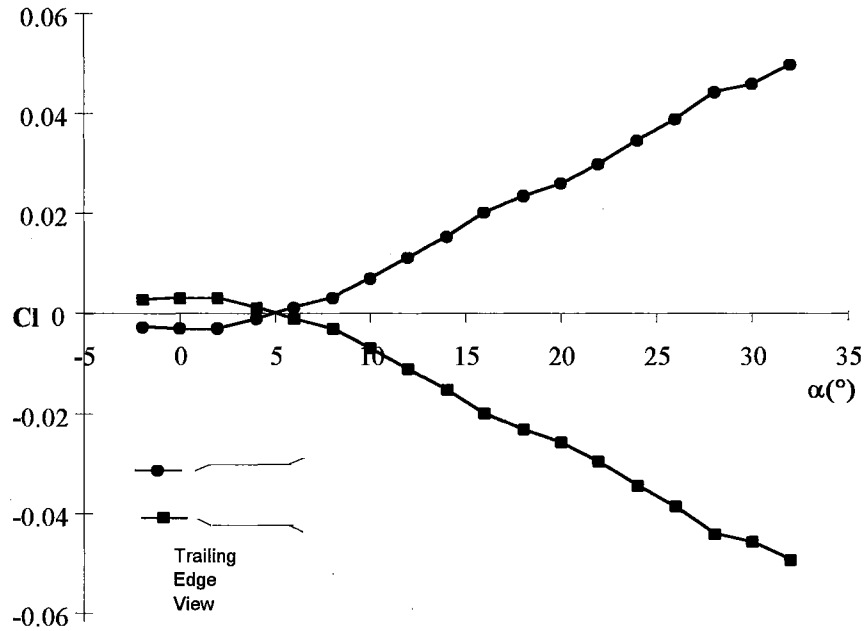


Figure 6.4. Effect of asymmetric flap deflection for opposite flap angles.

The graph shows that when the flaps are deflected asymmetrically in the opposite direction as the one shown in figure 6.3, the roll effect observed in figure 6.3 is the same, but in the opposite direction. It also shows that the torque sensor has the same resolution in both directions. Since the roll effect is symmetric, all the other experiments were performed with the 80° wing having asymmetric flap deflection shown in figure 6.3.

The 65° wing presented a similar roll reversal behavior as observed in the 80° wing, but the reversal occurred at different angles of attack. The effect of the flap deflection in the 65° wing is shown in figure 6.5.

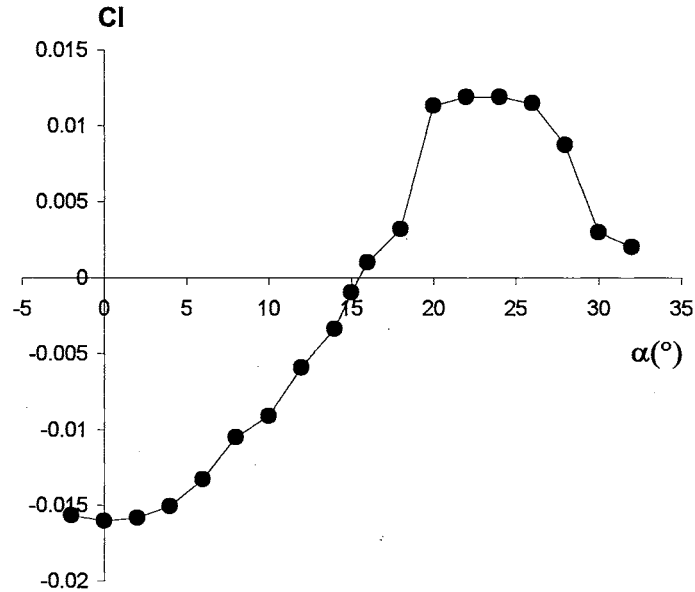


Figure 6.5. Effect of flap deflection on C_1 for different angles of attack for the 65° wing.

The figure indicates that above an angle of attack of approximately 15° , an increase in angle of attack increases control effectiveness up to 20° . For angles of attack between 20° to 26° the roll moment stays constant and for angles of attack higher than 26° the roll moment decreases. At an angle of attack of approximately 33° , the control effectiveness is essentially zero. It is speculated that the sudden increase in moment at 20° angle of attack and the subsequent decrease in control effectiveness is due to the effects of vortex breakdown which appears on the 65° plain wing for angles of attack greater than 20° (Wentz and Kolhman 1971).

The 65° delta wing exhibits a reversal in control effectiveness as was observed on the 80° wing. Note that below approximately 15° , the roll moment direction is negative, and for angles of attack higher than 15° it is positive. Although the effectiveness of the

flaps at large angles of attack is less than that observed with the 80° delta wing, the effectiveness in the negative direction is greater at the lower angles of attack.

The ability of the modified computational model to capture the behavior of roll moment when flaps are deflected for the 80° delta wing may be observed in figure 6.6.

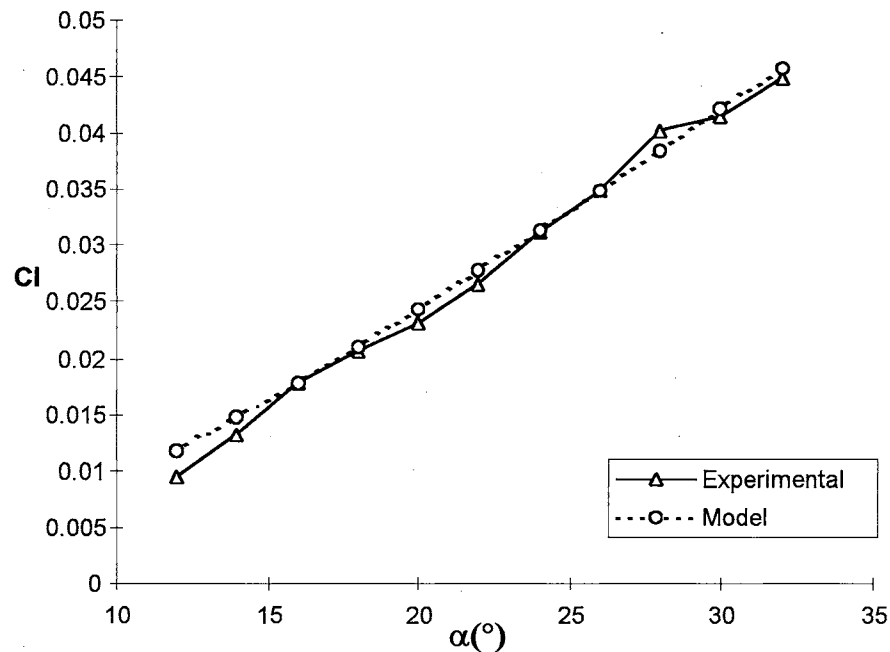


Figure 6.6. Comparison between experiment and model for 25° flap deflection, for the 80° wing.

Shown are the experimental data and computed roll moments over the range of validity of the assumptions for the model as discussed previously. The ability of the model to adequately predict the flow behavior demonstrates a potential for investigating the flow physics of problem in conjunction with experimental data.

From these results it can be observed that there are several different phenomena observed for the delta wings when leading edge flaps are deflected asymmetrically. First, effectiveness of the flaps appear to be a strong function of wing sweep angle and angle of

attack. Flap effectiveness for the 80° wing is very good at large angles of attack. Conversely, the effectiveness of the flaps on the 65° wing is degraded beyond approximately 26° , however, effectiveness is best at lowest angles of attack, although in the opposite direction.

Another significant observation for both wings is the reversal of roll moment with angles of attack. In each case there is a positive angle of attack for which control effectiveness is zero. Roll moment behavior due to asymmetric flap deflection is in the opposite direction for angles of attack on either side of this zero effectiveness point.

6.2 Trip Wires Effect on Roll Moment

Most of the experimental study that has been done with delta wings is at relatively low Reynolds number, due to the fact that the wind tunnels used have limited Reynolds number capability. It was shown by Hummel (1978) and Carcaillet et al. (1986) that Reynolds number has a significant effect on the flow over delta wings. This may be shown to be even more important when the wings have asymmetric flap deflection. This is because for the laminar flow the secondary separation line separates early, close to the center of the wing. In the turbulent case the vortices induce a higher suction peak, and the separation line moves closer to the leading edge (Hummel 1978 and Carcaillet, et. al 1986).

On the other hand, it has been shown that when a delta wing has a symmetric flap deflection the vortices are generated over the flap. The vortices have a different position than the ones that are generated when the flaps are not deflected. Therefore a combination

of high Reynolds number and asymmetric flap deflection is prone to change the vortices over the wing and the secondary and tertiary separation lines over the delta wings.

6.2.1 80° Wing Without Flap Deflection

To assess the effect of Reynolds number over the 80° wing, the boundary layer over the wing was tripped as mentioned in Section 2.2. The experiments were performed for the wing with and without asymmetric flap deflection.

For the wing without flap deflection, results are shown in figure 6.7,

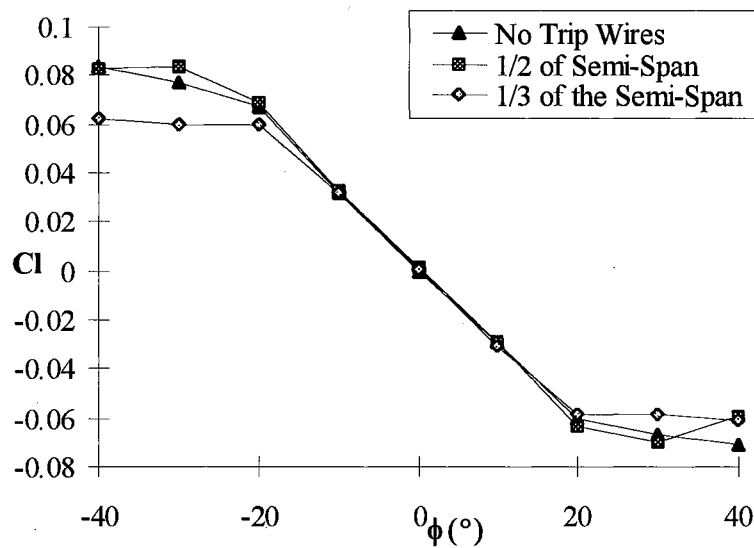


Figure 6.7. Roll moment for different trip wire position over the wing.

As it can be seen from the figure, the trip wires when placed at 1/2 of the semi-span have almost no effect on the roll moment. For the trip wires placed at 1/3 of the semi-span, there is no change in the moment for roll angles ranging from -20° to 20° . For angles higher than 20° and smaller than -20° , there is a small difference between the flow with trip wires at 1/2 and 1/3 of the semi-span.

The fact that the trip wires have no effect for 0° roll angle was expected, since the wing is symmetric and the vortices must be symmetric, therefore the force on the left and right side of the wing should be the same.

Since it is known that the trip wires change the pressure over the wing, it was expected that the roll moment coefficient for roll angles different than 0° would be different with and without trip wires. As shown in figure 6.7 this only happens for roll angles lower than -20° and higher than 20° . This indicates that the pressure distribution over the wing changes when the trip wires are placed on the wing.

The changes are more significant for the trip wires placed at $1/3$ of the semi-span, measured from the center of the wing. There is a 25% reduction in the moment due to the trip wires. For the trip wires located at $1/2$ of the semi-span there is very little change with the moment generated without the trip wires.

6.2.2 80° Wing With Asymmetric Flap Deflection

Noticing that the trip wires at $1/2$ of the semi-span had little effect on the wings between angles of attack -20° and 20° , without asymmetric flap deflection, it was decided that the experiments with the “flapped” wing would have the trip wires located only at $1/3$ of the semi-span. Another reason was that if the trip wires were placed at $1/2$ of the semi-span, they would be too close to the joint of the flap.

The graphic in figure 6.8 shows the roll moment for the 80° wing with asymmetric flap deflection,

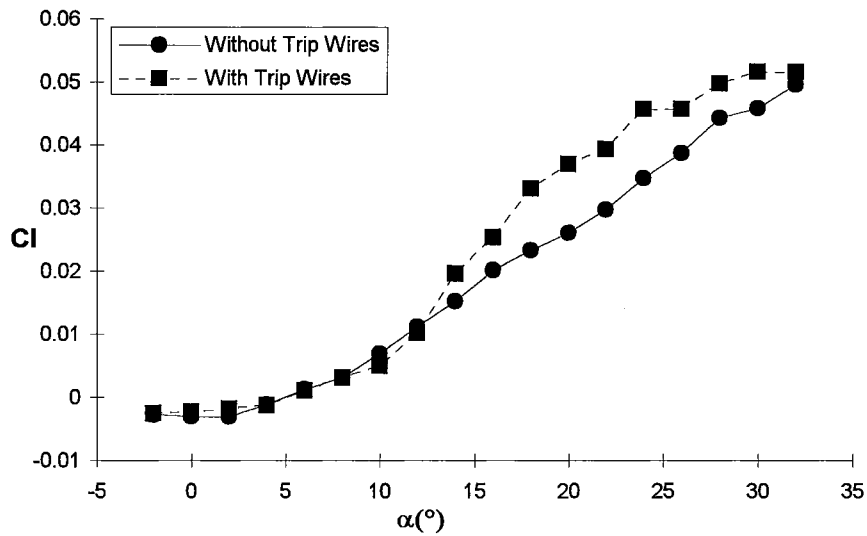


Figure 6.8. Effect of trip wire on the 80° wing with asymmetric flap deflection.

On the 80° wing with asymmetric flap deflection the trip wires have very little effect for angles of attack smaller than 12°. For angles of attack higher than 12° there is an increase in the roll moment indicating an improvement in flap effectiveness, that goes up to 32°.

It is interesting to notice that the angle of attack that the trip wires start to have some effect on the wing, is exactly the same that the computer model starts to be valid for the 80° wing, which is $\alpha=12^\circ$. Since the model uses potential vortices to model the leading edge vortices, it is only valid for angles of attack where the vortices are present. But this only starts to happen at angles of attack of 10° to 12°.

6.3 Surface Pressure Measurements

The surface pressure measurements were taken to complement the roll moment data, and to verify why there was a change in moment for the trip wires placed at 1/3 of the semi-span. The measurements were taken with the same wings used to take the roll moment data. This was done in order to minimize any possible error by using another wing with the same characteristics. The surface pressure measurements was performed using the procedure outlined in Section 5.6.

6.3.1 Pressure Distribution over the 80° Wing Without Flap Deflection

The pressure coefficient for the 80° wing without flap deflection at 30° angle of attack and several roll angles, is shown in figure 6.9.

As it can be seen from the figure, there is an increase on the pressure when the trip wires are placed on the wing. For $\phi=0^\circ$ the graph is symmetric for both conditions, with and without trip wires. This was expected since the wing has a centerline symmetry. The graph also show a small decrease in pressure right after the trip wire. This is probably where the boundary layer reattaches over the wing, after being tripped. It is important to notice that the graph for $\phi=0^\circ$ has the same trends as the one observed by Hummel (1978) and by Carcaillat, R. et al. (1986). When the wing is at $\phi=10^\circ$ the pressure of the reattachment point on the right side of the wing increases significantly. This increase in the pressure of the reattachment point would not happen if the flow had a high Reynolds number and did not have the trip wires. This phenomenon is due exclusively by the presence of the trip wires.

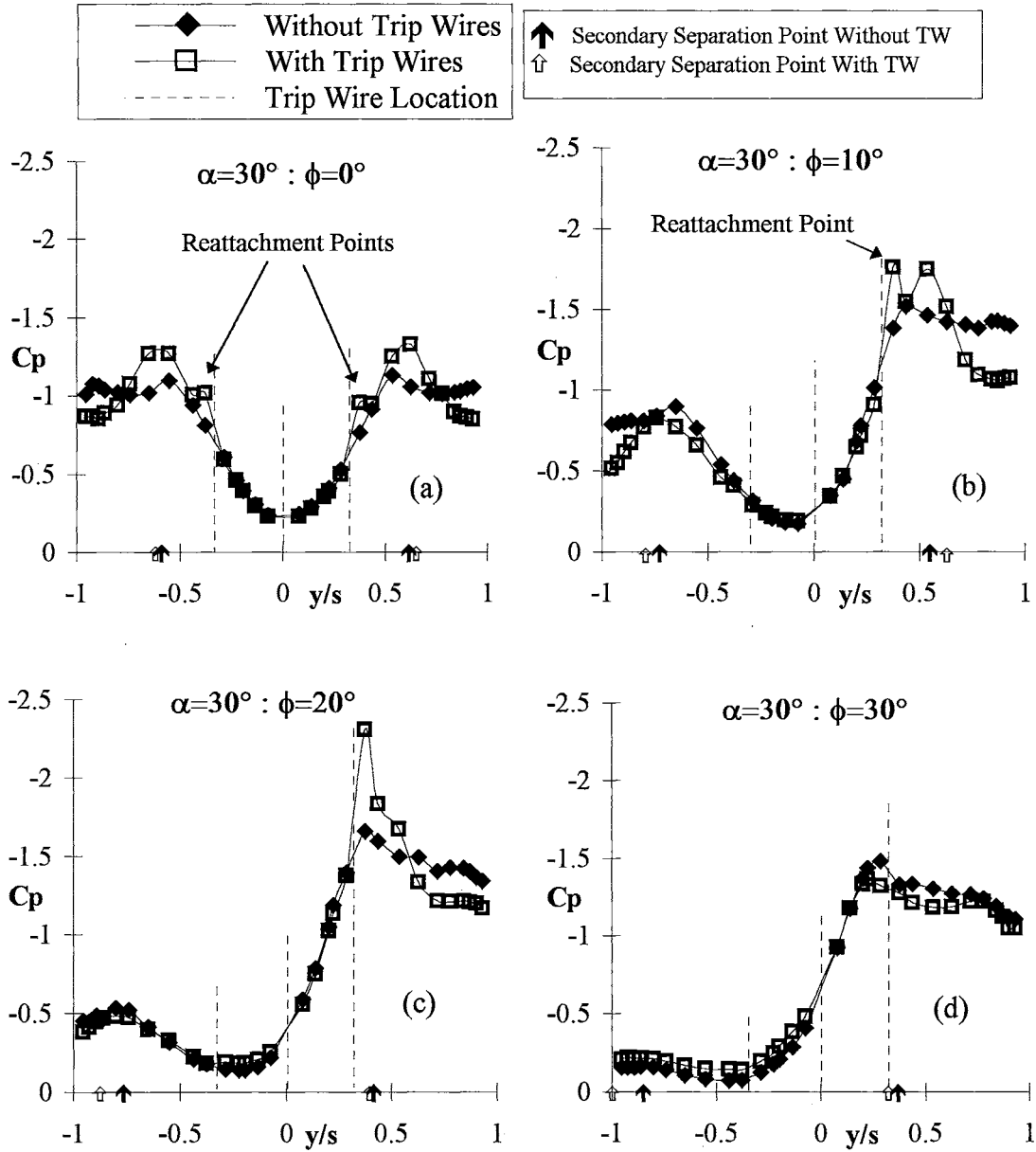


Figure 6.9. Pressure coefficient for the 80° wing with and without trip wires.

Even though the experiments with the trip wires were similar to those done by Hummel, he does not mention the existence of the reattachment points in his experiments. This difference in results may be due to the fact that the present experiments have a better resolution than Hummel had.

For $\phi=20^\circ$ the pressure due to the right vortex increases significantly and the pressure due to the reattachment of the boundary layer vanishes completely. When $\phi=30^\circ$ the pressure due to the right vortex decreases considerably and coincides with the pressure obtained without the trip wires. From the flow visualization results to be seen later, it is shown that at $\phi=30^\circ$ the secondary separation on the right side of the wing coincides with the trip wire. Therefore the pressure over the wing is the same as the one without trip wires, which is what figure 6.9(d) shows.

On the other hand, the left vortex had a decrease in pressure due to the trip wires for $\phi=10^\circ$. For $\phi=20^\circ$ and 30° , the pressure for both conditions are the same indicating that the trip wire is having very little effect on the left vortex as the wing is rolled in the positive direction.

The small effect that the trip wires have on the left vortex is due to the fact that when the wing is at a positive roll angle, the secondary separation line on the left side of the wing moves out of the wing. The flow seems completely separated from the top of the wing, making the trip wire useless. For the right vortex the opposite occurs. The secondary separation line moves inward towards the center of the wing up to a point where it coincides with the trip wire itself, making it useless.

The graphs in figure 6.9 also explain why the roll moment coefficient is nearly the same with and without trip wires, as shown in figure 6.7. By integrating the curves in figure 6.9 it is possible to determine the sectional moment over the wing with and without trip wires. Table I shows the results of the integration.

$\alpha=30^\circ$				
ϕ	0°	10°	20°	30°
Without TW	0.00	0.03	0.04	0.05
With TW	0.01	0.01	0.01	0.01

Table III. Roll moment coefficient over the 80° wing obtained from the pressure coefficient.

The numerical integration was performed using Trapezoid Rule shown in section 5.6. From the data shown, it can be seen that the moment due to the sectional pressure of the wing without trip wires is a little higher than the one with the trip wires. This is the same as observed in figure 6.7, where the moment of the wing without trip wires was a little higher than the one with the trip wires located at $1/3$ of the semi-span.

This shows that in this study the roll moment coefficient data alone, for wings with and without trip wires, can lead to erroneous conclusions, since it was shown that the pressure distributions over the wings change when the trip wires are present.

Even though the trip wires generates a high pressure due to reattachment, they also increase the pressure of the vortices. Therefore Reynolds number does affect the flow, and should be considered when studying the flow over delta wings.

6.3.2 Pressure Distribution over the 80° Wing With Asymmetric Flap Deflection

The pressure distribution over the 80° wing for several angles of attack and for zero roll angle is shown in figure 6.10, with and without trip wires.

From the figure it can be seen that for angles of attack between 0° and 5° , there is little difference in the pressure between the flow with and without trip wires and they are close to zero.

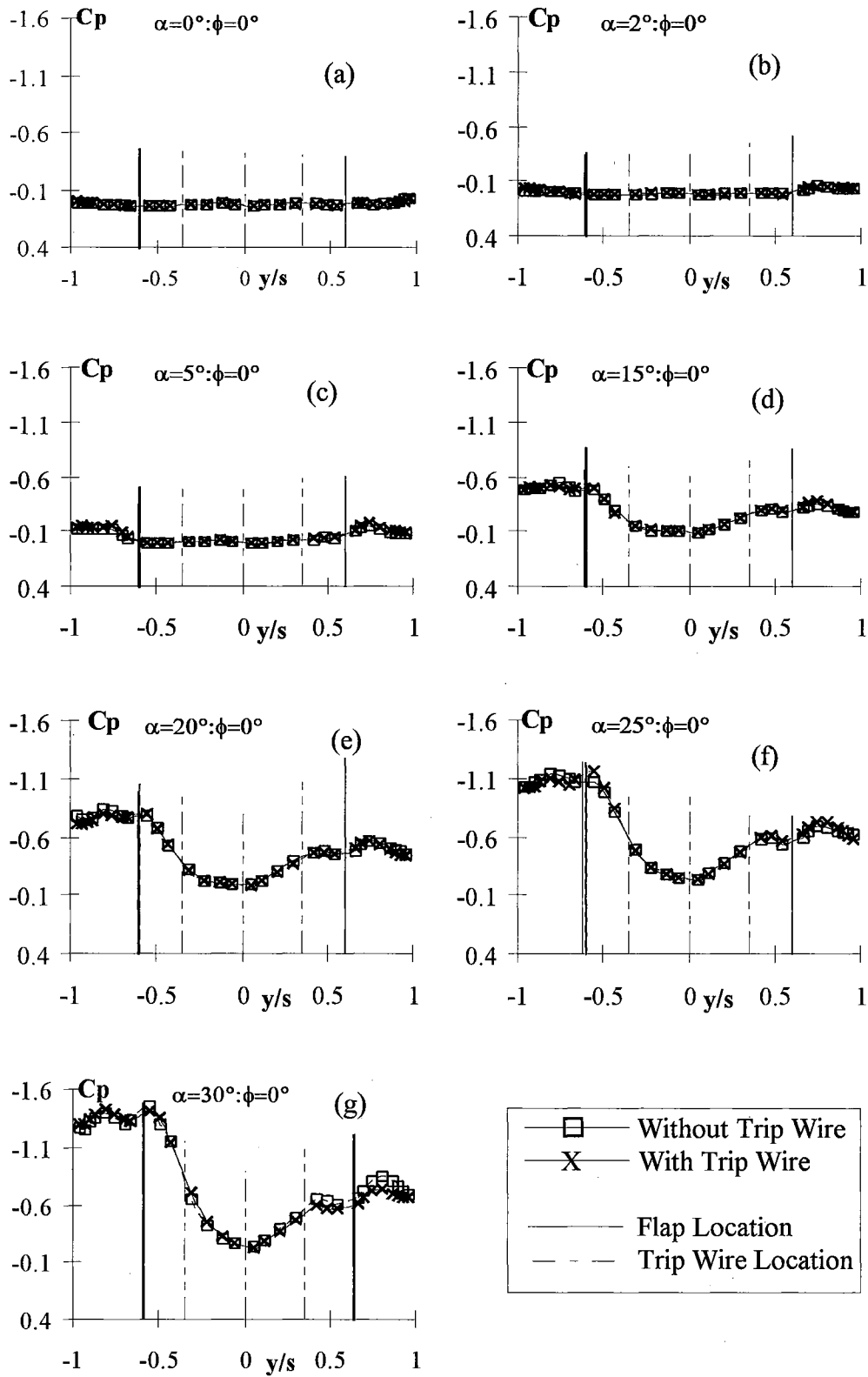


Figure 6.10. Pressure coefficient for the 80° wing with asymmetric flap deflection.

For angles of attack higher than 15° , a pressure difference starts to appear. The pressure is higher on the left side of the wing than on the right side of the wing, as the angle of attack increases. This is consistent with experiments performed by Marchman (1981), where he showed that the deflection of inverted flaps (deflected upward) the lift coefficient decreases. When the flaps are deflected downward (Marchman III, Plentovich and Manor (1980)) the lift is improved by moving the vortices towards the flaps and inducing additional thrust and reducing drag.

Therefore by deflecting the flaps asymmetrically (left flap upward, right flap downward) the right vortex has a higher lift than the left one generating a moment in the positive direction, which is the same conclusion obtained from the roll moment coefficient showed in figure 6.3.

It was expected that the trip wires would have some effect on the wing with asymmetric flap deflection as they had on the wing without flap deflection. From figure 6.10, it can be seen that the trip wires do affect the left and right vortices. It does not seem that the effect is the same on both vortices. The graph in figure 6.11 is a close-up of the graph in figure 6.8(g), which is the wing at $\alpha=30^\circ$ and $\phi=0^\circ$, and is the one that shows a greater difference for a wing with and without trip wires. The right side of the wing has the biggest difference in pressure between the flow with and without trip wires. When the trip wires are placed on the wing it generates a lower pressure on the right side of the wing, which increases the moment on the wing when compared with the no trip wires situation. This is consistent with the results obtained for the roll moment, shown in figure 6.8.

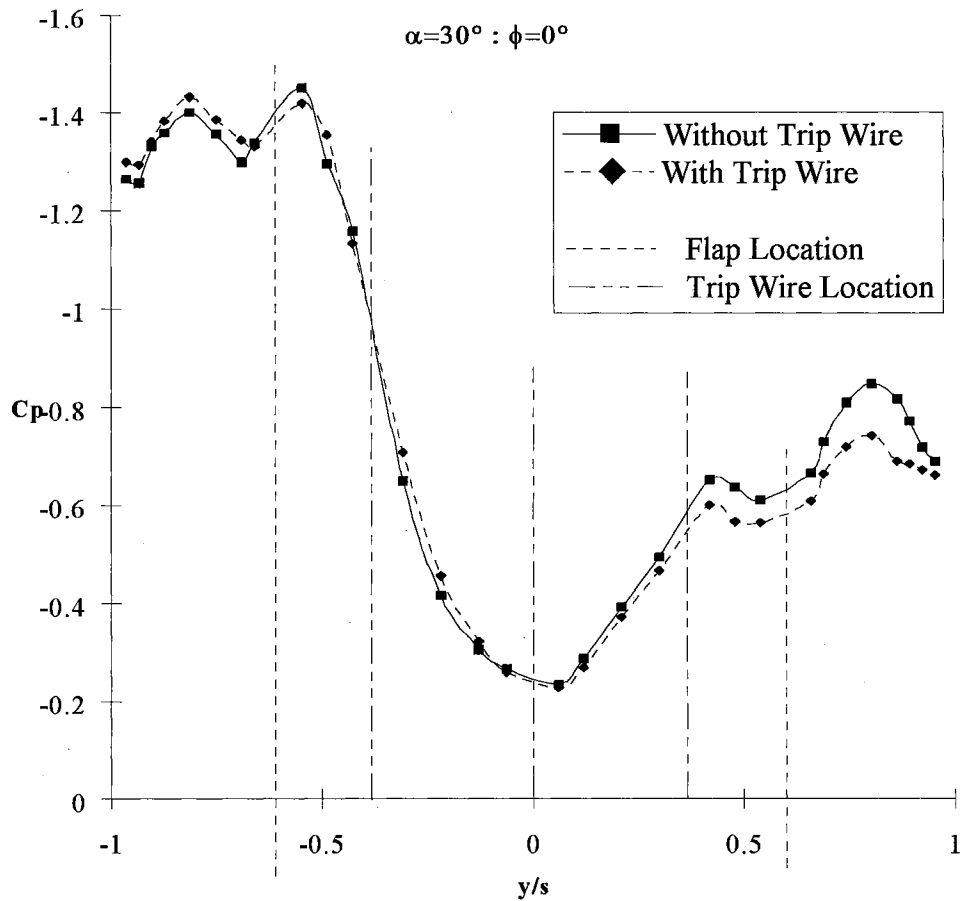


Figure 6.11. Pressure coefficient for the 80° wing with asymmetric flap deflection.

The graph shows that even though the curves have the same trend, the right vortex has a decrease in pressure with the trip wire, while the left vortex does not change with the trip wire. This generates a slightest higher roll moment to the right than the wing without trip wires, which is the same phenomenon shown in figure 6.8.

By placing the 80° wing with asymmetric flaps deflected and without trip wires at different roll angles, the pressure distribution changes over the wing as shown in figure 6.12.

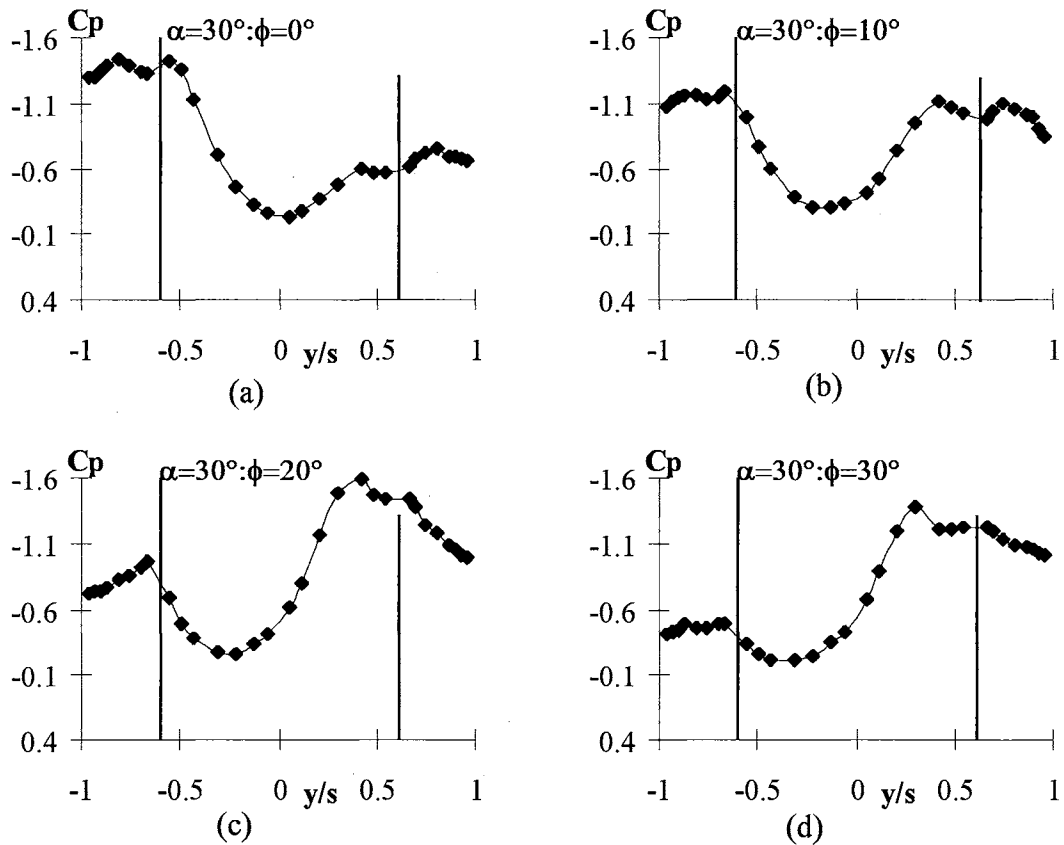


Figure 6.12. Pressure distribution of the 80° wing with asymmetric flap deflection at several roll angles.

The pressure distribution for a 0° roll angle, graph (a), shows that the left side of the wing has a higher pressure than the right side, generating a roll moment to the right. For a 10° roll angle, graph (b), the pressure distribution on both sides of the wing have approximately the same value. For 20° and 30° roll angles, graphs (c) and (d), the right side of the wing has a higher pressure, therefore generating a roll moment to the left. There is a change in the direction of the roll moment as the wing is rolled to the right when the flaps are deflected asymmetrically with the left flap downward and the right flap upward. Therefore for a 80° wing with asymmetric flap deflection, not only the angle of

attack is important on its behavior but the roll angle has also an important roll on the flow over the wing. The inversion in pressure distribution over the wing is going to be further explored on the free to roll experiments.

6.4 Flow Visualization

The flow visualization experiment was conducted on the wing to characterize the surface flowfield behavior. The experiment was conducted on the 80° wing over a wide range of angles of attack and roll angles. The purpose of this test was to correlate the flowfield behavior to the roll moment of the wing in order to verify the effect that the trip wires have on the flowfield over the wing.

6.4.1 Static Surface Flow Visualization for the 80° Delta Wing

Surface oil visualization experiments were performed to investigate how the surface flow is affected by changes in angle of attack and roll angle when trip wires are present on the top of the wing.

Flow visualization on the surface gives an indication of how the primary reattachment line and secondary and tertiary separation lines behave on the top surface of the delta wing. Figure 6.13 is a photograph of the surface flow field on the 80° delta wing without asymmetric flap deflection and without the trip wires, at $\alpha=30^\circ$ and $\phi=0^\circ$. Some of the major features of the surface flow field are shown in the figure. The most notable feature of the surface flowfield is the secondary separation line.

Due to the large adverse pressure gradient near the leading edge of the wing, the boundary layer on the surface of the wing separates and forms a secondary and at times a tertiary vortex, as shown in the figure. There have been studies that analyzed the surface flow on delta wings with various sweep angles and angles of attack. Hummel (1978) presented surface oil visualization on a 76° delta wing at 20.5° angle of attack, having a Reynolds number of 900,000.

In the present study the Reynolds number was 700,000 for the 80° delta wing. Based on the experience of other researchers, the boundary layer on the upper surface of the wing at this Reynolds number should be laminar. Results were also obtained with trip wires on the surface of the wing to create a turbulent boundary layer and using the same Reynolds number. The laminar boundary layer separated sooner and resulted in a stronger secondary vortex than that seen for the turbulent case. In the present study the Reynolds number used for the 80° wing was 700,000 and the wing was placed at angles of attack of 15° , 30° and 40° , and roll angles of 0° , 10° , 20° and 30° .

It is important to note that the boundary layer over the wing goes from the center of the wing towards the leading edge. Wherever there is a separation line, most of the time this line is conical. When vortex breakdown occurs the separation lines show a curve over the wing, indicating that the separation is not conical anymore, as shown in figure 6.14 for a 80° wing at 40° angle of attack and 0° roll angle.

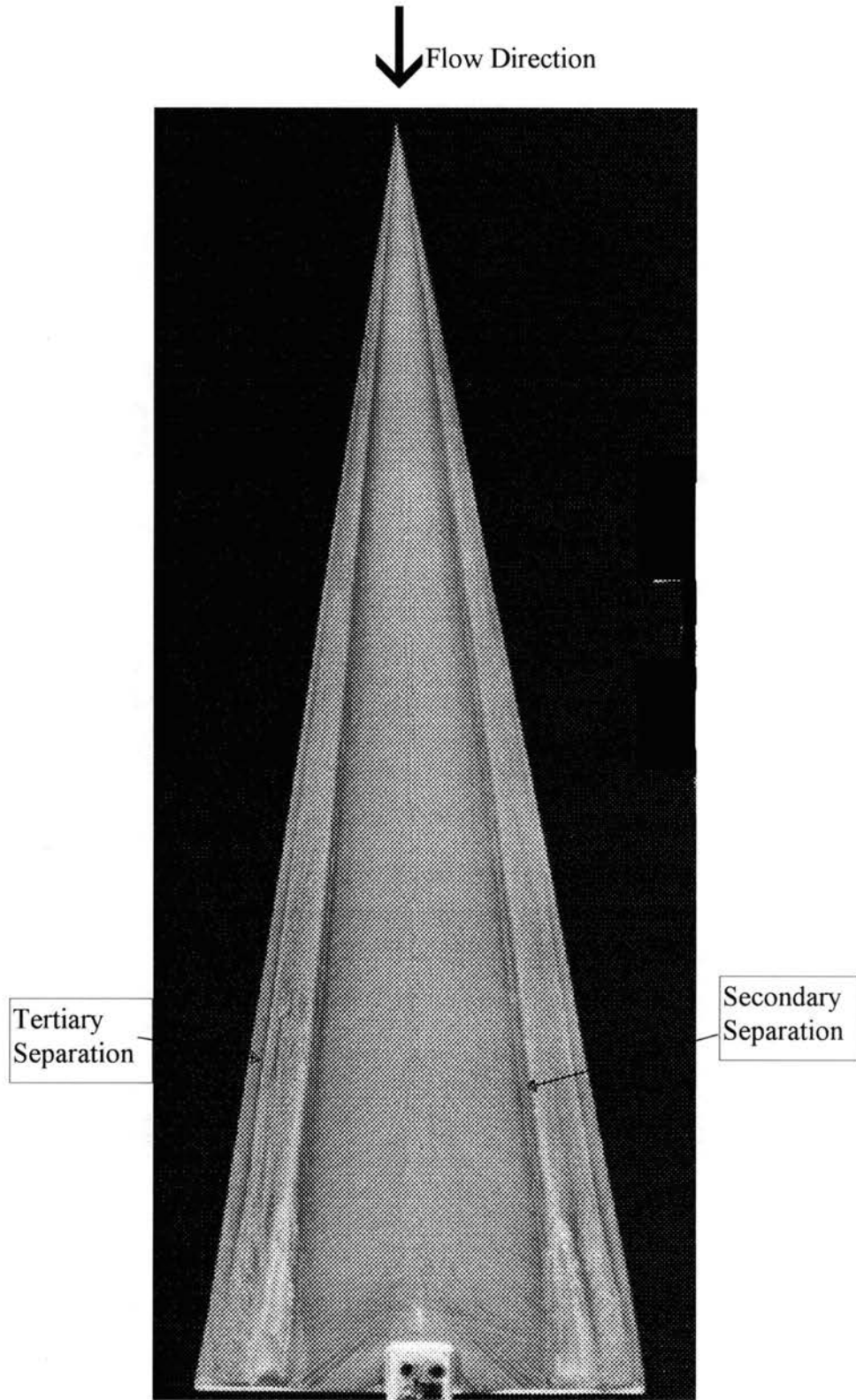


Figure 6.13. Surface flow field for a 80° wing at $\alpha=30^\circ$ and $\phi=0^\circ$.

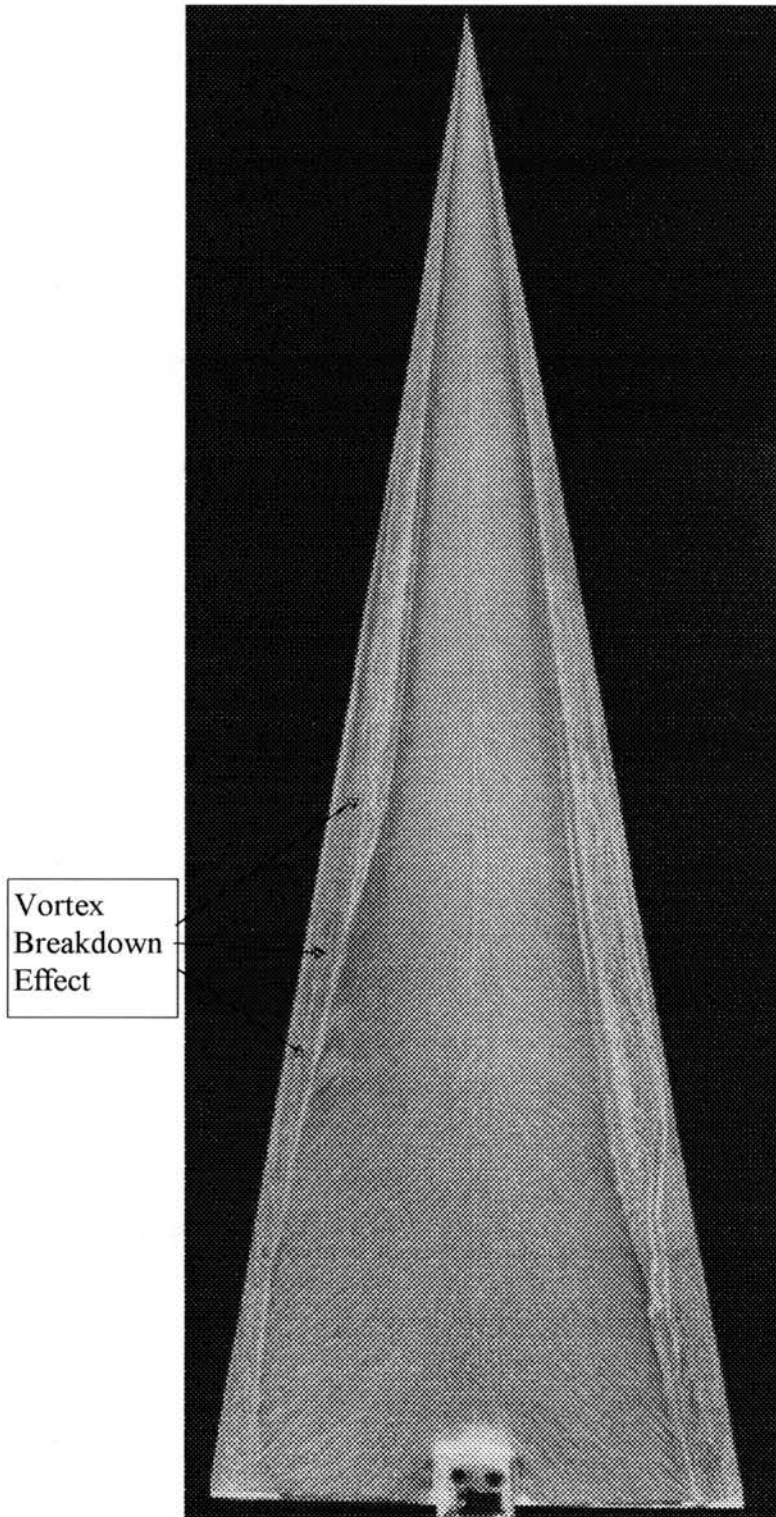
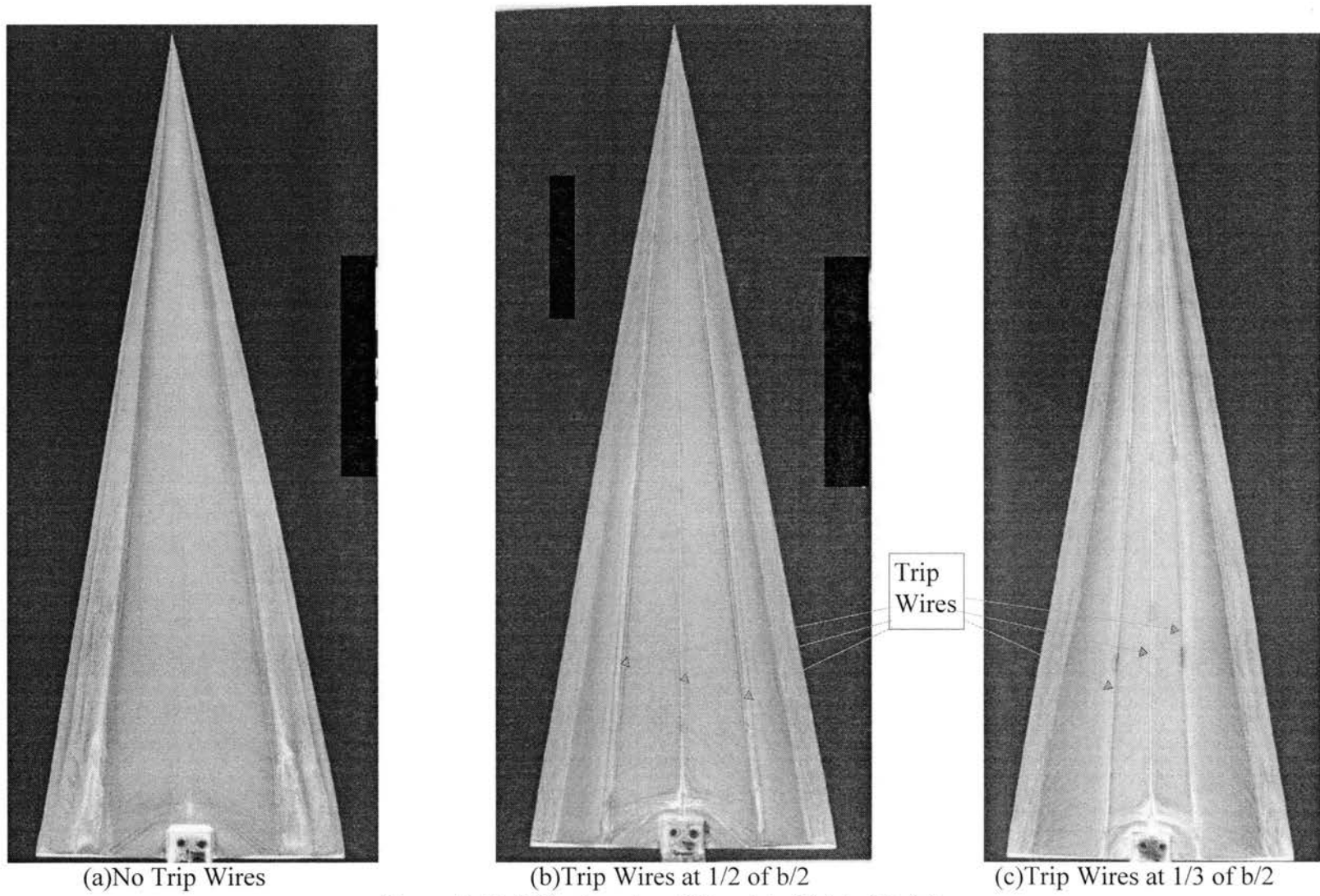


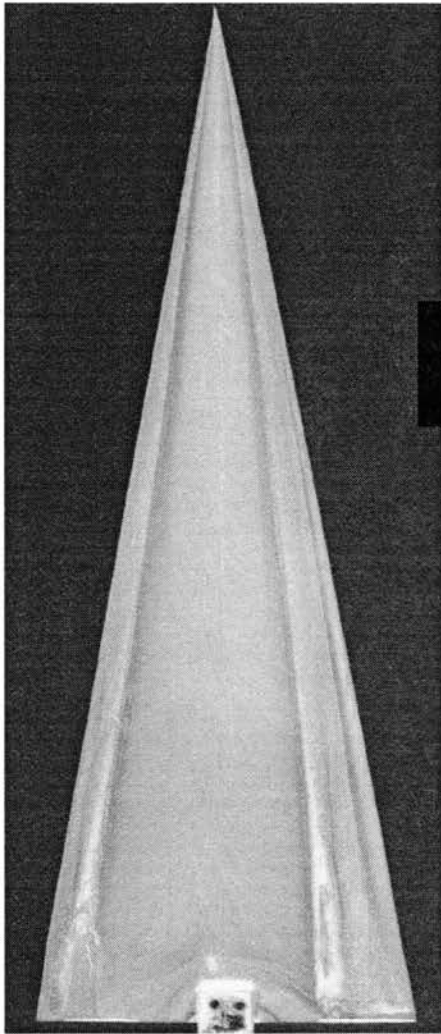
Figure 6.14. Vortex breakdown effect on a 80° wing at $\alpha=40^\circ$ and $\phi=0^\circ$.

For one experiment trip wires were placed at $1/2$ of the semi-span location and at the centerline, and in another experiment at $1/3$ of the semi-span, measured from the center of the wing and at the centerline of the wing.

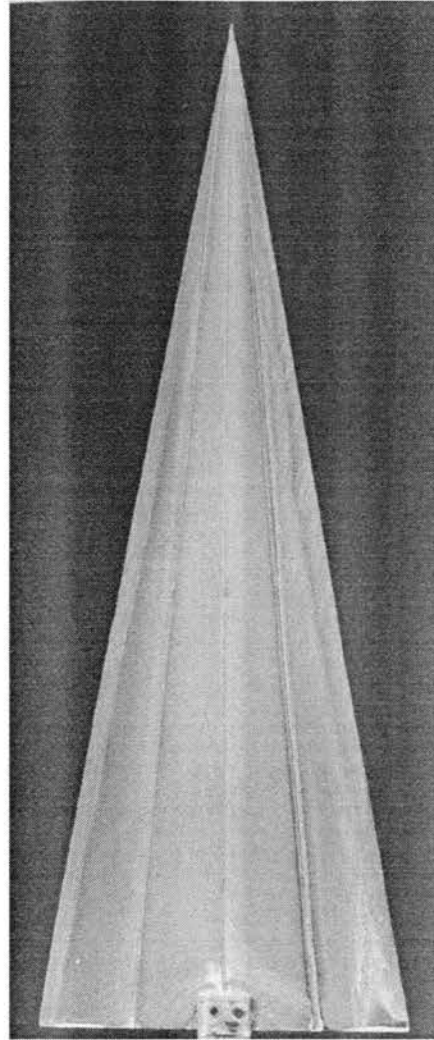
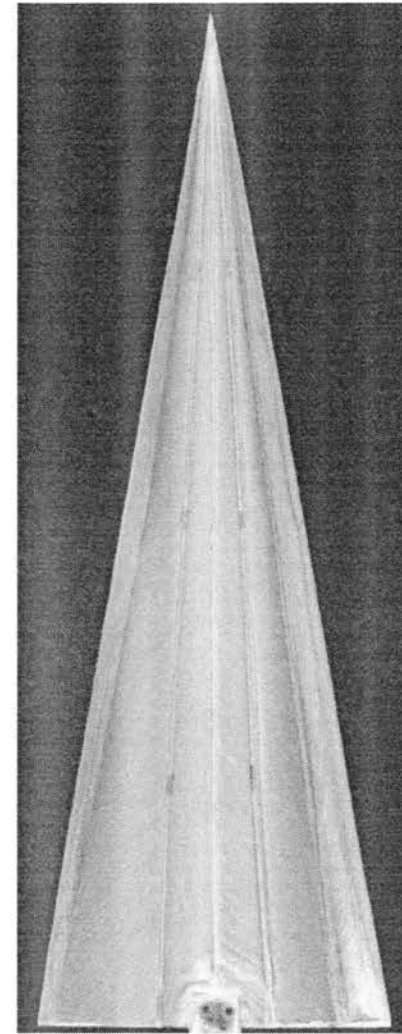
Due to the number of photographs taken, only the results for the 80° wing at 30° angle of attack and 0° , 10° , 20° , and 30° roll angles are shown. The results obtained at 15° , 30° and 40° angle of attack at 0° roll angle are also shown.

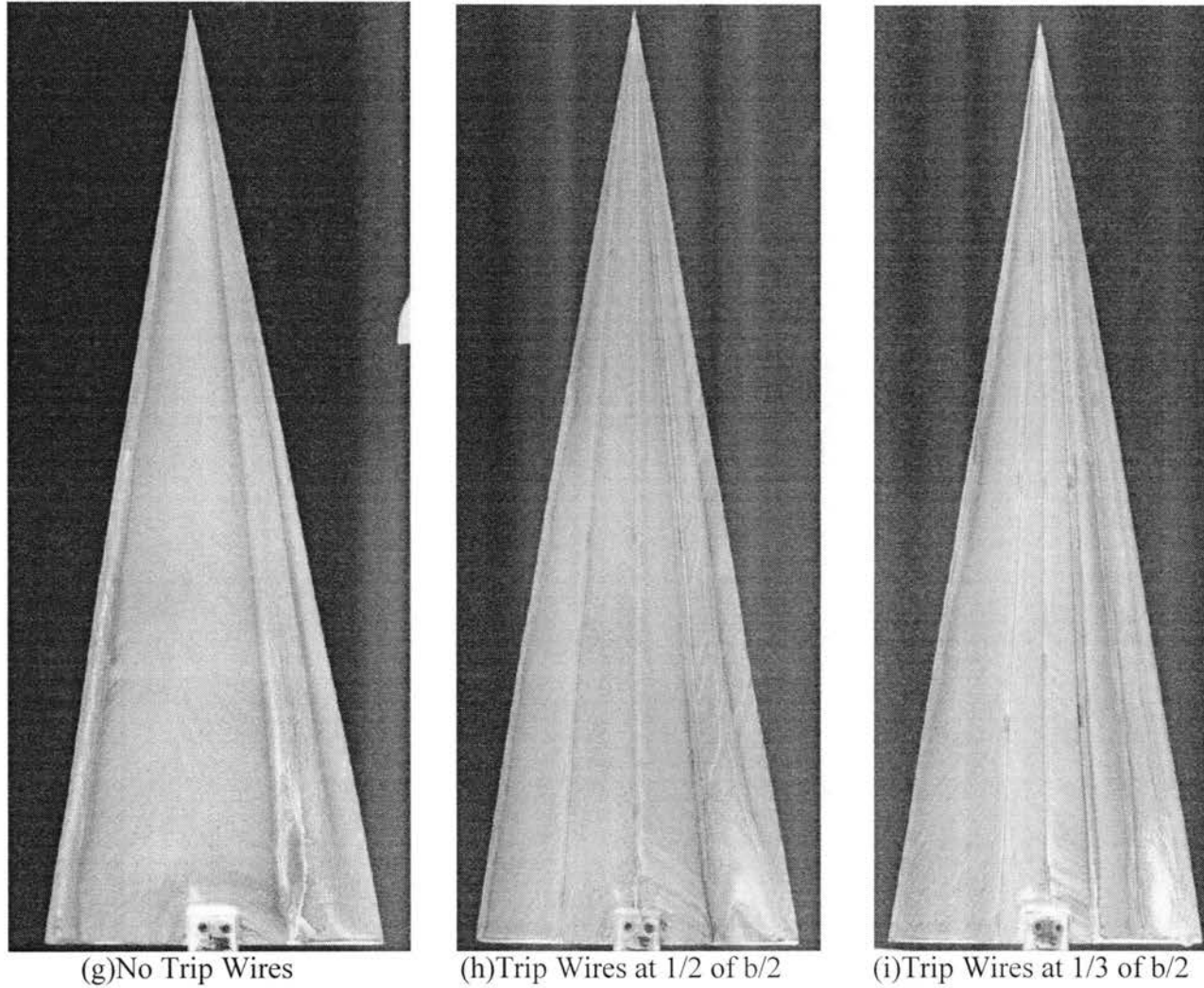
Figure 6.15 through figure 6.18 shows the surface flow visualization results for the 80° wing at 30° angle of attack and at different roll angles for different trip wires location. Photo (a), looks similar to that obtained by other researchers in that the primary reattachment is visible along the centerline, and the secondary and tertiary separation lines are clearly visible. For photos (b) and (c), the trip wires clearly moved the secondary separation line closer to the leading edge of the wing. Both photos show the secondary separation line on the same position on the wing. There is a small difference between the two photographs. Photo (b) has line right after the trip wires, which does not appear on photo (c). It is speculated that this line could be the secondary separation line, or it could be the reattachment line of the boundary layer, right after it was tripped, as shown in the surface pressure measurement. As the wing is rolled to a larger roll angle, the primary reattachment line, and secondary and tertiary separation lines move toward the upward side of the wing, photos (d), (g) and (j). For the wing with trip wires at $1/2$ of the semi-span, the primary reattachment line and the secondary and tertiary separation lines also moved toward the upward wing. The difference is that there is no separation line on photo (e), which indicates that the line is right over the trip wire.

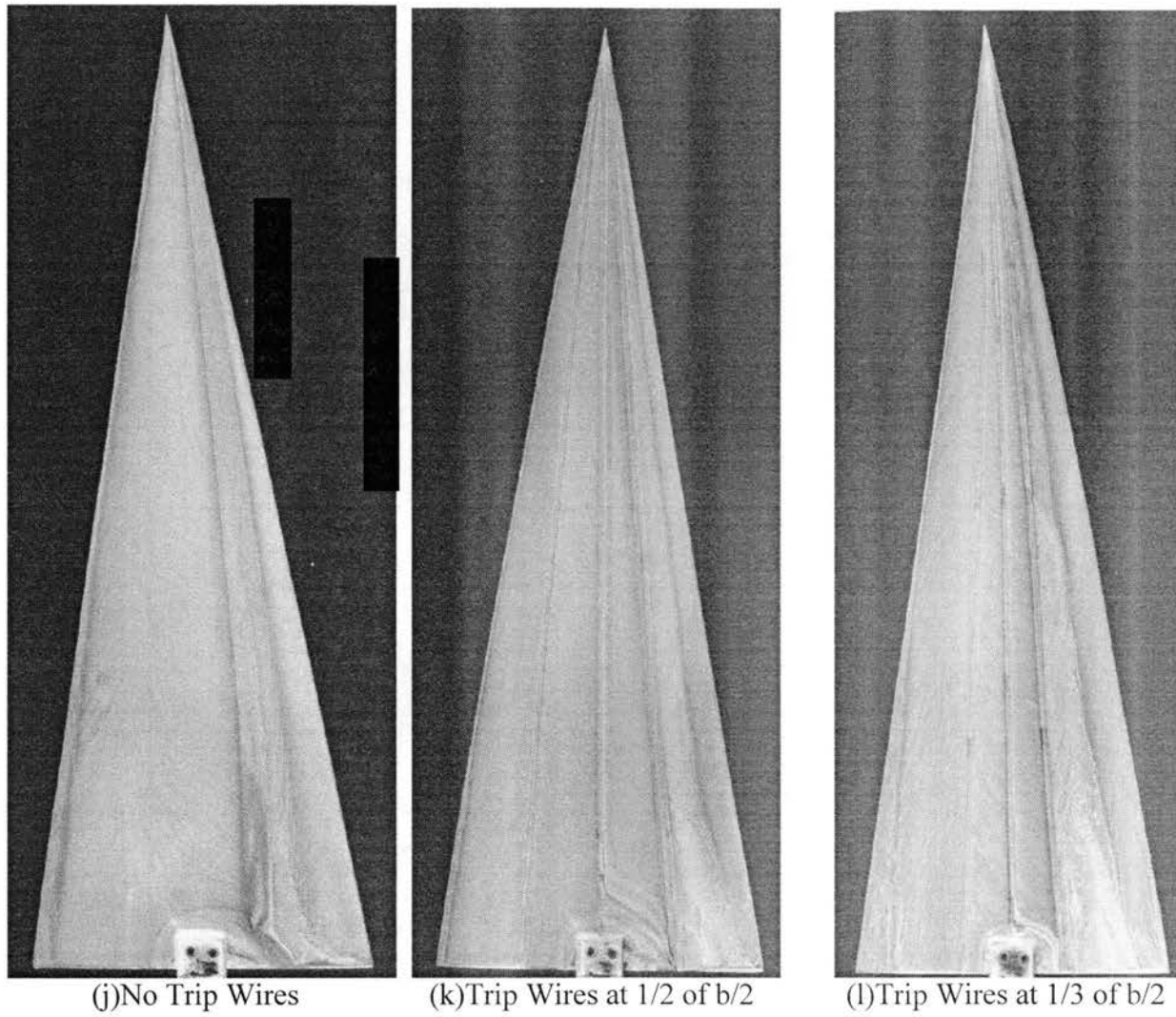




(d) No Trip Wires

(e) Trip Wires at $1/2$ of $b/2$ (f) Trip Wires at $1/3$ of $b/2$ Figure 6.16. 80° wing at $\alpha=30^\circ$ and $\phi=10^\circ$ (d), (e), (f).



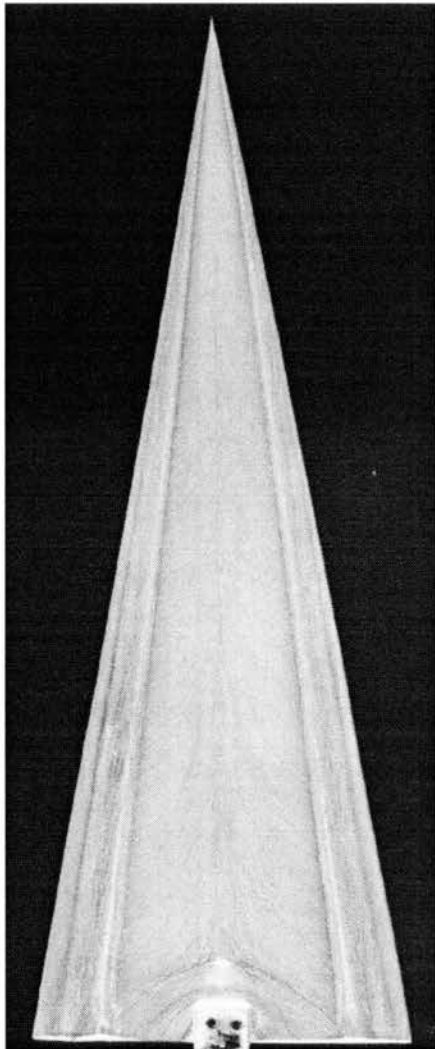


For photos (h) and (k) the secondary separation line can be seen before the trip wire, making it ineffective in tripping the boundary layer. On the other hand when the trip wires are placed at 1/3 of the centerline, they seem to be effective up to 20° roll angle, photos (f) and (i). For a roll angle of 30°, the secondary separation line coincides with the trip wire.

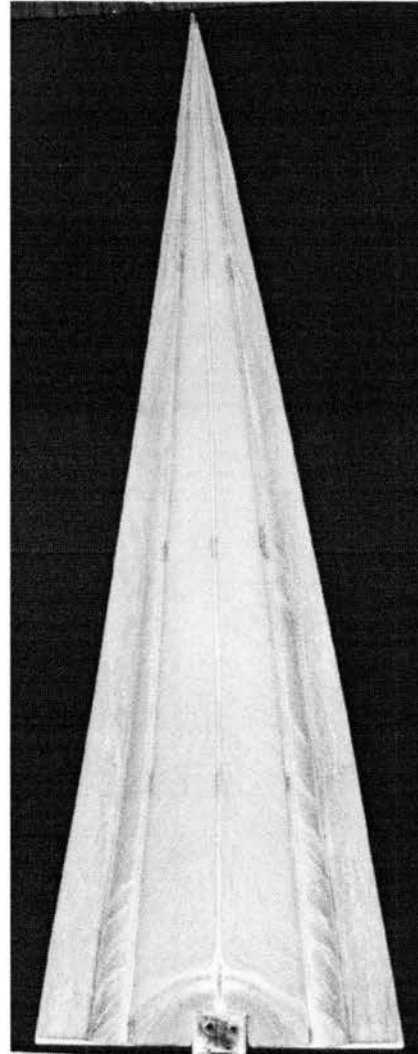
The results indicate that for the wing without trip wire, the primary reattachment line as well as the secondary and tertiary separation lines move toward the upward side of the wing, as the wing rolls. The trip wires do delay separation up to a roll angle where the separation line does not coincide with the trip wires.

From figures 6.19 and 6.20, it can be seen that by changing the angle of attack, from 30° to 15° and keeping the roll angle constant, the secondary separation point moves towards the center of the wing, as shown in figures 6.19(b),(c) and 6.20(e),(f). The location of the secondary separation is the same for both trip wires: located at 1/2 of the semi-span and 1/3 of the semi-span. This indicates that Reynolds number is not only important for the wing at different roll angles, but also at different angles of attack.

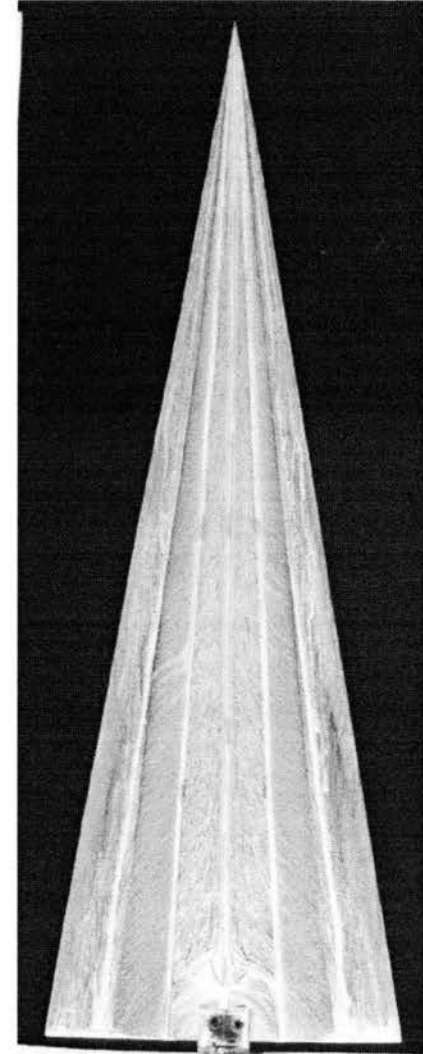
The graphics in figure 6.21 show a quantitative view of the secondary separation lines for 15° and 30° angles of attack at several roll angles. The data was taken from the pictures shown in figures 6.19 and 6.20 for 0° angle of attack. The secondary separation line was measured at 75% of the chord station for each of the pictures. Since the pictures do not have the same size, the position of the secondary separation line was non-dimensionalized by each local semi-span. As it can be seen from the figure, for the wing without trip wires, as the wing rolls right, the secondary separation lines move toward the upward side of the wing.



(a) No Trip Wires

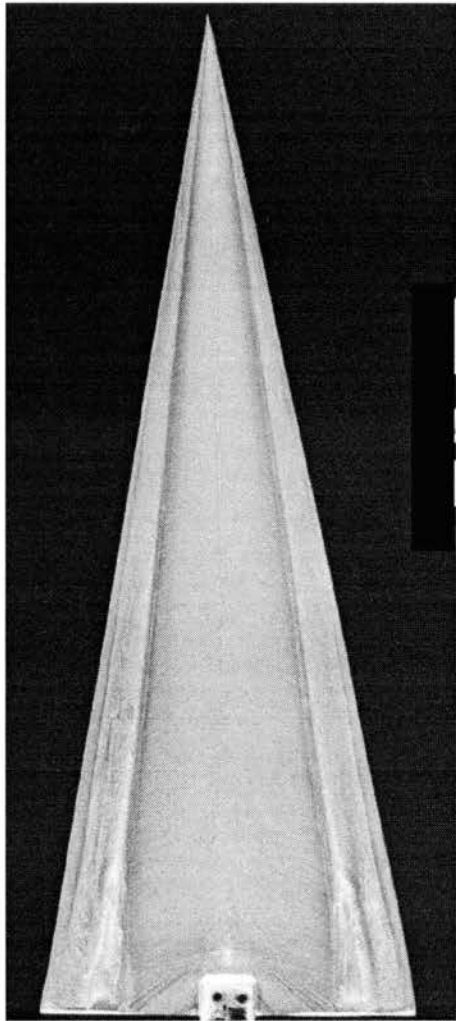


(b) Trip Wires at $1/2$ of $b/2$

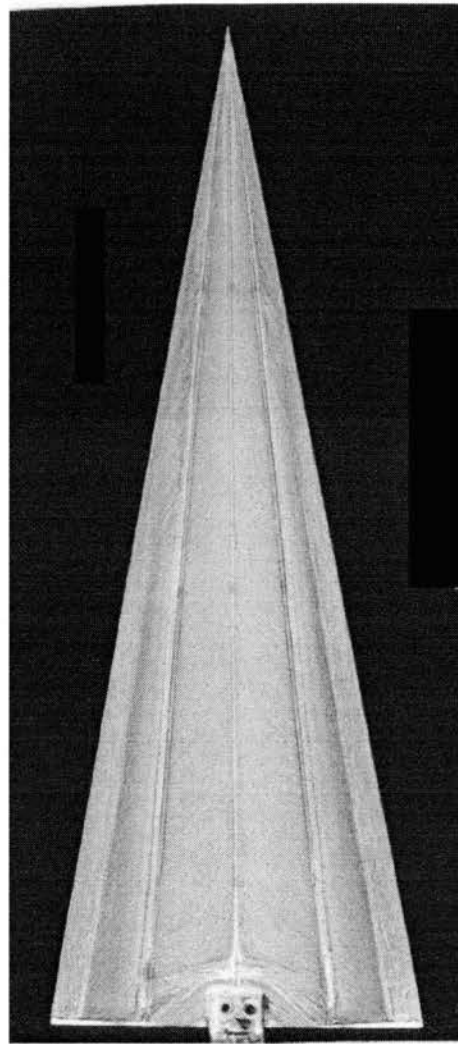


(c) Trip Wires at $1/3$ of $b/2$

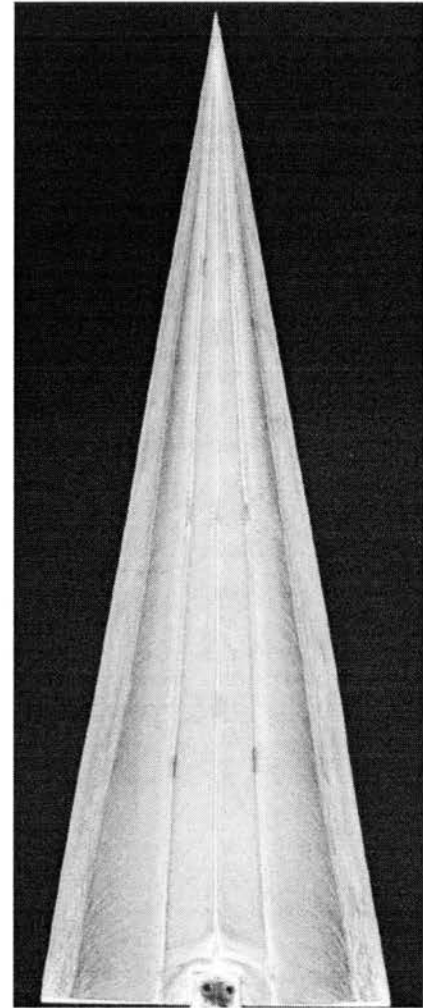
Figure 6.19. 80° wing at $\alpha=15^\circ$ and $\phi=0^\circ$ (a), (b), (c).



(d) No Trip Wires



(e) Trip Wires at $1/2$ of $b/2$



(f) Trip Wires at $1/3$ of $b/2$

Figure 6.20. 80° wing at $\alpha=30^\circ$ and $\phi=0^\circ$ (d), (e), (f).

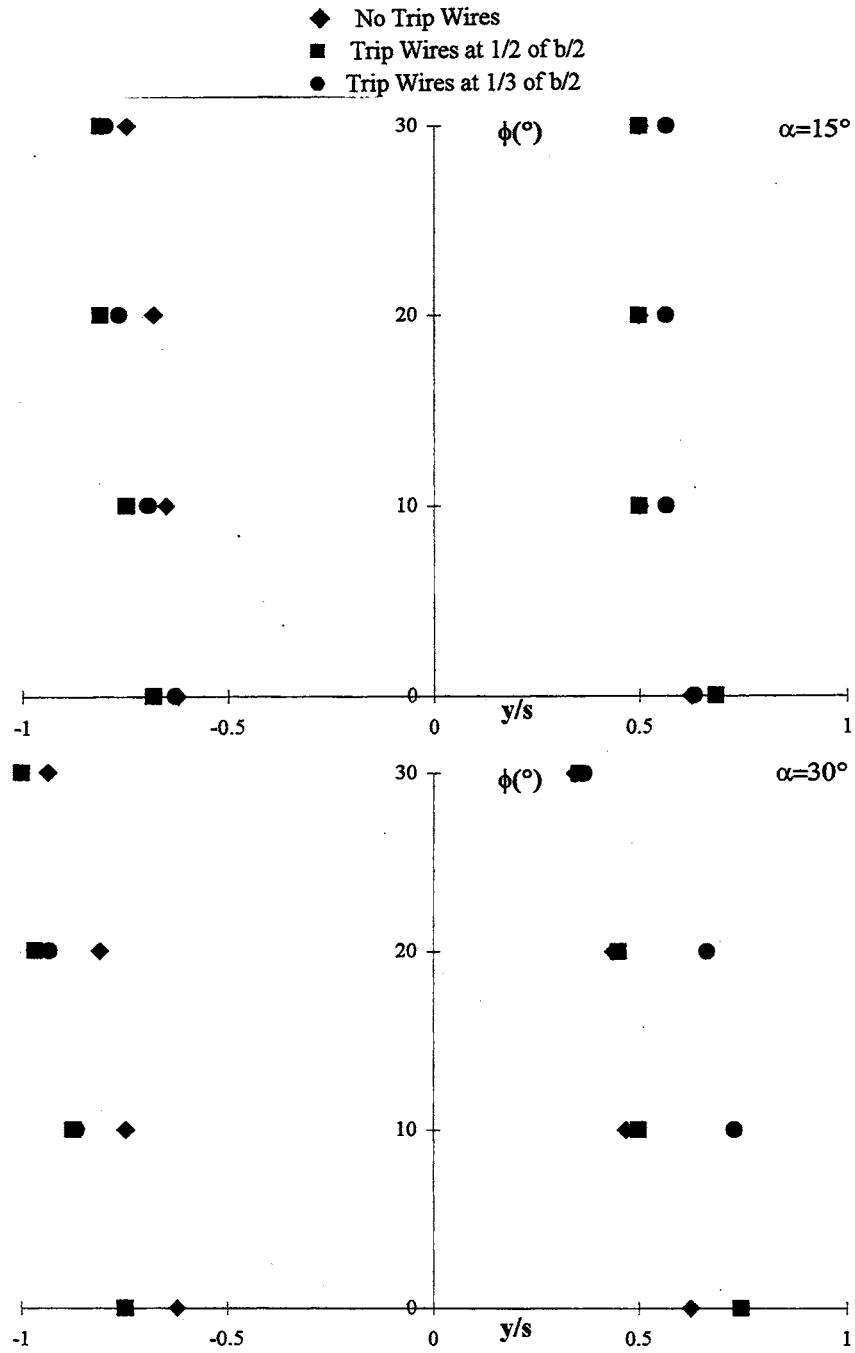


Figure 6.21. Secondary separation line for the 80° wing at $\alpha=15^\circ$ and 30° .

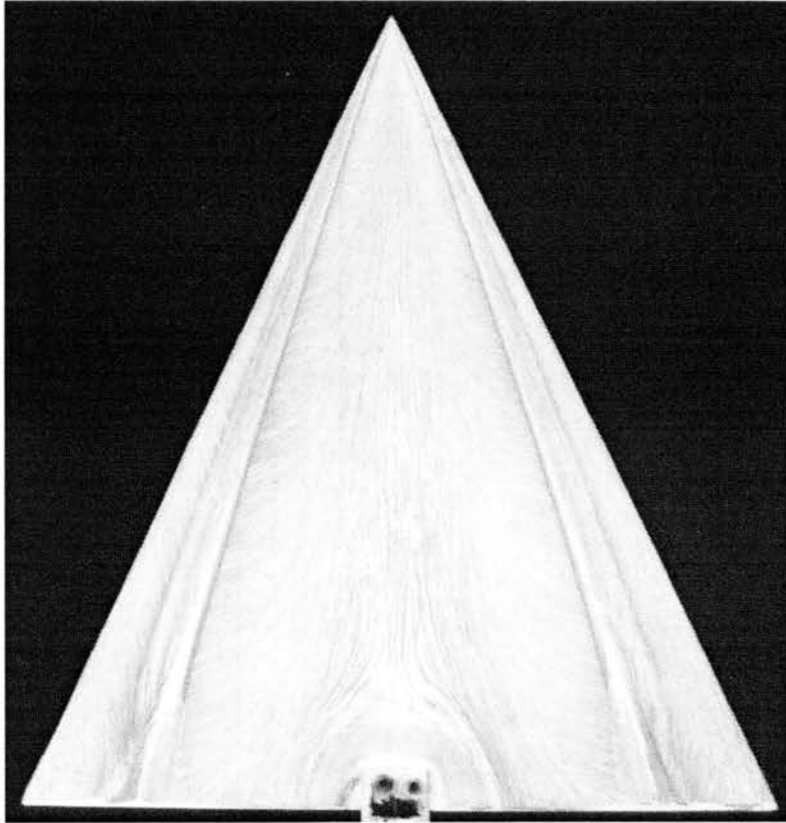
When the trip wires are placed at 1/2 of the semi-span, the right separation has a different behavior than the left separation line. On the left side of the wing the trip wire is able to delay separation all the way up to 30° roll angle for both angles of attack. On the right side of the wing the trip wire is only effective up to the point where the separation

line coincides with the trip wire itself. For the trip wire placed at 1/2 of the semi-span, the right separation line is effective up to 10° roll angle for both angles of attack. For the trip wire placed at 1/3 of the semi-span, measured from the center of the wing, the trip wire is effective up to 30° roll angle for 15° angle of attack, and up to 20° roll angle for 30° angle of attack. After that point the trip wire becomes ineffective because the separation line coincides with the trip wire.

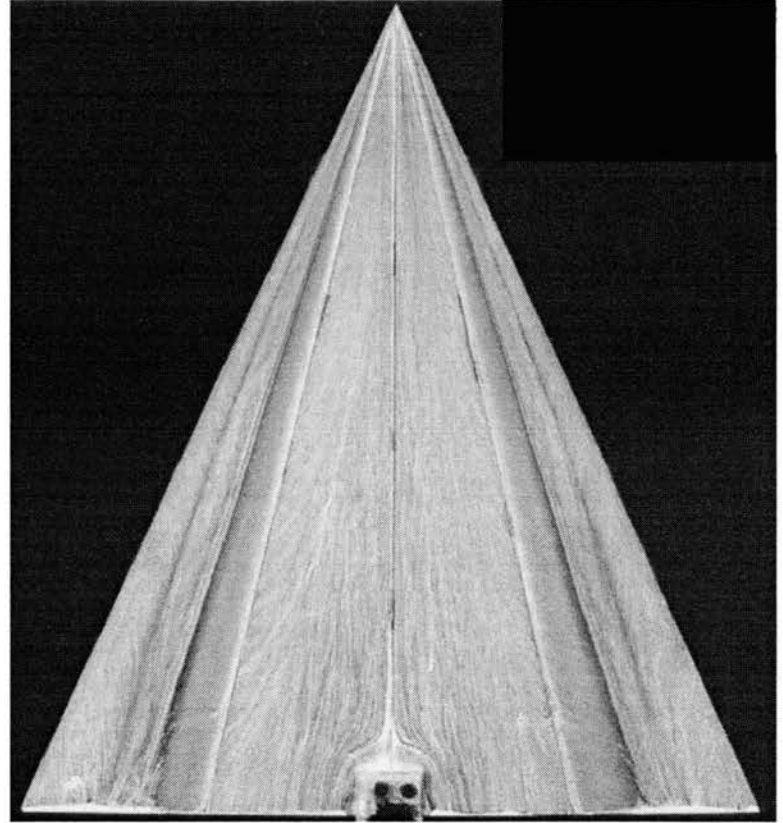
6.4.2 Static Surface Flow Visualization for the 65° Delta Wing

The trip wires had the same effect on the 65° wing that they had on the 80° wing. For the wing at 15° angle of attack at several roll angles, they were able to move the secondary separation line toward the leading edge of the wing, as shown in figure 6.22 through 6.25. The photographs in figure 6.22(a) and (b) clearly show that the trip wires not only move the secondary separation line toward the leading edge of the wing, but is also able to reattach part of the boundary layer that separated close to the trailing edge of the wing, in figure 6.22(a). From the pictures the secondary separation line was moved by 8% towards the leading edge from its original position, when measured from the wing without trip wires. The measurement was made at 85% chord station. As the wing is rolled the same effect can be noticed on the other figures.

When the wing was kept at 0° roll angle, and the angle of attack was increased, starting at 10°, the boundary layer start to show signs of vortex breakdown discussed previously for the 80° wing. The secondary separation line start to curve from half of the wing to the trailing edge. Figures 6.26 to 6.29, show the wing at 0° roll angle, and at 10°, 15°, 20°, and 30° angle of attack.

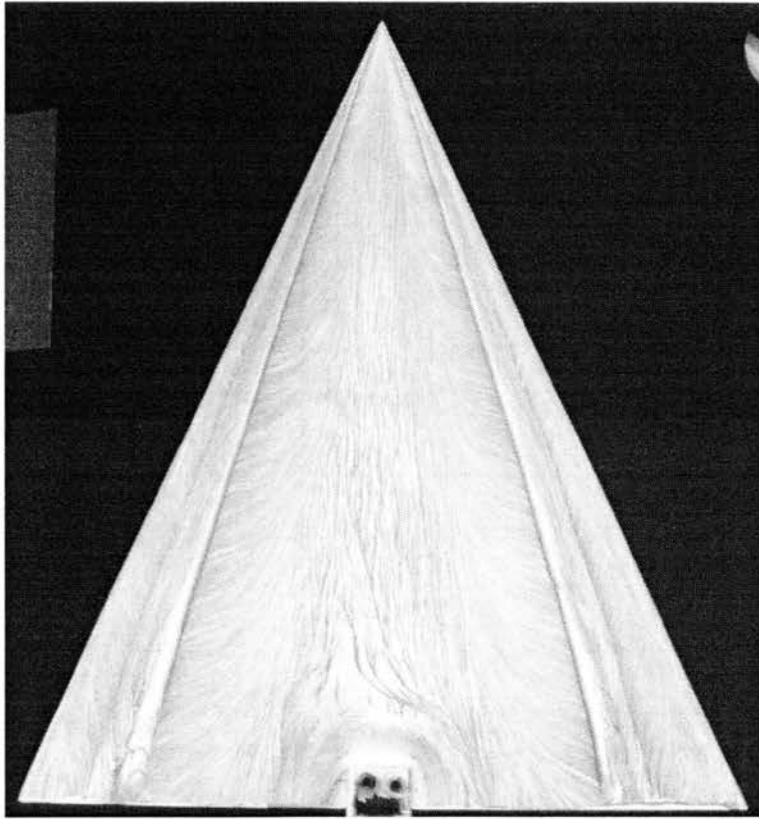


(a) No Trip Wires

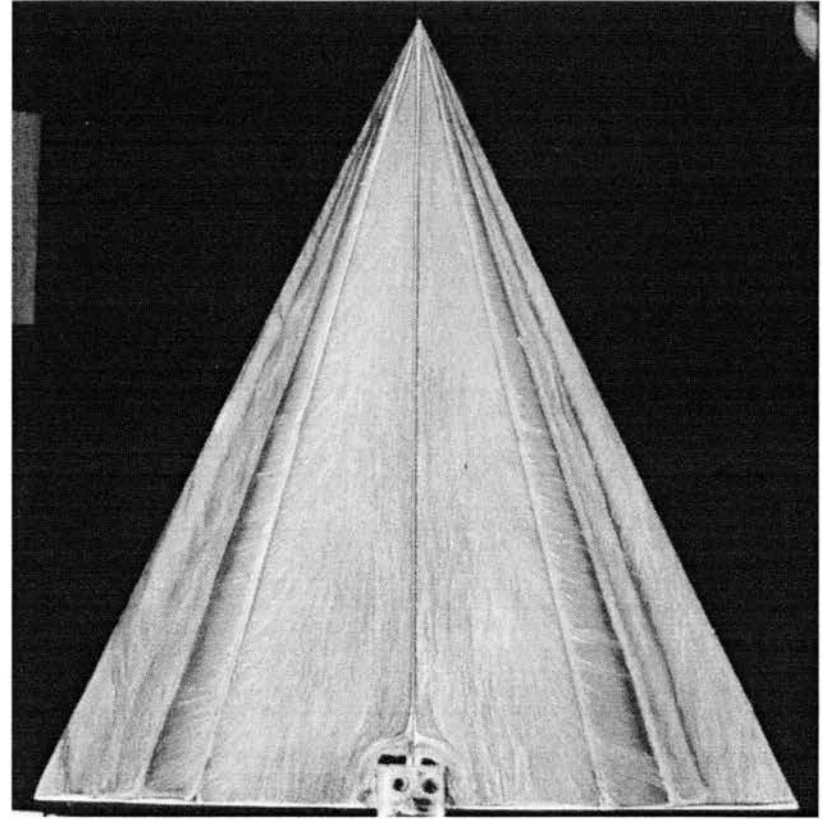


(b) Trip Wires are $1/2$ of $b/2$

Figure 6.22. 65° wing at $\alpha=15^\circ$ and $\phi=0^\circ$ (a) and (b)

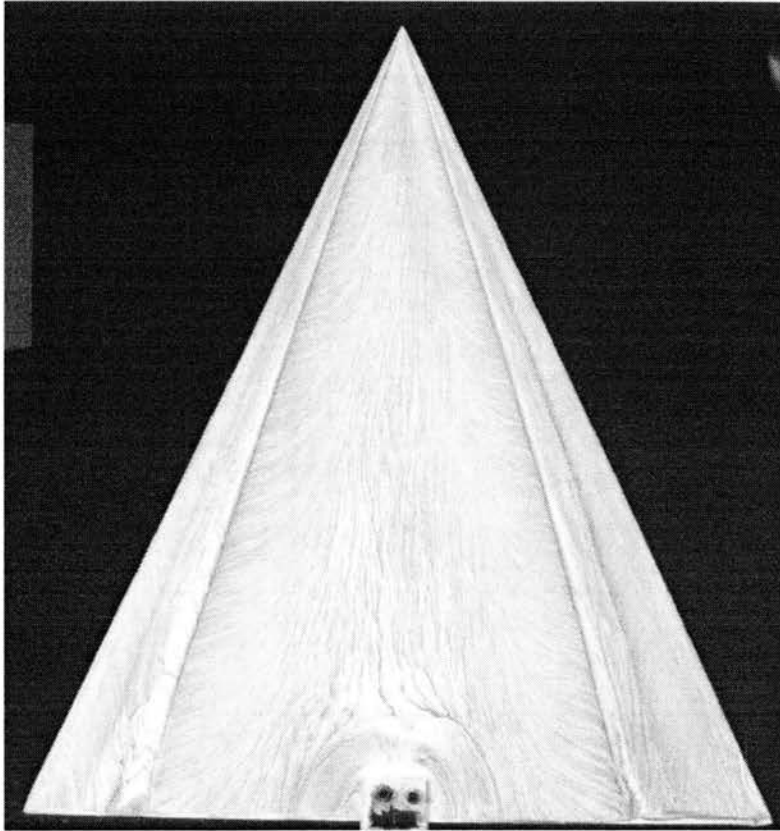


(c) No Trip Wires

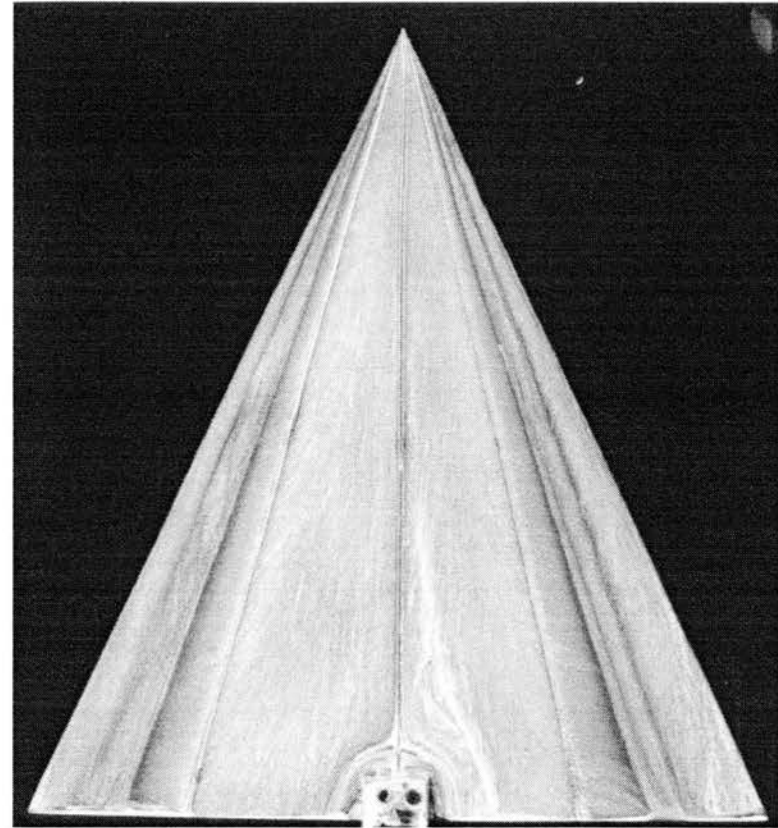


(d) Trip Wires at $\frac{1}{2}$ of $b/2$

Figure 6.23. 65° wing at $\alpha=15^\circ$ and $\phi=10^\circ$ (c) and (d).

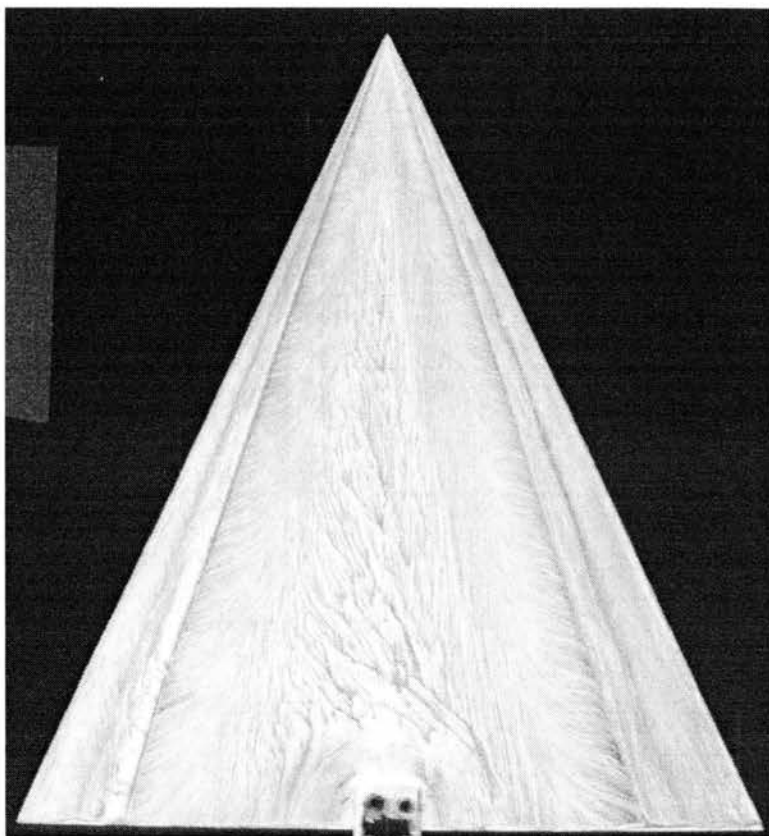


(e) No Trip Wires

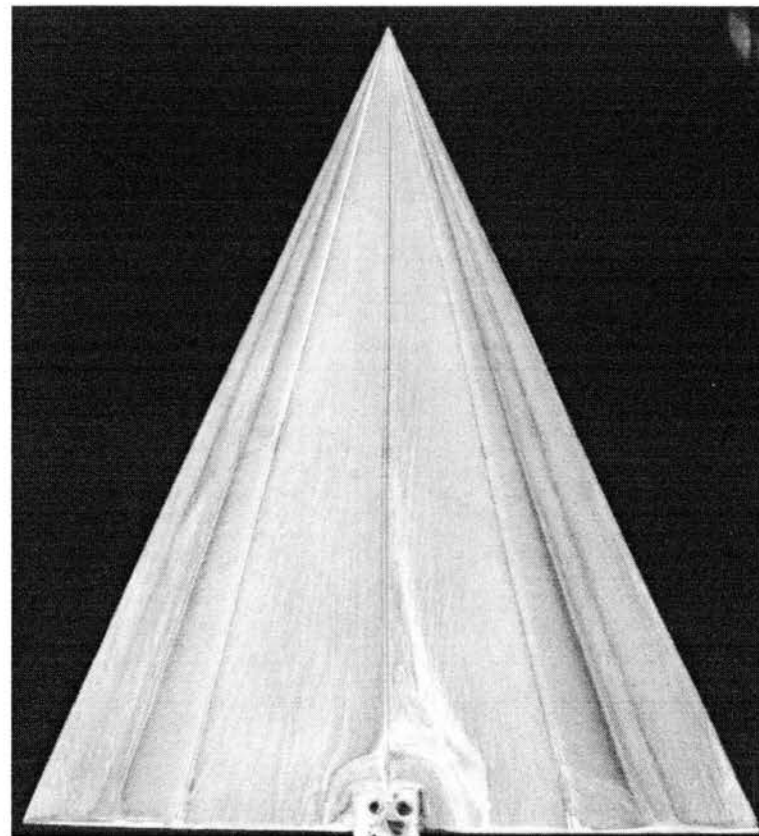


(f) Trip Wires at $1/2$ of $b/2$

Figure 6.24. 65° wing at $\alpha=15^\circ$ and $\phi=20^\circ$ (e) and (f)

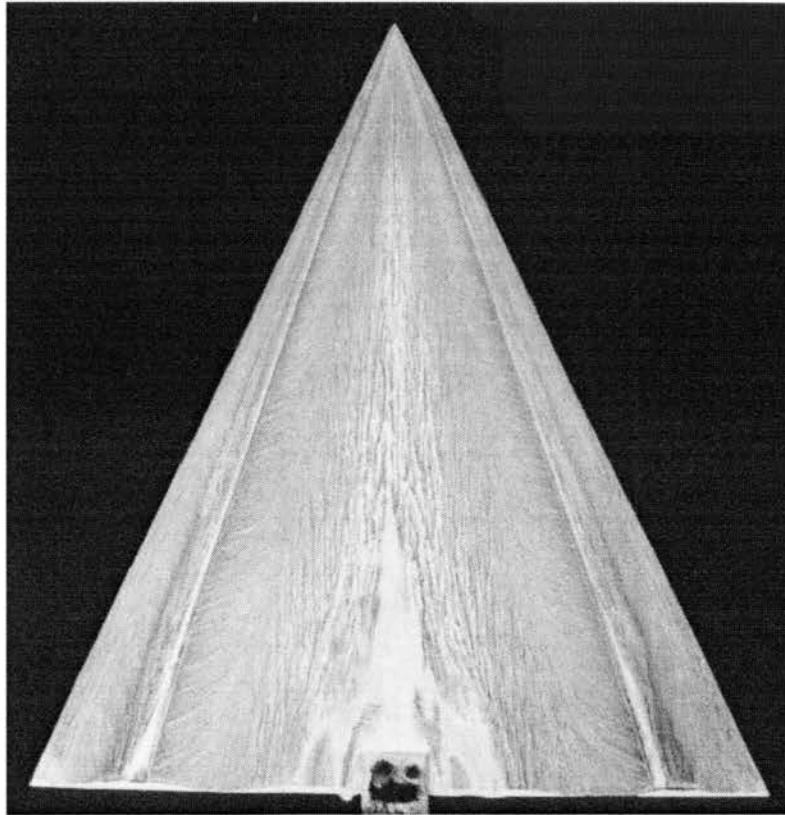


(g) No Trip Wires

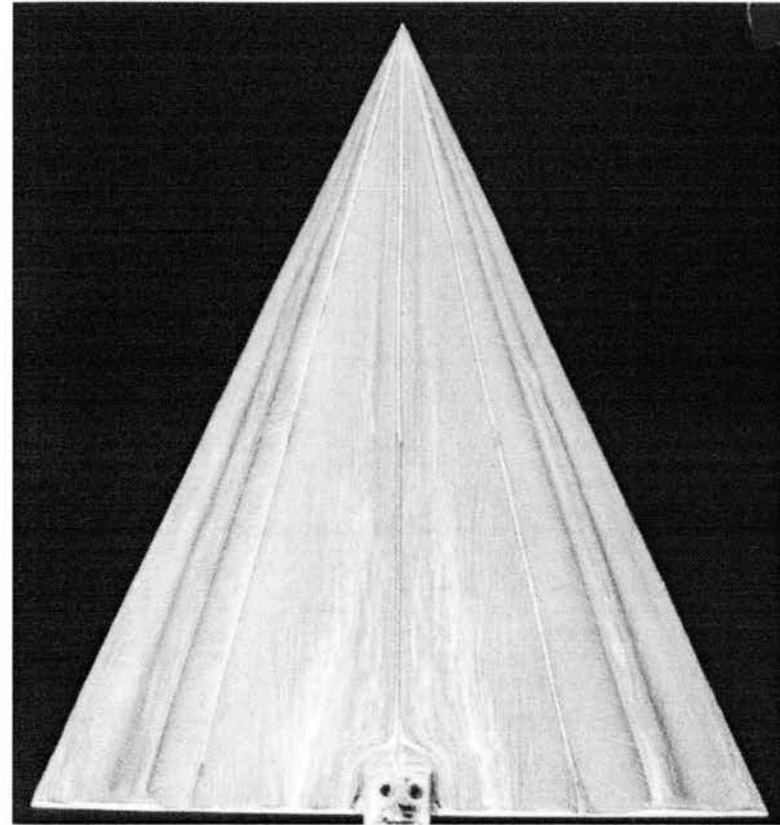


(h) Trip Wires at 1/2 of b/2

Figure 6.25. 65° wing at $\alpha=15^\circ$ and $\phi=30^\circ$ (g) and (h)

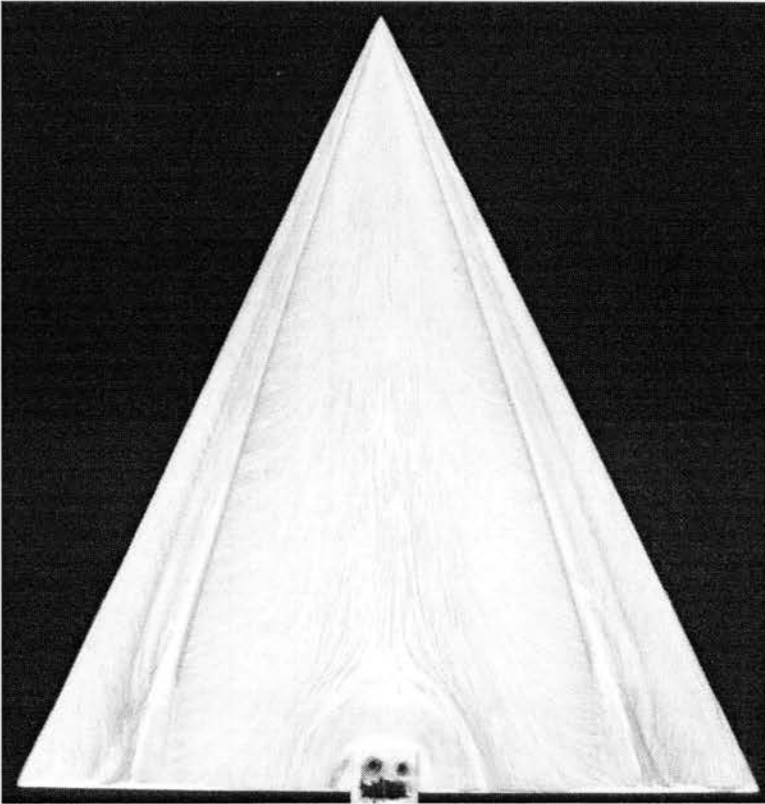


(a) No Trip Wires

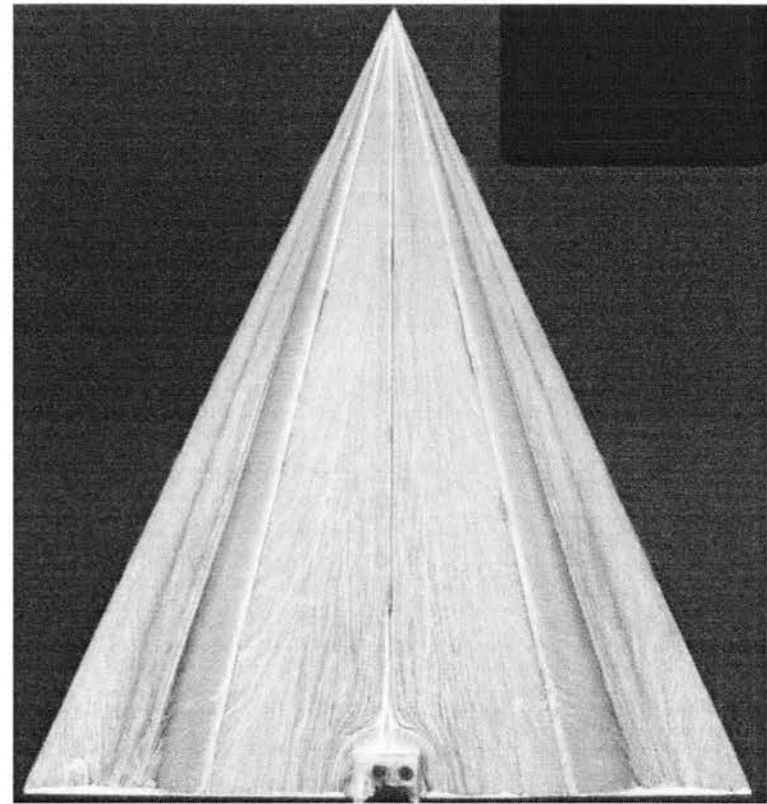


(b) Trip Wires at 1/2 of b/2

Figure 6.26. 65° wing at $\alpha=10^\circ$ and $\phi=0^\circ$ (a) and (b).

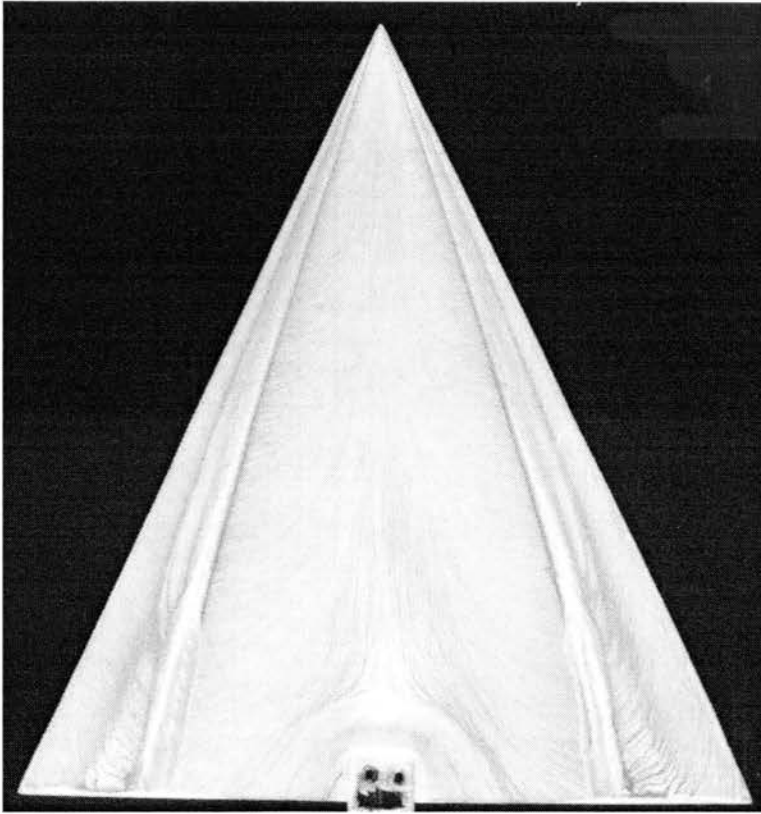


(c) No Trip Wires

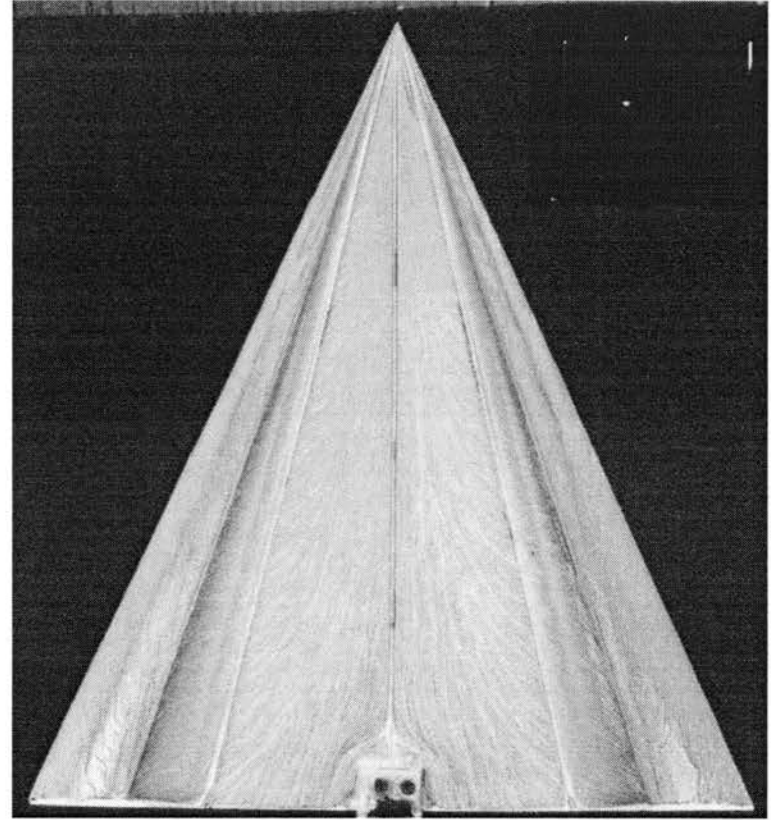


(d) Trip Wires at 1/2 of b/2

Figure 6.27. 65° wing at $\alpha=15^\circ$ and $\phi=0^\circ$ (c) and (d).

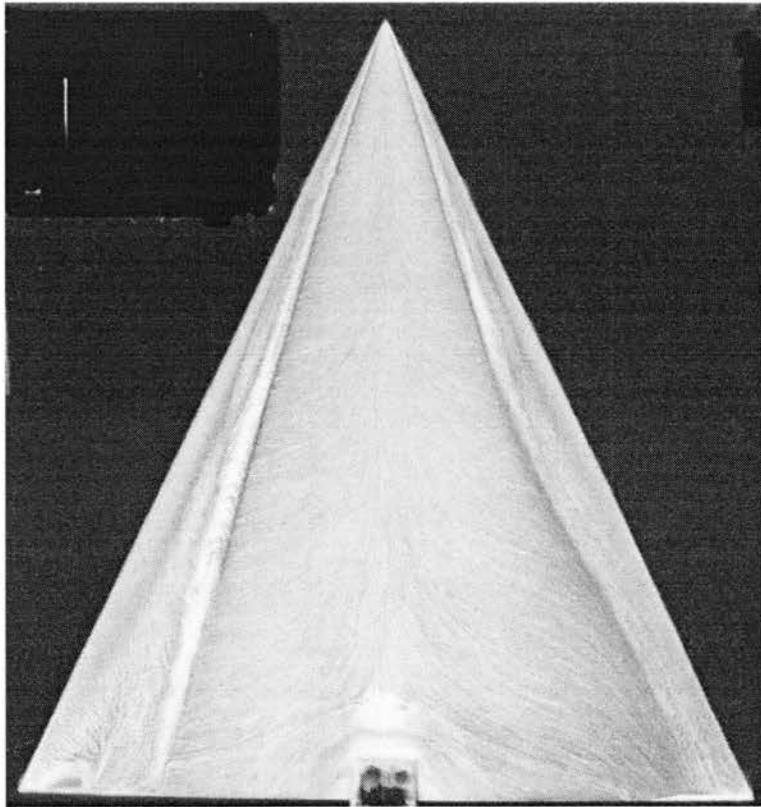


(e) No Trip Wires

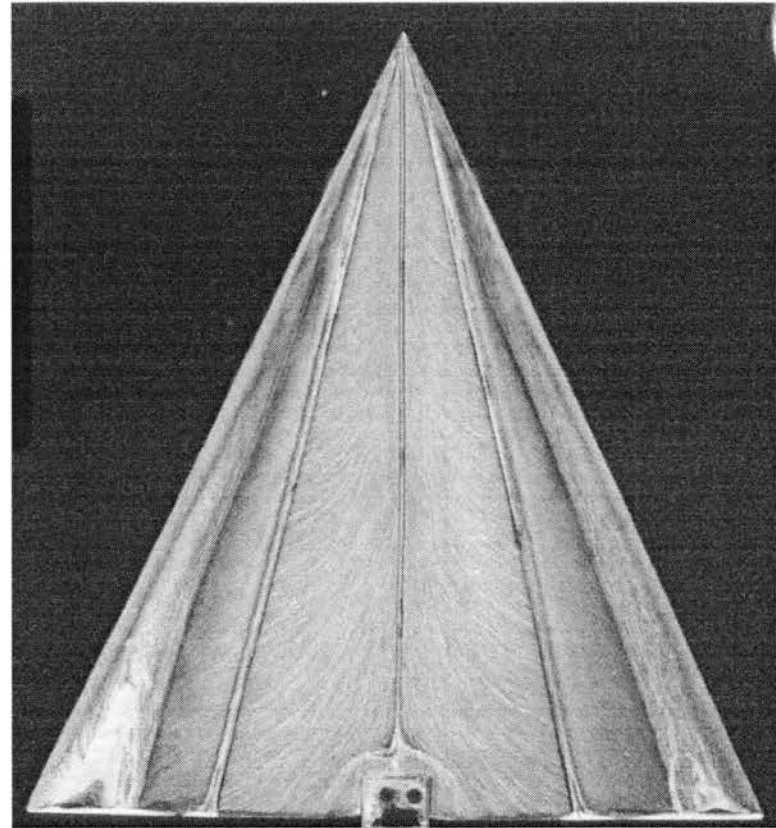


(f) Trip Wires at $1/2$ of $b/2$

Figure 6.28. 65° wing at $\alpha=20^\circ$ and $\phi=0^\circ$ (e) and (f).



(g) No Trip Wires



(h) Trip Wires at $1/2$ of $b/2$

Figure 6.29. 65° wing at $\alpha=30^\circ$ and $\phi=0^\circ$ (g) and (h).

At 10° angle of attack the secondary separation line does not seem to change position with the trip wire, indicating that the trip wire may not have an effect at this angle of attack. As the angle of attack increases to 15° and 20° , the secondary separation line seems to vanish at about $1/3$ of the chord from the trailing edge of the wing. This is theorized to be an end effect of the vortices on the oil used for flow visualization. This means that at the trailing edge of the wings the vortices are not strong enough to move the oil, which makes the oil to run off on the trailing edge. It is interesting to notice that, the same reattachment of this end effect showed for the wing at 15° angle of attack is shown at 20° angle of attack, shown in figure 6.28(e) and (f). As the angle of attack is further increased to 30° , vortex breakdown occurs as shown in figure 6.29(g). From figure 6.29(h) it appears that at the trailing edge of the wing, the trip wires were able to prevent vortex breakdown, but when looking close to the apex of the wing, it seems that vortex breakdown is still present. At this point there is no guarantee that the trip wires did prevent vortex breakdown. Further investigation may be necessary to determine this theory.

From the results it is concluded that the change in Reynolds number does affect the flow over the 65° and 80° delta wings at high angles of attack and at different roll angles.

6.5 Free to Roll System

Free to roll experiments were performed to verify dynamically the reversal of roll moment observed on the 80° and 65° delta wings with asymmetric flap deflection. The experiments were conducted to qualitatively test the behavior of the wings at different angles of attack.

The tests were conducted with the flaps deflected at $\delta=25^\circ$ asymmetrically and for the wings placed at several angles of attack.

An interesting phenomenon occurred as the angle of attack changed. The wings either rolled left, did not roll or made a static roll to the right. Both wings had this behavior, but it occurred at different angles of attack, as shown in the roll moment coefficient plots in figures 6.3 and 6.5. A qualitative plot of the behavior of the wings is shown in figure 6.30.

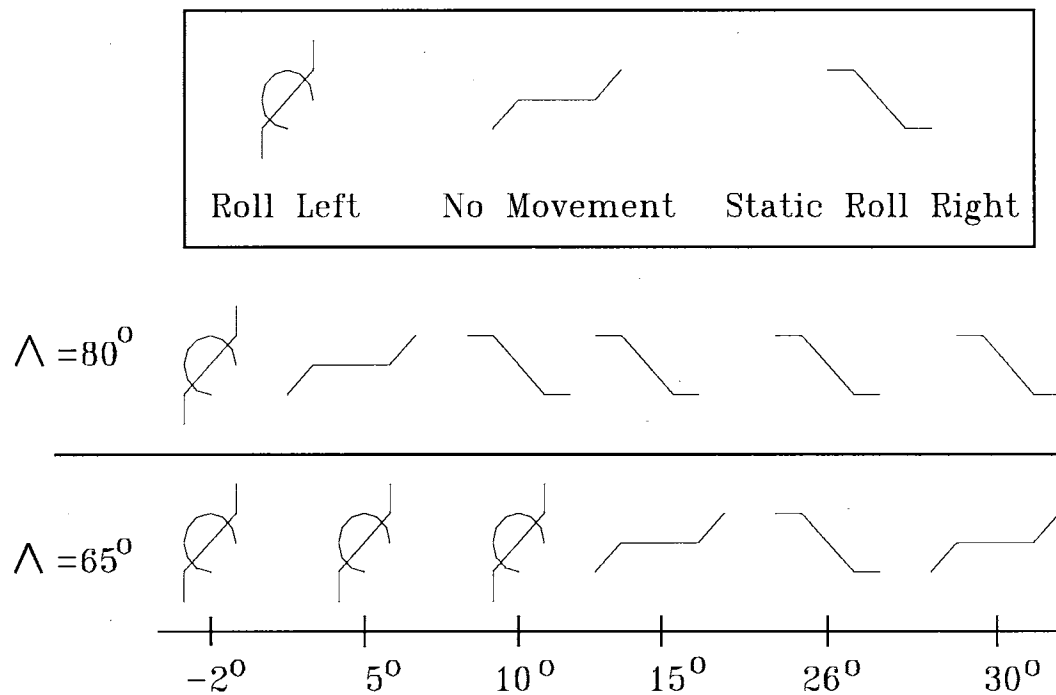


Figure 6.30. Behavior of the delta wings for different angles of attack.

The 80° wing rolled left for $\alpha = -2^\circ$ to 6° , it did not roll for $\alpha \cong 7^\circ$ and it made a static roll to the right for $\alpha > 7^\circ$.

The 65° wing did also roll left, but for $\alpha = -2^\circ$ to 14° , it did not roll for $\alpha \cong 15^\circ$, and made a static roll to the right for $\alpha = 16^\circ$ to 30° .

Static roll in this case means that the wing started to roll and stop at some roll angle different than zero. When the wing rolled, it was a continuous roll, until the wind tunnel was turned off.

Comparing figure 6.30 with figures 6.3 and 6.5, the results are all consistent with each other. When the 80° delta wing with asymmetric flap deflection (left flap downward and right flap upward) is placed at angles of attack between 0° and 6° the wing does a dynamic roll to the right. When the wing is placed at approximately 7° angle of attack it does not roll, and when placed at angles of attack higher than 7° , it performs a static roll to the right.

6.6 Roll Reversal Phenomenon

The explanation for the behavior of the roll reversal on the wings when the flaps are deflected asymmetrically, may be understood by considering both longitudinal and lateral flow effects. At low angles of attack, 0° to 4° for the 80° wing and 0° to 14° for the 65° , as the leading edge flap is deflected upwards, the local angle of attack is increased, as shown in figure 6.31, and vice versa on the opposite flap. This will increase the effective angle of attack, consequently increasing the lift on the upward flap. This creates a roll moment toward the downward deflected flap as shown in figure 6.3 for the 80° delta wing and figure 6.5 for the 65° delta wing. The roll moment generates a continuous roll on the wing toward the downward flap, as seen in the free to roll experiments.

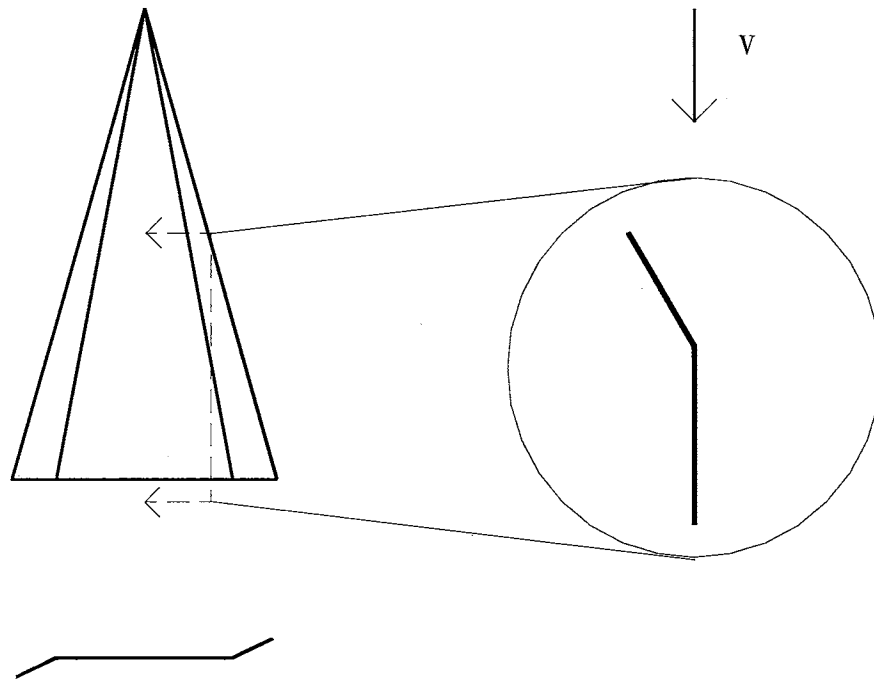


Figure 6.31. Flap effect at low angles of attack.

Conversely, at larger angles of attack, 10° to 32° for the 80° delta wing and 16° to 32° for the 65° wing, the crossflow becomes dominant due to the leading edge vortex formation. A downward deflected flap results in stronger vortex closer to the wing as shown in figure 6.32. This result is confirmed by the pressure distribution shown in figure 6.10, for several angles of attack, and by the roll moment coefficient distribution seen in figures 6.3 and 6.5 for the 80° and 65° wings respectively. As the angle of attack increases, the vortices over the wing start to form. Figure 6.10 shows that the downward flap has a stronger vortex than the right flap. This was confirmed by Marchman (1981), and Marchman and Thomas (1981), in two separate works, where it was shown that flaps deflected downward generate stronger vortices than flaps deflected upward. The difference is that in his work the flaps were never deflected asymmetrically. Since the

downward flap deflected vortex has a higher pressure than the upward flap deflected vortex, the wing generates a moment to the right as shown in figure 6.3 and 6.5.

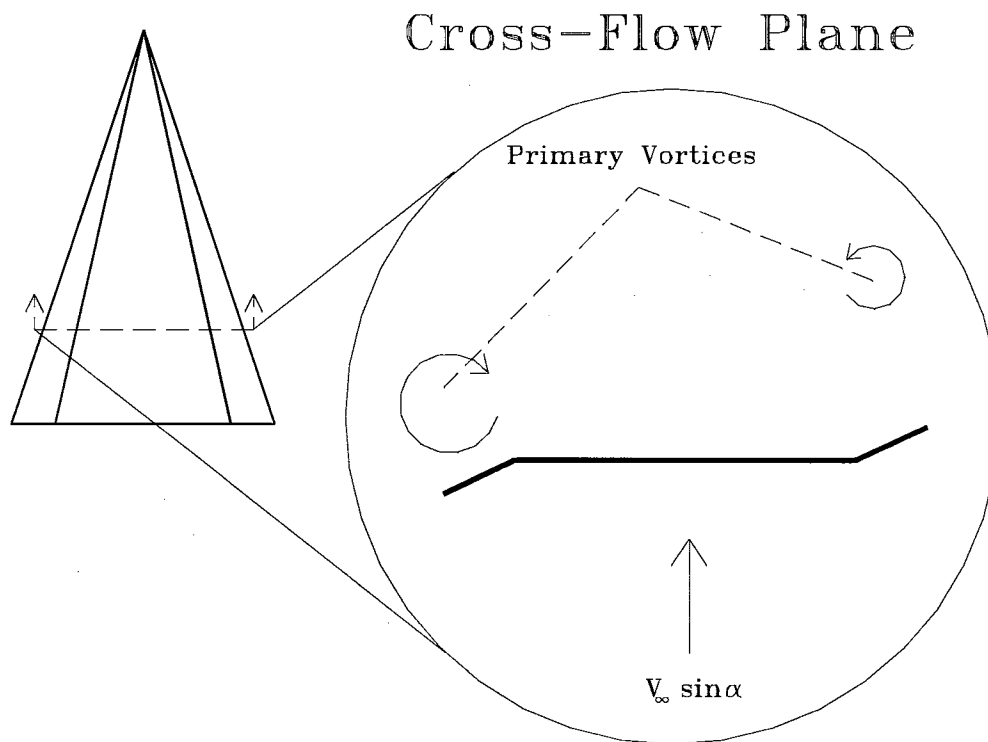


Figure 6.32. Change in vortex position, for asymmetric flap deflection on the 80° wing.

But as the wing rolls, the flap deflection changes the strength of the vortices, as shown in figure 6.12(a). At a certain roll angle, between 8° and 12° , the pressure distribution over both sides of the wing becomes similar figure 6.12(b), and the wing stops to roll. This was confirmed by the free to roll experiments, where the wing would make a static roll to the right when placed at 30° angle of attack and 0° roll angle and released.

This behavior would then be further modified by the appearance of vortex breakdown, on the 65° wing, which is suspect in creating the decrease in effectiveness beyond 26° angle of attack. This comes from the fact that for a 65° swept angle plain

wing, the vortex breakdown starts at $\alpha=19^\circ$ at the trailing edge and reaches the leading edge when the wing is at $\alpha=37^\circ$, as shown in figure 6.33, by Wentz and Kohlman (1971).

It is important to note that even through there have been several studies with LEVF's in delta wings with different sweep angles, the phenomenon of the wings rolling left, right and not rolling for different angles of attack, was never reported, to the best of my knowledge.

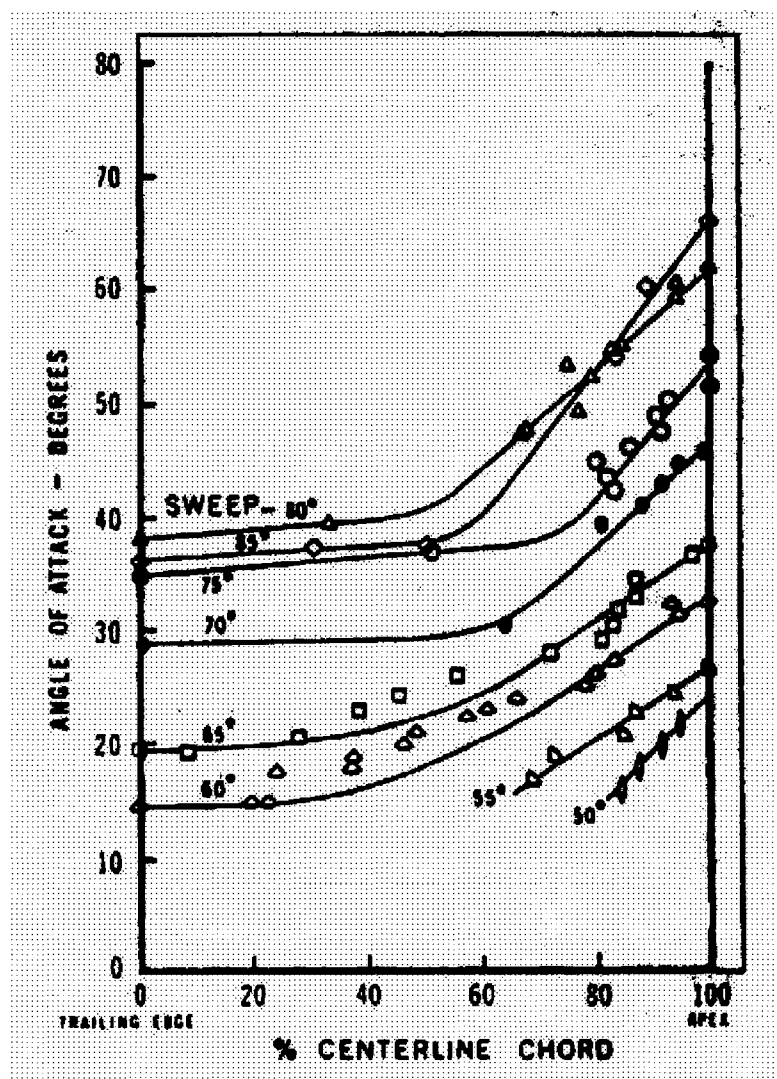


Figure 6.33. Vortex breakdown position for delta wings (Wentz and Kohlman 1971).

CHAPTER VII

CONCLUSIONS AND RECOMMENDATIONS

7.1 Conclusions

The conclusions section is divided into three major categories. Specific conclusions based on the results of the computational model are presented first. Similarly, conclusions based on the results of experiments performed on the 80° wings presented. Finally, specific conclusions based on the results of the experiments on the 65° wings are presented.

The goals of the use of the computer model were to assess the roles that the unsteady boundary condition and spanwise camber play in wing rock, and to apply these concepts in developing a control strategy for alleviating wing rock. Simulation data have been collected that indicate not only the quasi-steady and dynamical aspects of the model motion, but a wide range of data that are indicative of the fluid physics involved. Results indicate that quasi-steady effects have a damping effect on the motion primarily because of the hysteresis behavior of vortex position normal to the wing. Additionally, spanwise camber when applied proportional to roll rate has been shown to be capable of alleviating the wing rock motion by mitigating the lag in normal vortex position.

The results obtained by the flow visualization experiments for the 80° at 30° angle of attack and 0° roll angle, without flap deflection, and with and without trip wires are very similar to those obtained by Hummel (1978). It indicates that there is a difference on the primary reattachment point in the center of the wing, and on the secondary and tertiary separation points over the wing, when the trip wires are present. This is indicative that

Reynolds number is important when studying the flow over delta wings. As the wing rolls, the trip wires change the reattachment and separation points position, up to the point where secondary separation does not coincide with the trip wire location, as seen for the case where the trip wire was placed at 1/2 of the semi-span, at 10° roll angle, and for the case where the trip wire was placed at 1/3 of the semi-span, at 30° roll angle. If trip wires are used to study the turbulent boundary layer over the wing, the location where they are placed over the wing becomes very important, mainly if the wing is going to be studied in roll angles different than zero.

Results indicated that for angles of attack higher than 20° on the 80° delta wing there was a difference in the roll moment for the plain wing with and without trip wires. This prompted to concluded that the pressure distribution over the wing changes when the trip wires are present.

The pressure distribution data showed that when the wing is in roll, the pressure over the downward side is larger than the one on the upward side of the wing. Integrating the sectional pressure coefficient curves, it was found that the sectional roll moment coefficient is different, with and without trip wires. This is the reason why there is a change in the roll moment with the trip wires. For a roll angle of 30°, the pressure on the downward side drops drastically, indicating that there has been separation of the boundary layer. This was confirmed by the flow visualization experiments, showing that the secondary separation coincides with the trip wire, making it ineffective in tripping the boundary layer.

For a 25° asymmetric flap deflection (left flap downward and right flap upward) on the 80° delta wing, the roll moment results showed that an interesting phenomenon occurs

with the wing as the angle of attack goes from 0° to 32° , and when the wing is at 0° roll angle. For angles of attack between 0° to 5° , the wing has a negative roll moment. For an angle of attack of approximately 6° , the wing has roll moment equals to zero. For angles of attack higher than 6° up to 32° , the wing has a positive roll moment. There is a reversal in roll moment as the angle of attack increases. The increase would probably go up to 35° which is the angle where vortex breakdown starts to appear on the 80° delta wing.

The free to roll experiments showed that when the wing is placed at angles of attack from 0° to 5° , it has a continuous roll to the right. When placed at 6° angle of attack, the wing does not roll to either side. It just stays at 0° roll angle, with very small oscillations, like it is hovering. For angles of attack higher than 6° , the wing would make a static roll to the right. This means that it would roll a few degrees to the right and would stop. This is indicative that the pressure of the vortices over the wing balances each other and stops the roll of the wing.

Further investigation of the pressure determined that when the wing is at 0° roll angle, the pressure distribution over the wing is close to zero, for angles of attack from 0° to 5° . As the angle of attack increases the downward flap has a higher pressure than the upward flap, generating a roll moment to the right. This happened for both conditions, with and without trip wires. The curves for both conditions were very similar to each other, up to 30° angle of attack. Results for 30° angle of attack and several roll angles show that the pressure distribution over the wing for 10° roll angle is symmetric. This symmetry is changed as the wing is further rolled to 20° and 30° roll angles. The pressure over the upward flap becomes higher than the one on the downward flap, generating a roll moment to the left.

The 65° delta wing demonstrated a different behavior than the 80° delta wing. The roll moment distribution also had a roll reversal behavior, but it occurred at different angles of attack. The wing presented a negative roll moment for angles of attack between 0° and 14°. It would not roll either side for an angle of attack of 15°, and it would have a positive roll moment for angles of attack higher than 15°. The positive roll moment increased up to 20° angle of attack, after that it stayed constant until 26° angle of attack. For angles of attack between 26° and 32° the moment decreased almost to zero. It is suggested that the decrease in roll moment on the wing is due to vortex breakdown, which starts to appear at the trailing edge of the 65° delta wing at about 20° angle of attack, and reaches the apex of the wing at about 35° angle of attack.

By combining all the experimental results it is concluded that:

1st) the reversal in the roll of the wings can be explained by considering both the longitudinal and lateral flow effects. At low angles of attack the upward flap has a higher local angle of attack, and vice-versa for the downward flap. This increases the effective angle of attack, which increases the lift and generates a moment toward the downward flap. At large angles of attack, the crossflow becomes dominant due to the formation of the leading edge vortices. The downward deflected flap results in a stronger vortex closer to the wing, generating a roll moment in the direction of the upward flap.

2nd) trip wires do affect the flow over the wing considerably, by moving the location of the primary reattachment point and the secondary and tertiary separation points. The trip wires have also a negative effect on the secondary separation point. When

the wing is rolled, the location of the secondary separation point can coincide with the location of the trip wire, making it inefficient.

7.2 Recommendations

1. Increase the angle of attack of the 80° wing beyond vortex breakdown, to determine its effect on the roll moment, and compare with the roll moment obtained for the 65° .
2. Measure the pressure distribution on the 65° wing with and without flap deflection, and with and without trip wires. Results should be interesting since it is known that vortex breakdown is present on the wing for angles of attack between 20° and 35° .
3. Use a different method to trip the boundary layer over the wing. This would have to be a method that is not so intrusive as the trip wires. The point would be to avoid the location of the secondary separation line to coincide with the trip wire.
4. Perform a smoke flow visualization. This would help in determining the location of vortex breakdown on the 65° delta wing and would also help determine if the trip wires do avoid vortex breakdown or not.

REFERENCES

Arena Jr., A.S., "An Experimental and Computational Investigation of Slender Wings Undergoing Wing Rock", Ph.D. Dissertation, University of Notre Dame, April 1992.

Arena, Jr., A.S., and Nelson, R. C., "Unsteady Surface Pressure Measurement on a Slender Delta Wing Undergoing Limit Cycle Wing Rock", AIAA Paper 91-0434, January, 1991.

Arena, Jr., A.S., and Nelson, R. C., "Experimental Investigation on Limit Cycle Wing Rock of Slender Wings", Journal of Aircraft, Vol.31, No.5, Sept.-Oct., 1994.

Arena, Jr., A.S., Nelson, R. C., and Schiff, L.B., "An Experimental Study of the Nonlinear Dynamic Phenomenon Known as Wing Rock", AIAA Paper 90-2812, August 1990.

Arena, Jr., A.S., and Nelson, R. C., "A Discrete Vortex Model for Predicting Wing Rock of Slender Wings", AIAA 92-4497, August, 1992.

Carcaillet, R. et al., "Leading Edge Vortex Flow Over a 75 Degree-Swept Delta Wing-Experimental and Computational Results", ICAS, Sept. 1986, 15 pgs.

Deng, Q. and Gursul, I., "Effect of Leading-Edge Flaps on Vortices and Vortex Breakdown", Journal of Aircraft, Vol.33, No.6, November-December, 1996, pp.1079-1086.

Grantz, A.C. and Marchman III, J.F., "Trailing Edge Flap Influence on Leading Edge Vortex Flap Aerodynamics", Journal of Aircraft, Vol.20, No.2, February 1983, pp. 165-169.

Hoffler, K.D., and Rao, D.M., “An Investigation of the Tabbed Vortex Flap”, *Journal of Aircraft*, Vol. 22, No. 6, 1985, pp. 490-497.

Hoffler, K.D.; Rao, D.; Frassinelli, M.C., “Basic Studies on Delta Wing Flow Modifications by Means of Apex Fences”, *Vortex Flow Aerodynamics, Volume I, Proceedings of a Conference - Hampton, VA, USA, Oct 8 -10, 1985*, pp.203-217.

Hsing, Ting-ding; Zhang, Zi-qiang, and Zhuang, Feng-gan, “The Impact of Apex-Flap on Vortex-Flapped Delta and Double Delta Wings”, AIAA Paper 91-3218.

Hummel, I.D., “On the Vortex Formation Over a Slender Wing at Large Angles of Incidence”, AGARD CP-247, 1978.

Ize, C. and Arena, Jr., A. S., “Spanwise Camber and Quasi-Steady Effects During Wing Rock”, *Journal of Aircraft*, Vol.35, No.3, May-June 1998, pp.495-497.

Ize, C. and Arena, Jr., A.S., “Effects of Asymmetric Leading Edge Flap Deflection on Delta Wings in Roll”, AIAA Paper 97-3486, Atmospheric Flight Mechanics Conference, August 11-13, New Orleans, Louisiana, 1997b.

Levin, D. and Seginer, A., “Experimental Investigation of Vortex Flaps on Thick Delta Wings”, *Journal of Aircraft*, Vol.31, No.4, 1994, pp.988-991.

Marchman, III, J.F., “Aerodynamics of Inverted Leading-Edge Flaps on Delta Wings”, *Journal of Aircraft*, Vol.18, No.12, 1981, pp. 1051-1056.

Marchman, III, J.F., Plentovich, E.B., and Manor, D., “Performance Improvement of Delta Wings at Subsonic Speeds Due to Vortex Flaps”, AIAA Paper 80-1802, AIAA Aircraft Systems Meeting, Anaheim, California, August 4-6, 1980.

Marchman, III, J.F., “Effectiveness of Leading-Edge Vortex Flaps on 60 and 75 Degree Delta Wings”, *Journal of Aircraft*, Vol.18, No.4, 1981, pp. 280-286.

Marchman, III, J.F., and Thomas, R.H., "Effects of Yaw on Leading Edge Vortex Flap Aerodynamics", AIAA Paper 81-1660, AIAA Aircraft Systems and Technology Conference, Dayton, Ohio, August 11-13, 1981.

Marchman III, J.F. and Hollins, M.L., "Fuselage Effects in Leading Edge Vortex Flap Aerodynamics", ICAS-82-6.7.5, 1982, pp. 1302-1308.

Nguyen, L.T., Yip, L. and Chambers, J.R., "Self Induced Wing Rock on Slender Delta Wings", AIAA Paper 81-1883, August, 1981.

Oh, S., and Tavella, D., "Analytical Observations on the Aerodynamics of a Delta Wing with Leading Edge Flaps", AIAA Paper 86-1790, 9 pgs.

Rao, D. M., "Upper Vortex Flap - A Versatile Surface for Highly Swept Wings", ICAS-82-6.7.1, 1982.

Rao, D. M., "Towards an Advanced Vortex Flap System - The "Cavity" Flap", Vortex Flow Aerodynamics, Volume I, Proceedings of a Conference - Hampton, VA, USA, Oct 8 -10, 1985, pp.219-230.

Rinoie, K.; Fujita, T.; Iwasaki, A., and Fujieda H., "Behaviours of Leading-Edge Separation Vortex Formed on a Delta Wing with Vortex Flaps", 20th ICAS, Sorrento, Napoli, Italy, 8-13 September, 1996, pp.2252-2259.

Rinoie, K. and Stollery, J.L., "Experimental Studies of Vortex Flaps and Vortex Plates", *Journal of Aircraft*, Vol.31, No.2, March-April 1994, pp. 322-329.

Roberts, S.D. and Arena, Jr., A.S., "An Inviscid Model for Evaluating Wing Rock Suppression Methodologies", AIAA 94-0808, 32nd Aerospace Sciences Meeting & Exhibit, January 10-13, 1994, Reno, NV.

Schoonover, Jr., W. E., and Ohlson, W.E., "Wind Tunnel Investigation of Vortex Flaps on a Highly Swept Interceptor Configuration", ICAS-82-6.7.3., pp.1276-1290.

Walton, J., and Katz, J., "Reduction of Wing Rock Amplitudes Using Leading-Edge Vortex Manipulations", AIAA-Paper 92-0279, 30th Aerospace Sciences Meeting & Exhibit, January 6-9, Reno, NV, 1992.

Wentz, Jr., W.H., and Kohlman, D.L., "Vortex Breakdown on Slender Sharp-Edged Wings", *Journal of Aircraft*, Vol.8, No.3, March 1971, pp.156-161.

APPENDIX

A.1. Torque Sensor Construction

A.1.1 Mechanical Part

All parts of the torque sensor are made out of 1/8" thick aluminum. The main parts of the sensor are shown in figure A1.

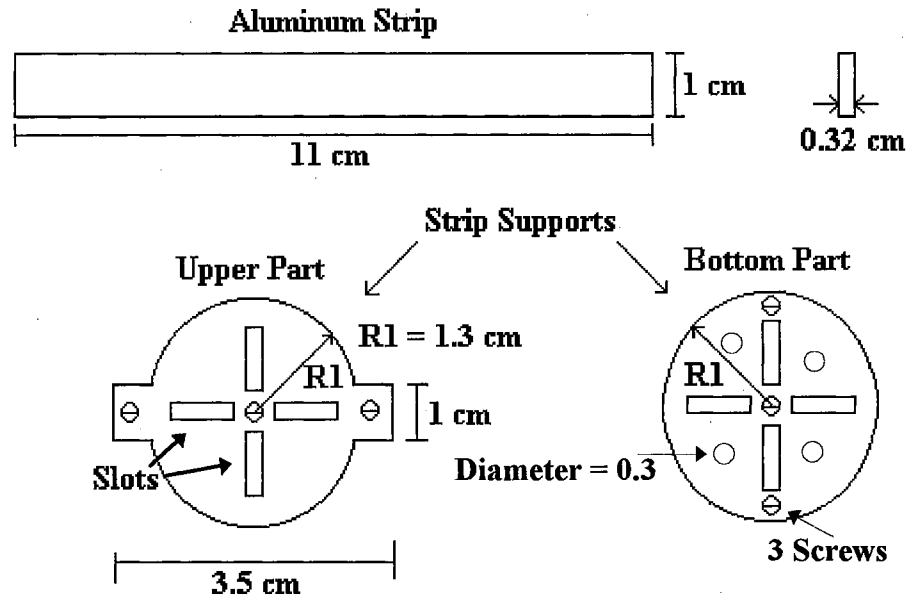


Figure A1. Main parts of the torque sensor.

It is important to have the slots of the upper part aligned with the one of the bottom part, otherwise the strip will not be straight when the torque sensor is finished. The slots have the same size as the strips, so that the strips can fit exactly on them. The bottom support should have four holes on the sides of the slots, so the wires from the strain gages can pass through it.

The next step is to put the strip on the slot and fix them in there. There are two possible ways to do that: by welding and gluing. The method used for the experiments was by glue. It was suggested that welding could be used, but it was unknown how the

welding is going to affect the aluminum. The glue used was transparent epoxy, that cures in 2 hours.

There is one disadvantage when using glue to fix the parts together, that the torque sensor does not withstand a high pressure. If a high pressure is going to be used on the wind tunnel, it might be advisable to try to fix the parts by welding them together.

There is no right way to put the parts together. The easiest way is probably to put all the strips in one of the supports first, and then fix the other support on the strips. The final assemble of the parts should look like the one in figure A2.

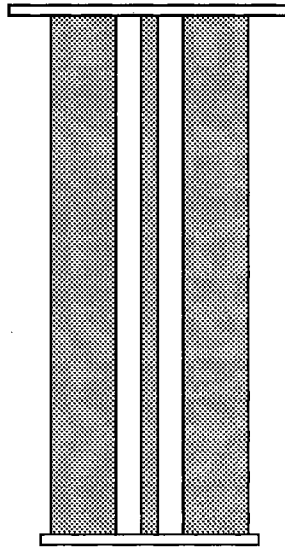


Figure A2. Final assemble of the strips and the supports.

The next step is to the support of the wing the support of the sensor itself. The parts needed for that are shown in figure A3. The support of the torque sensor was made of a plastic tube. It is suggests that the tube be made of aluminum. The support is hollow and a hole is made on the side so a Allen screw can be placed on it. If the support is made

out of plastic there is a good chance that the threads of the Allen screw will get damaged due to continuous use.

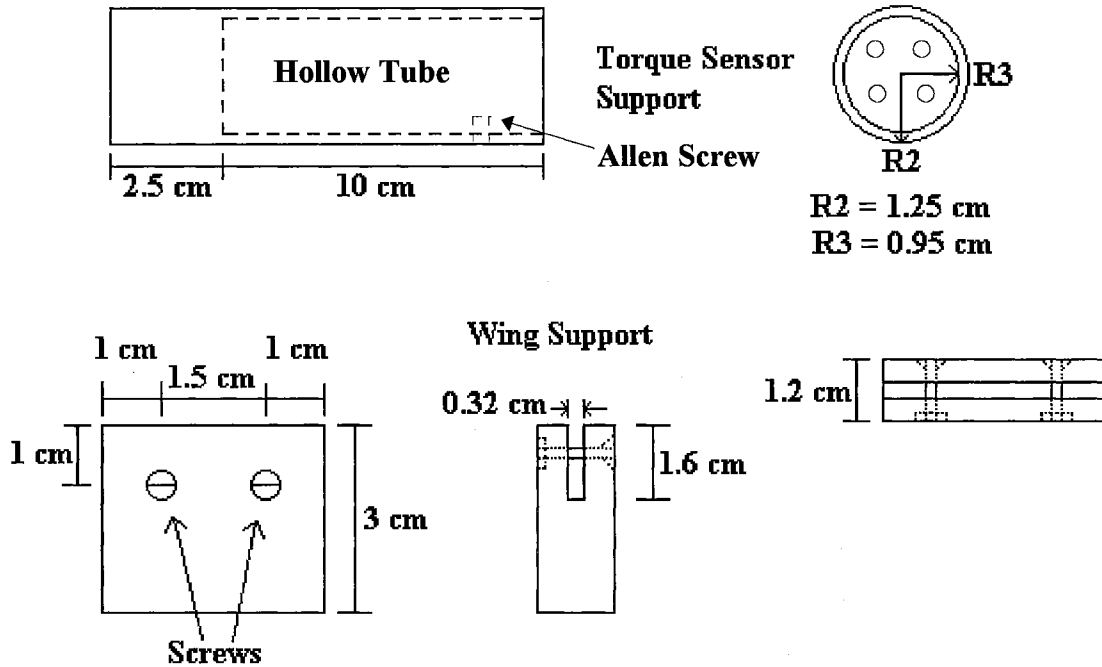


Figure A3. Support for the torque sensor and for the wing.

This is the reason it is suggested that the support for the sensor be made of aluminum, so the threads of the Allen screw will not get damage with continuous use of the system. The torque sensor is attached to the support by the 3 screws placed on the bottom part of the sensor and by epoxy. If necessary additional screws can be placed in any free space on the bottom of the sensor.

The support of the wing is a block of aluminum with a open slot where the wing is placed. The slot used was 1.6 cm deep, but it can be deeper than that if necessary. Two screws were placed on the side of the support in order to hold the wing. The support of the wing was connected to the torque sensor by the three screws on the top part of the

sensor. It was also glued with epoxy to ensure a good bond. The final assembly with the wing support and the torque sensor support should look like figure A4.

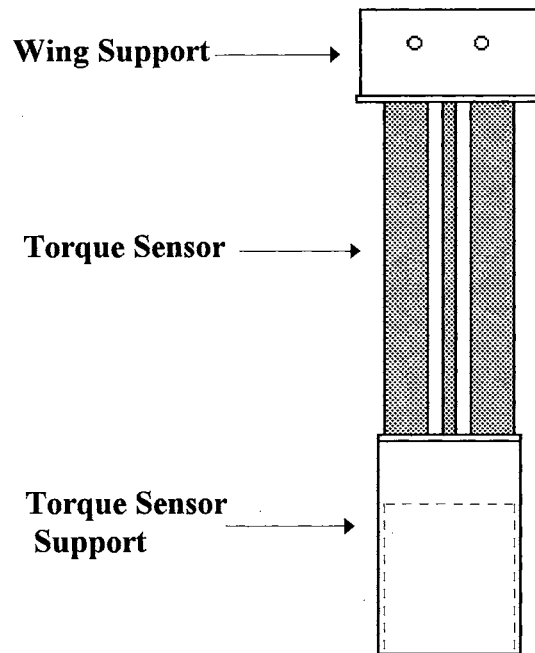


Figure A4. Final assemble of the torque sensor with wing support and sensor support.

The final step on the assemble of the torque sensor is the placement of the strain gages on the aluminum strips. For easy visualization, the torque sensor is going to be shown only with the wing support. Figure A5 shows the place where the strain gages should be placed. The strain gages should be the last component to be placed on the torque sensor. It is necessary to have 4 strain gages in order to have a full Wheatstone Bridge.

The position in the strips where the strain gages are placed, depends how much sensitivity the user needs from the torque sensor.

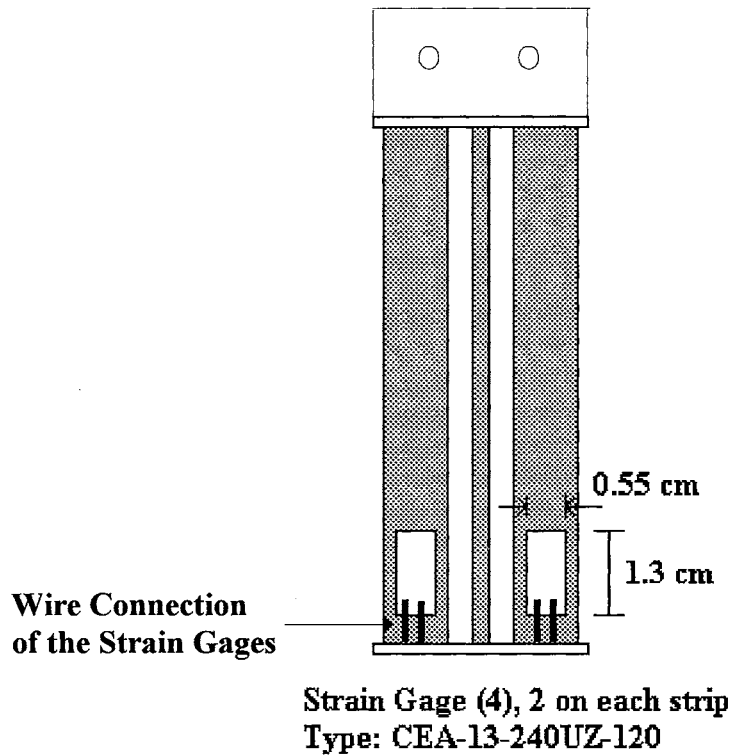


Figure A5. Placement of the strain gages on the torque sensor.

By placing the strain gages close to the wing support the sensitivity of the sensor decreases, and vice-versa by placing them close to the torque sensor support. The strain gages must be placed in two opposite strips and on both sides of the strips. All for gages should also be placed on the same height. For convenience the gages were placed on the strips that had the width on the same side as the wing support.

After choosing the place where the strain gages are going to be placed, it is necessary to clean the surface of the strips. First, the user needs to sand any dirt on the strips. After that, ammonia should be used to clean the aluminum powder deposited by the

sanding of the strips. Finally the strips should be cleaned with alcohol, to ensure a clean surface for the strain gages.

To fix the strain gages on the surface of the strips, first take a piece of Scotch tape, and tape the upper surface of the strain gage. Take the tape with the gage and drop 1 or 2 drops of super glue on the back of the strain gage. Place the strain gage and the Scotch tape on the surface of the aluminum strip. Wait a few minutes for the Super glue to cure completely. Peel the Scotch tape out, very carefully not to take the strain gage out. In case the strain gage does not stick to the aluminum strip, all the process has to be repeated, starting from the cleaning of the aluminum strips.

After the strain gages are all in place, the final step is to solder the wires on each of the strain gages. The soldering of the wires on the strain gages is very delicate and should be done by a experienced technician. After the wires are soldered on the strain gages they should go through the holes made on the bottom part of the sensor and on the sensor support, in order to avoid any undesired pull, that can take them from the strain gages, and damage the gages. To protect the points where the wires are soldered on the gages, it is suggested to drop a few drop of candle wax on these points.

In the current experiment the torque sensor was placed on a pipe that was connected to the floor of the wind tunnel, as described in Section 2.3.1.

A.1.2 Electronic Part

The components needed for the electronic part of the torque sensor are: 2 potentiometer of 10 Ohm and 10 turns, 1 resistor of 100 Ohm, 1 resistor of 68Kohm, 1 power supply with ± 5 Volts output, and 1 power supply with ± 11 Volts output.

The user is also going to need an Op Amp to amplify the output signal from the torque sensor. The Op Amp used in this experiment was a 741 with an amplification of 680 times. The schematic of the electronic circuit used is shown in figure A6.

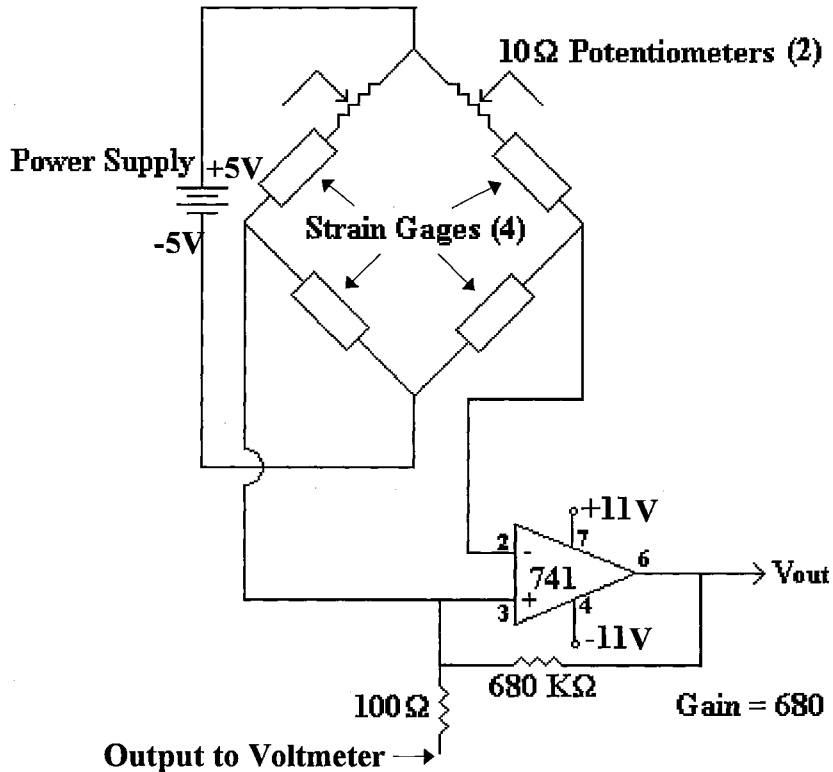


Figure A6. Schematic of the electronic circuit for the strain gages and amplifier.

One thing to be noticed in the circuit above is that there is no part of the circuit is grounded. If any part of the circuit is grounded the output voltage is going to be zero.

The power supply to the strain gages does not need to be exactly ± 5 Volts. It can be as high as the strain gages can support. It is important though, that the power to the strain gages be kept constant during the data acquisition process. If the voltage supplied to the strain gages fluctuates during data acquisition, the output voltage will also fluctuate,

giving incorrect data. In this experiment the voltage supplied to the circuit was -1.76 and 2.11 Volts. These were the lowest voltages that the power supply provided and they were monitored to ensure that there would be no fluctuation.

If a different Op Amp is used the connections of the circuit shown in figure A6 may have to be changed. To increase the amplification of the voltage output, the 680 K Ω resistor has to be changed to the desired amplification value.

B.1. Computer Code Used for Data Acquisition

The computer code used was written in C language. It acquires 1000 points and averages it, and then starts all over again, until the computer is turned off. The process is shown in the screen all the time.

```
#include "d16.h"
void main()
{ int counter=0,sample;
float volts,avgvolts,volt=0;
int datavalue;
clrscr();
boardsetup();
set_gain(1);
chan_scan();
printf("Enter number of sample to be taken:");
scanf("%i",&sample);
clrscr();
while (counter <= sample)
{   counter++;
    datavalue=a2din();
    volts=datavalue*(2./4095.)-1.;
    volt=volt+volts;
    avgvolts=volt/counter;
    gotoxy(7,10);
    printf("%8.4f",volts);
    printf("%8.4f",avgvolts);
}
}
```


VITA

Carlos Ize

Candidate for the Degree of

Doctor in Philosophy

Thesis: EFFECTS OF ASYMMETRIC LEADING EDGE FLAP DEFLECTION ON DELTA WINGS

Major Field: Mechanical Engineering

Biographical:

Personal Data: Born in São José dos Campos, São Paulo, Brazil, On November 27, 1961, the son of Antonio F. Izé and Marlene B.A. Izé.

Education: Received Bachelor degree in Physics from the University of São Paulo, Physics Institute of São Carlos, São Carlos, São Paulo, Brazil, August 1988. Received Master degree in Mechanical Engineering from the University of São Paulo, School of Engineering of São Carlos, São Carlos, São Paulo, Brazil, August 1991. Completed the requirements for Doctor in Philosophy in Mechanical and Aerospace Engineering at Oklahoma State University in July 1998.

Experience: Employed as a teaching assistant at Oklahoma State University from Spring 1996 to Summer 1998: graduate research assistant at the Department of Mechanical and Aerospace Engineering, 1993 to present.

Professional Membership: American Institute of Aeronautics and Astronautics.